IMMOBILIZATION OF METAL CLUSTER CARBONYL COMPLEXES ON LAYERED SILICATES

By

Emmanuel P. Giannelis

A DISSERTATION

Submitted to

Michigan State University

in partial fulfillment of the requirements

for the degree of

DOCTOR OF PHILOSOPHY

Department of Chemistry

1985

ABSTRACT

IMMOBILIZATION OF METAL CLUSTER CARBONYL COMPLEXES ON LAYERED SILICATES

By

Emmanuel P. Giannelis

Several metal cluster carbonyl complexes have been immobilized on Na^+-hectorite and alumina pillared montmorillonite and characterized by a variety of spectroscopic techniques.

Adsorption of the protonated metal cluster carbonyl $HOs_3(CO)_{12}^+$ on Na^+-hectorite leads to a preferential dispersal of $Os_3(CO)_{12}$ centers at the hydroxylated edge sites of the silicate layers. Under conditions where surface migration is slow, the edge bound clusters react with surface hydroxyl groups to form complexes of the type $[Os(CO)_{2,3}(O\text{-}Si\equiv)_2]n$, whereas clusters adsorbed on basal planes are stable.

The difference in reactivity of $Os_3(CO)_{12}$ with different clays and the dependence on the drying method is rationalized in terms of a clay flocculation model in which both lamellar (face-face) and delaminated (edge-edge, edge-face) interactions of the layers can take place, depending in part on the layer-morphology.

The phosphonium-phosphine ligand $Ph_2PCH_2CH_2\overset{+}{P}Ph_2CH_2Ph$ (abbreviated $P\text{-}P^+$) has been used as a means of inducing positive charge on otherwise neutral metal carbonyl clusters. $Ru_3(CO)_9(P\text{-}P^+)_3$, $H_4Ru_4(CO)_8(P\text{-}P^+)_4$, $Ir_4(CO)_9(P\text{-}P^+)_3$, $Os_3(CO)_{11}(P\text{-}P^+)$, and $H_2Os_3(CO)_{9,10}(P\text{-}P^+)$ have been

intercalated in hectorite and characterized by IR and electronic spectroscopy, x-ray diffraction and elemental analysis.

The intercalated $H_2Os_3(CO)_9(P\text{-}P^+)$-hectorite has been used as an olefin isomerization catalyst. The reaction is found to be dependent on the extent of interlayer swelling. In toluene, the intercalated catalyst exhibits a pseudo first-order behavior with $k_{obs} = 0.022\ h^{-1}$.

The mechanism of metal cluster binding to alumina pillared montmorillonite has been investigated by IR and electronic spectroscopy. $Os_3(CO)_{12}$ and $Ru_3(CO)_{12}$ are found to form protonated species of the type $HOs_3(CO)_{12}^+$ and $HRu_3(CO)_{12}^+$ which can be extracted from the surface by ion exchange with KPF_6. In contrast, $H_4Ru_4(CO)_{12}$ and $Ir_4(CO)_{12}$ are simply physisorbed on the surface of the clay. Significantly, $H_2Os_3(CO)_{10}$ reacts with the pillared clay to form a pillar-grafted hydrido triosmium cluster of the type $HOs_3(CO)_{10}(O\text{-}Al\lessdot)$. In addition, adsorption of $[CpFe(CO)_2]_2$ on the surface leads to cationic species of the type $[CpFe(CO)_{2,3}]^+$ electrostatically bound to the clay.

TO MY PARENTS

ACKNOWLEDGEMENTS

I would like to thank Dr. T.J. Pinnavaia for his guidance, independence, and encouragement offered throughout the years of graduate school. I am also grateful to Dr. H.A. Eick for his editorial assistance in improving my writing. Helpful discussions with Dr. D.G. Nocera are particularly acknowledged.

Finally, I would like to thank the members of Dr. Pinnavaia's research group whose help, advice, and encouragement made graduate school a unique experience.

TABLE OF CONTENTS

LIST OF TABLES

LIST OF FIGURES

CHAPTER I

INTRODUCTION

A. Structure and Properties of Layered Silicates

1. Structure

The term "clay" refers to finely divided mineral sediments having particles with dimensions of less than 2μ. However, a material exhibiting certain properties such as plasticity, small particle size, and specific chemical composition (i.e. as consisting largely of silica, alumina, and water) might be loosely defined as clay[1]. The term "clay minerals" refers to specific structural types of 2μ particles which can be divided into crystalline and non-crystalline classes. It should be recognized, however, that recent advances in X-ray crystallography and structural analysis have affirmed that completely ordered clay structures represent no more than ideal models[2,3].

The swelling phyllosilicates, known as smectite clay minerals, have a layer lattice structure made up by the stacking of two-dimensional oxyanion sheets, often with intermediate layers of hydrated metal cations[4]. The major building units of these two-dimensional arrays are silica tetrahedra and octahedra of magnesia or alumina. The silicate tetrahedra are usually oriented so that the three basal oxygen atoms of each tetrahedron lie on

the same plane, while the fourth oxygen atom (apical) defines a second common plane. The octahedral sheet contains a cation, usually Al (gibbsitic) or Mg (brucitic), surrounded by six hydroxy ions in an octahedral arrangement. Condensation of the tetrahedral and octahedral sheet in a way that some hydroxyl ions of the brucite or gibbsite structure are replaced by apical silicate oxygens results in a composite layer structure.

Hectorite and montmorillonite, like all smectite clays, are classified as 2:1 layer minerals. This designation refers to a structure in which two tetrahedral sheets sandwich an octahedral sheet (Figure 1). A common example of a 1:1 layer structure is kaolinite, where a tetrahedral sheet is paired only to an octahedral sheet to form a layer[5]. Montmorillonite contains mainly aluminum in the octahedral sites and since only two-thirds of these sites are occupied, the mineral is referred as a "dioctahedral" clay. On the other hand, a "trioctahedral" mineral has all octahedral sites filled by metal cations, as in hectorite, where all sites are occupied principally by magnesium ions.

Cations at particular locations of the silicate structure can be replaced by various other cations with similar ionic radii without changing the structural characteristics of the mineral. If the replacing cation has a lower valence, a net negative charge will develop as a result of isomorphous substitution. Charge neutrality is achieved by either an opposing substitution with cations of higher valence or, as is usually the case, by the presence of additional cations in the interlayer region of the structure.

The replacement of Mg^{2+} for Al^{3+} in the octahedral sheet of montmorillonite results in the development of a net anionic charge. In hectorite the layer charge arises from the isomorphous substitution of octahedral Mg^{2+} by Li^{+} ions. Normally, arrays of hydrated alkaline earth

Figure 1 Idealized structure of a smectite clay mineral. (O) Oxygen atoms; (●) hydroxyl groups. Silicon and sometimes aluminum normally occupy tetrahedral positions in the oxygen framework. Aluminum, magnesium, iron, or lithium may occupy octahedral sites. $M^{n+} \cdot xH_2O$ represents the interlayer exchange cation.

or alkali metal cations are located in the interlamellar space or the regions between the basal surfaces of the negatively charged silicate layers. The charge balancing cations are usually located adjacent to the points of anionic charge on the basal planes. However, small anhydrous cations, mainly H^+ or Li^+, can migrate through the oxygen sheet to the neighborhood of the substitution, where the anionic charge arises. It has been reported that H^+ ions coordinate with the hydroxyl groups of the octahedral sheet rather than react with tetrahedral oxygen atoms[6].

The idealized unit cell compositions for hectorite and montmorillonite are

$$M_{0.67}\,[Mg_{5.33}Li_{0.67}]^{VI}(Si_{8.0})^{IV}O_{20}(OH,F)_4$$

and

$$M_{0.67}[Al_{3.33}Mg_{0.67}]^{VI}(Si_{8.00})^{IV}O_{20}(OH)_4$$

respectively, in which the superscripts (IV) and (VI) refer to the respective cation in tetrahedral and octahedral sites, and M represents a univalent or equivalent compensating cation[2]. The thickness of the unit structure (layer plus interlayer assembly), which can be calculated from a series of 00ℓ X-ray basal reflections, will depend on the amount of interlayer water and the nature of interlayer cation.

2. Ion Exchange

The hydrated compensating cations of the native minerals are exchangeable and can be replaced with other hydrated metal cations and with various organic and organometallic cationic species. However, the extent of ion replacement may be size limited, especially in the case of

large complex cations. Hectorite, for example, exhibits a cation exchange capacity (CEC) of about 70 milliequivalents per 100 grams. Based on the CEC and the a and b unit cell parameters of the mineral (5.25 x 9.18 Å), the average distance between exchange sites is calculated to be about 8.7 Å[7]. Thus, cations with cross-sectional diameters greater than this value can fill the interlamellar spaces before an homoionic clay is achieved.

The exchange reaction can be represented by the following equation:

$$\overline{\underline{Na^+(solv)}} + M^{n+} \xrightarrow{\text{solvent}} \overline{\underline{M^{n+}(solv)}} + Na^+ \qquad (1)$$

where the horizontal lines represent the negatively charged silicate layers. The kinetics and equilibria of the above equation depend on several variables[8,9]. However, an attempt will be made to generalize some of the qualitative features concerning the tendency of a cation to exchange onto a negative surface. The exchange equilibrium in general favors **a)** cations with higher valence charge; **b)** the larger cation between species of a particular valence; and **c)** certain cations (i.e. K^+, Ba^{2+} and NH_4^+) that because of their size can take up a very favorable interlayer position. The rate of the reaction is determined mainly by the interlayer cation accessibility, which in turn depends on the swelling properties of the mineral.

3. Swelling of Smectites

Smectite clays exhibit basal spacings larger than the corresponding 9.2 Å of their uncharged analogues because of the presence of hydrated compensating cations. The values of basal spacings depend mainly on the mineral, the exchangeable cation, and the partial pressure of water vapor in equilibrium with the clay sample[10].

The basal spacing of dehydrated Na^+-montmorillonite is 9.5 Å. As the

water content increases spacings of 12.4, 15.4, and 18.6 Å are observed, corresponding to the presence of one, two, or three layers of water associated with the Na^+ ion respectively. Further swelling can occur when Na^+-montmorillonite is suspended in water. In fact, the aluminosilicate layers are completely dispersed, the interlayer spacing being practically infinite[11].

The osmotic swelling of smectite clays is limited by the electrostatic interactions between the anionic silicate layers and the compensating interlayer cations. As the dielectric constant of the swelling media decreases, the Coulombic interactions between the opposing silicate surfaces and the interlamellar cations increase, which results in smaller basal spacings[12].

Increasing the concentration of clay suspensions in aqueous or ionizing media can form thixotropic porous structures, that may gel. This gelation phenomenon results from extensive layer edge-to-face and edge-to-edge interactions generating a "house of cards" structure[10].

A wide variety of neutral molecules other than water can also be intercalated on smectite clays. Protonation and ionic interactions, coordination to interlamellar cations, and dipolar interactions are among the mechanisms involved in the intercalation processes. The intercalation of ammonia on Mg^{2+}-montmorillonite involves the protonation of the base and leads to bound ammonium ions[13]:

$$\underline{\overline{Mg(H_2O)_x^{2+}}} + NH_3 \longrightarrow \underline{\overline{[Mg(OH)(H_2O)_{x-1}]^+ + NH_4^+}} \qquad (2)$$

Transition metal ion exchanged minerals intercalate pyridine through coordination to the metal ions[14]:

$$\underline{\overline{[Cu(H_2O)_x]^{2+}}} + py \xrightarrow{-H_2O} \underline{\overline{[Cu(py)_4{}^{2+}]}} \qquad (3)$$

The swelling and increase in basal spacings on treatment with polar solvents not only can be used as a means of identification of these minerals, but plays a very important role in catalytic reactions as well.

4. Acidity

Among the very significant properties of silicate minerals is their ability to exhibit strong surface acidity upon removal of their adsorbed or intercalated water. Though both Lewis and Bronsted acid sites may contribute to the surface acidity, protonic acidity is more important in catalytic reactions involving the minerals. In some cases native minerals possess sufficient surface acidity to catalyze several "natural" processes, e.g., the chemical transformation of organic molecules, the degradation of pesticides, and petroleum-forming reactions. The surface acidity is related in origin and is often comparable to that of amorphous acidic silica-alumina and zeolites that have been used as petroleum cracking catalysts.

Polarized water molecules coordinated to the compensating interlamellar cations are the most important source of Bronsted acidity in smectite clays. The degree of dissociation of water coordinated to interlayer cations is higher than that of the bulk liquid. Thus, hydrated cations are more acidic in the clay interlayers than in homogeneous aqueous solution[15,16]. The acidity can be correlated with cationic polarizing power which increases with increasing charge-to-radius ratio. In addition, the acidity increases as the amount of interlamellar water decreases.

5. Catalysis and Interlayer Dynamics

Smectites have been known and used for many years as efficient heterogeneous catalysts for a number of reactions[17]. Acid modified smectites were used extensively in the petrochemical industry for the cracking of petroleum feed stock to valuable products until they were replaced by the more thermally stable zeolites. The use of silicates as polymerization catalysts is also known and discussed extensively in many textbooks[18-20]. Because of their "two-dimensional" interlamellar environment, smectite minerals offer the possibility of controlling chemical transformations with the prospect of obtaining products different from those obtained in a less restrictive homogeneous medium.

A recent development in the area of clay catalysts is the intercalation of known, well studied, complex catalysts on smectite interlayers by utilizing simple ion exchange techniques. Electron spin resonance (ESR) and nuclear magnetic resonance (NMR) studies have provided an insight into the nature of clay intercalates[21-23]. At low degrees of interlayer solvation the interlamellar cations adopt a dynamic orientation and rotate anisotropically about certain molecular axes. At high degree of interlayer solvation, swelling beyond the coordination sphere of the solvated cation separates efficiently the anionic silicate layers from the solvated complex and provokes rapid tumbling. Thus, intercalated metal catalysts exhibiting solution-like mobility should be comparable in terms of catalytic activity to their homogeneous counterparts. In addition, surface chemical phenomena may favor the intercalation of a particular catalytic species from those involved in an equilibrium and may alter the specificity and selectivity of the catalyst.

6. Pillared Clays

A serious drawback associated with the use of naturally occurring smectites as adsorbents and heterogeneous catalysts at elevated temperature is the loss of adsorbed solvent and collapse of the layers to van der Waals contact. Under these circumstances the surface area drastically diminishes and interlamellar catalytic reactions are precluded. Efforts to overcome this practical problem led to intercalation of robust cations, which act as molecular props or pillars, so that internal surface is available for adsorption and catalysis even in the absence of a swelling solvent. Among the various cationic species that have been used in pillaring layered silicates are alkylammonium ions, bicyclic amine cations, metal chelate complexes, and polynuclear hydroxy metal cations.

More than 25 years ago Barrer and MacLeod introduced the concept of pillaring smectite clays to prepare porous forms of montmorillonite by ion exchange with tetraalkylammonium ions[24]. Tetramethylammonium and ethylenediammonium forms of montmorillonite, hectorite, and fluorohectorite possessing interlayer porosity were also prepared[25]. These systems exhibit a very small interlayer spacing (Δd = 3-4 Å) and show low resistance to swelling solvents. Cationic species derived from rigid or cage-like amines also have been used as pillaring agents. For example, the intercalation of protonated 1,4-diazabicyclo[2,2,2]-octane(triethyldiamine) in smectites results in a material exhibiting d00ℓ interlamellar spacing of 14.2 Å[26]. Moreover, this material shows typical molecular sieving properties and markedly higher catalytic activity for esterification of carboxylic acids with alkanols than does R_4N^+-montmorillonite. However, these systems are not thermally stable and decompose below 250°C[27].

Derivatives with higher thermal stability (<450°C) were prepared by

introducing large metal chelates complexes such as $Fe(Phen)_3^{2+}$, $Cu(Phen)_3^{2+}$, $Fe(bp)_3^{2+}$, $Cu(bp)_3^{2+}$, and $Ru(bp)^{2+}$[28,29]. An unusual characteristic of these products is the incorporation of anions in the interlayer region in the form of cation-anion pairs. This binding of excess salt is believed to result from a screening of the electrostatic charge of the silicate layers by the large complex cation.

A turning point in the preparation of genuine pillared phases was achieved by intercalation of polynuclear hydroxy metal cations formed by hydrolysis over a specific range of OH^-/M^{n+} ratios. These products exhibit high thermal stability, considerable surface areas, and intracrystal acidity and can function as cracking catalysts[30-40]. Most of the work in this area has been devoted to using hydroxy aluminum cations. ^{27}Al NMR studies along with potentiometric titration data indicate that the predominant species in base- or metal-hydrolyzed $AlCl_3$ at the OH^-/Al^{3+} ratios used to prepare the pillaring agent is $Al_{13}O_4(OH)_{28}^{3+}$[39,41]. In addition the lattice expansion ($\sim$ 9.5 Å) of smectites pillared with hydroxy aluminum cations is consistent with the estimated van der Waals diameter for an intercalated Al_{13} Keggin ion.

The introduction of polynuclear oxycations in the interlamellar region of the mineral, followed by dehydroxylation at elevated temperatures to produce small oxide aggregates, provides a versatile method for preparing a new class of molecular sieves with pore size range (6-40 A) larger than faujasite-type zeolites. By varying the size of the molecular pillar and/or the population density of the interlayer region one could tailor the pore size to a particular application.

B. Concept of Supported Metal Complexes

Efforts to prepare superior hybrid catalysts possessing the advantages

of both homogeneous and heterogeneous catalytic systems with few disadvantages led to immobilization of soluble transition metal complexes on inert solid supports such as organic polymers and refractory metal oxides[42-50]. One can appreciate the recent interest in supported complex catalysts by comparing them with traditional homogeneous and heterogeneous catalysts.

A commonly employed class of homogeneous catalysts is that of the organotransition metal complexes. Since these complexes exhibit a well defined structure and stoichiometry, and advances in analytical techniques permit proper characterization in solution, homogeneous catalysts are better studied and understood. In addition, because of the availability of all metal centers in a sufficiently dilute solution, their catalytic activity can be easily interpreted. For the same reason they allow for an efficient and totally reproducible use of metal atoms. Furthermore, transition metal complexes exhibit electronic and steric properties that can be selectively modified or controlled through ligand substitution or variation of the solvent system. Finally, homogeneous catalysts usually possess one type of active site making them more specific and easier to tailor to a particular application.

Though in principle homogeneous catalysis seems highly efficient and attractive, it suffers from three major technical problems that may be prohibitive in industrial applications. The main disadvantage of homogeneous catalysts is the problem of separating the catalyst form the products at the end of the reaction. Separation of the two usually can be accomplished by distillation below the decomposition point of the catalyst, a procedure that is generally ineffective and highly expensive. Second, organotransition metal complexes lack the stability exhibited by traditional heterogeneous catalysts, such as pure metals and inorganic oxides, under severe reaction

conditions, that might be necessary for a particular process. Finally, homogeneous catalysts suffer from a limited solubility in suitable solvents, a problem clearly not present with a heterogeneous catalyst.

The major advantages of heterogeneous catalysts are their capacity for use in packed or fluidized bed reactors and ready separation from substrate and reaction products. Because of their high activity for a wide range of reactions they have been traditionally employed for a number of important industrial applications. However, certain undesirable properties make them less attractive. Heterogeneous catalytic reactions take place at the interfaces of the solid catalyst and the liquid or gaseous substrate. Only a fraction of the potential catalyst centers is exposed to substrate molecules; the atoms not present at the surface are inaccessible and remain unused. Despite recent advances in the area of surface characterization[51-53], complicated processes, such as chemisorption and catalysis, are not well understood. Thus the design and modification of heterogeneous catalysts is often limited due to poorly defined active sites. Moreover, their specificity is generally lower compared to homogeneous catalysts because of the several types of active site present on the surface. The major advantages and disadvantages associated with traditional homogeneous and heterogeneous catalysts are listed in Table 1.

The most common method in heterogenizing a transition metal catalyst is anchoring of the catalyst to a variety of solid supports through an ionic or covalent interaction. The metal complex may be also physically dispersed on the surface of the support by using an impregnation technique. However, the physisorption technique leads to species interacting weakly with the support, that can be readily desorbed from the surface, when the reaction involves solid-liquid phases.

Table 1

Advantages and Disadvantages of Homogeneous and Heterogeneous Catalysts[54]

Process	Advantages	Disadvantages
Homogeneous Catalysis	1) Well studied and interpreted catalytic activity	1) Separation problem
	2) Reported activity under mild reaction conditions	2) Sensitive to extreme reaction conditions
	3) Efficient and reproducible use of metal atoms	3) Solubility or solvent problem
	4) Electronic and steric properties easily varied and controlled	
Heterogeneous Catalysis	1) Acceptable thermal and mechanical stability	1) Design and improvement difficult due to ill defined active sites
	2) High activity for a wide range of reactions	2) Limited accessibility and effectiveness
	3) Ready separation from reaction products	3) Severe and costly reaction conditions

The new hybrid catalyst systems that appear heterogeneous at the bulk level but are essentially homogeneous on a molecular level, typically exhibit ease of separation, considerable thermal and mechanical stability, and efficiency in multistep or batch processes, properties commonly associated with heterogeneous catalysts. On the other hand properties such as specificity, efficiency, reaction control, and reproducibility are ordinarily associated with homogeneous systems. Additional advantages that may result from the immobilization process per se include **1)** higher activity or specificity by inhibiting the number of undesirable side reactions; **2)** substrate selectivity based on introduction of preferred orientations and different stereochemistry about the central metal atom; and **3)** preferential stabilization of catalytically active but normally unstable structures[42,55].

The components of the hybrid catalyst must be designed to fulfill the reaction requirements. From a chemical viewpoint the support should be inert to the reagents and products. The important engineering considerations are thermal and mechanical stability, enabling it to withstand the required reaction conditions, porosity, and acceptable surface area. Typical organic supports are polystyrene, polyamines, polyvinyls, polyamino acids, urethanes, acrylic polymers, and cross-linked dextrans. The list of usually used inorganic supports includes silica, alumina, glass, zeolites, and clays[56,57]. Though inorganic supports possess better thermal and mechanical stability than their organic counterparts, various synthetic routes to organic polymers offer a wide range of surface functionalization, pore size and surface area.

The catalytically active portion of the metal complex should remain stable under reaction conditions and must be "soluble" in the reaction medium. The optimum catalytic activity of immobilized catalysts is achieved in a solution-like environment in which metal complexes maintain their vibrational

and rotational degrees of freedom. To enhance activity it may be preferable to anchor the metal complex to the support via a long chemical chain rather than directly attach it to the surface. Close proximity of the support with the metal complex may result in strong stereochemical interactions with the active site. Though immobilization through an electrostatic interaction appears to exert the fewest restrictions on rotational and vibrational motions of the catalyst, the major problem lies with the availability of catalytically active charged species that remain stable when electrostatically bound to the appropriate support.

C. Some Aspects of Cluster Chemistry and Catalysis

1. Metal Cluster Carbonyls

Metal clusters are discrete molecular species consisting of a framework of metal atoms or ions in triangular or polyhedral arrays. The metal skeleton is surrounded and stabilized by various ligands such as carbonyls, hydrides, phosphines, or halides. However a small subclass of "naked" clusters with no ligands attached to the metal core[58] includes ions like Bi_5^{3+}, Sn_5^{3-}, Ge_9^{4-}, and Sn_9^{4-}. Hundreds of cluster complexes are known, many so stable that their structures have been determined by a variety of techniques including X-ray crystallography, NMR, infrared, and Raman spectroscopy[59-62].

One metal cluster subclass of particular interest is metal carbonyls. CO molecules at terminal or bridging positions are coordinated to the transition metal framework. The strength of metal-metal bonds increases within a group as the size or atomic weight of the metal increases. This effect is clearly demonstrated by comparing the chemistry of iron and ruthenium triangle derivatives of the type $M_3(CO)_{12}$ (M = Fe and Ru). The iron triangle in $Fe_3(CO)_{12}$ is generally less stable and is broken more readily

than is the metal core in $Ru_3(CO)_{12}$ upon reaction with reagents such as tertiary phosphines.

$Ru_3(CO)_{12}$ and $Os_3(CO)_{12}$ consist of a triangle with four terminally bonded CO ligands attached to each metal atom[63,64]. One unusual aspect of the trinuclear metal unit in ruthenium and osmium dodecacarbonyl clusters is their weak but detectable basicity[65]. Thus, they dissolve readily in concentrated sulfuric acid to give a solution exhibiting a high field ^1H NMR resonance at around δ -19 to -20, indicative of a hydride bridging two transition metal atoms. Precipitation and isolation of the stable $[HM_3(CO)_{12}][PF_6]$ is easily accomplished by adding NH_4PF_6 to the sulfuric acid solutions.

An interesting trinuclear metal cluster, $H_2Os_3(CO)_{10}$, is obtained by passing hydrogen gas through a refluxing octane solution of $Os_3(CO)_{12}$. Its unusual chemistry arises from the presence of an unsaturated site, thus, it readily adds donor molecules to attain the stable 48-electron configuration[67]. $Ir_4(CO)_{12}$ and $H_4Ru_4(CO)_{12}$ possess a tetranuclear core structure in a tetrahedral arrangement with three terminally bonded CO molecules coordinated to each metal atom[68,69]. It is believed that the four hydrogen atoms in $H_4Ru_4(CO)_{12}$ bridge the four long edges of the Ru_4 framework[69].

Metal cluster carbonyl complexes undergo a wide range of substitution reactions. The main synthetic route in preparing carbonyl substituted derivatives until recently was thermally or photochemically facilitated CO dissociation as illustrated by equation 4[70].

$$Mm - CO \xrightarrow[h\nu]{\Delta} Mm\text{-}\square + CO \qquad (4)$$

However, a serious drawback associated with this method makes it less

attractive. As may be anticipated, it leads to a mixture of products that normally require separation by chromatographic techniques. A recent advance employs Me_3NO for the oxidative decarbonylation of a thermally inert metal cluster[71]. The reaction mechanism involves nucleophilic attack on the metal bound carbonyl to give carbon dioxide and trimethylamine (equation 5)[70]

$$Mm\text{-}CO \xrightarrow{Me_3NO} Mm\text{-}\square + CO_2 + Me_3N \qquad (5)$$

The advantage of using Me_3NO is that both reaction byproducts are gaseous and are easily removed. In addition, an unsaturated center is left free to coordinate any added ligand. By controlling the stoichiometry of the reaction one can influence its specificity and obtain a certain derivative rather than a mixture of products. Of particular interest to our work is the substitution reaction with phosphine ligands. Thermal substitution of carbon monoxide with a tertiary phosphine occurs progressively on different metal centers, the substituted derivative attaining a stereochemical arrangement that minimizes steric interactions between phosphine ligands[72].

2. Catalysis by Metal Clusters

Metal cluster compounds find several uses in catalysis by exhibiting interesting catalytic properties in their own right, by acting as catalyst precursors, or by serving as models for complicated processes such as chemisorption and catalysis[73-78]. They can catalyze reactions as diverse as hydrogenation, isomerization, hydroformylation, water-gas shift, cyclisation, and oxidation[78]. By virtue of their structure and properties cluster compounds offer new opportunities in catalysis. Since they possess discrete well defined structures, high selectivity can be anticipated. Neighboring metal centers provide multiple bonding of a reactant molecule

that cannot be realized with mononuclear complexes. Moreover, different reagents can coordinate to neighboring positions, offering the possibility for synthesis gas ($CO + H_2$) conversion. Since transformations of the ligands can be transmitted through the metal-metal bonds, the reactivity and catalytic activity can be influenced, allowing for tailoring of the cluster to specific application.

From the standpoint of cluster-surface analogy it is important to demonstrate that discrete metal clusters can catalyze a number of reactions which can be brought about by conventional heterogeneous catalysts, but not by their homogeneous counterparts. Reactions catalyzed by conventional dispersed metal catalysts include the hydrogenation of nitrogen to give ammonia, the hydrogenation of carbon monoxide to give methane or methanol, and the hydrogenolysis of saturated hydrocarbons. Indeed $Os_3(CO)_{12}$ and $Ir_4(CO)_{12}$ were found active for the methanation reaction and the conversion of n-hexane to a mixture of C_4 to C_8 alkanes can be catalyzed by the "naked" cluster Bi_5^{3+}[74].

However the task of establishing beyond reasonable doubt that the actual catalyst is indeed a cluster compound and not a product of dissociation or aggregation is extremely difficult. The fact that the metal cluster complex may have been present initially in solution and may have been recovered intact at the end does not consitute a strong indication that the cluster integrity was maintained throughout the reaction. As a matter of fact, the opposite is believed to be the case, that is, some reactions are thought to be catalyzed by highly active mononuclear species formed by the fragmentation of the cluster under the reaction conditions[78].

Laine has formulated a set of five criteria that can be useful in identifying a homogeneously-catalyzed reaction as a cluster-catalyzed

reaction[79]. Cluster catalysis is suggestted if,

1. the turnover frequency increases with increasing concentration of catalyst,

2. the product selectivities obtained using cluster catalyst precursors are different from those obtained using mononuclear catalyst precursors, or the products themselves cannot be reconciled with mechanisms that involve only mononuclear species,

3. it is possible to modify the catalyst or the reaction conditions to favor metal-metal bond formation and the modification results in increased catalytic activity,

4. catalytic asymmetric induction is observed or chiral products can be obtained using chiral metal clusters in which the asymmetry resides in the metal framework or is a basic skeletal property,

5. a specific combination of two or more different metals can be used to enhance the rates of the reaction or change the product selectivity or allow catalysis of a reaction not catalyzed independently by any one of the metals.

D. Supported Metal Cluster Carbonyls

1. Immobilized Metals, Mononuclear Complexes, and Cluster Compounds on Solid Supports

Supported metals, a subclass of traditional heterogeneous catalysts are capable of activating C-C and C-H bonds in saturated hydrocarbons as well as hydrogenating carbon monoxide[80]. Dispersion of the metal aggregates on an inorganic oxide increases the effective surface area per gram of catalyst and at the same time offers the potential of better temperature control.

On the other hand, homogeneous catalysts comprise soluble mononuclear metal complexes and exhibit high selectivity[81]. However, the only homogeneous processes presently of major industrial significance are olefin hydroformylation[82], methanol carbonylation[83], and butadiene hydrocyanation[84]. Although anchoring of metal complexes on solid supports is believed to bridge the gap between conventional homogeneous and heterogeneous catalysts, the new hybrid catalysts have not yet found industrial application, because of problems associated with catalyst stability[45].

Supported metals and transition metal complexes on solid supports constitute the limits of a hierarchy defined by the degree of metal aggregation[85]. Supported metal clusters, a new class of materials, possess an intermediate position. Since small metal particles are normally more efficient catalysts, the use of supported metal clusters offers a new dimension to the preparation of highly dispersed heterogeneous catalysts. A subclass of metal clusters that has received considerable attention in the preparation of supported metallic particles is metal carbonyls. This route allows for the preparation of highly dispersed metal particles on both organic[86] and inorganic supports[87]. Metal clusters might also serve as potential precursors for the synthesis of supported metal oxides[88]. They can offer the following differences/advantages over conventionally prepared supported metal catalysts[78]:

1. Non-aqueous solvents can be used in catalyst preparation, since metal clusters are soluble in organic media.

2. The reduction by hydrogen at high temperatures can be avoided, for metal clusters comprise metal atoms formally in a zerovalent state.

3. A halide free-route to supported catalysts is usually advantageous, since halide atoms can reduce catalytic activity by poisoning the active

sites and they might be responsible for sintering of the catalyst.

4. Heteronuclear clusters of certain stoichiometry are known and they may be used for the preparation of alloys of well defined stoichiometry and composition.

The two major methods commonly employed for heterogenizing transition metal complexes are also used for immobilization of metal cluster compounds.

The first preparative route involves impregnation of the support with a solution of the cluster carbonyl compound followed by either partial or complete removal of CO molecules under various reaction conditions. The main problem associated with this method is that considerable aggregation may occur during ligand removal, leading to a pocrly dispersed metal.

An alternative approach, resulting in actual supported clusters, uses chemically modified supports such as phosphine functionalized polymers and silica. The anchoring of the carbonyl complex is realized through a chemical bond between the cluster and the functionalized support. Methods such as ion exchange of the cluster compound or a precursor into the cavities of zeolites and metal vapour deposition have also been employed[89,90].

Infrared spectroscopy has been used extensively in characterizing physically supported and chemically bound metal cluster carbonyls. The supported metal clusters are usually identified by comparison of their infrared spectra in the carbonyl stretching region with those of their molecular analogs. Although it is a very powerful technique, providing structural information as well as the extent of ligand substitution[91], it is the rule in surface analysis to use more than one method. Thus, several spectroscopic techniques, including Raman, EXAFS, NMR, ESR, and Mossbauer, have also been employed.

2. Anchored Metal Carbonyls on Functionalized Polymers

The main route in supporting metal cluster carbonyls on organic polymers involves ligand exchange between the cluster compound and the functionalized support. Cluster carbonyl complexes are known to undergo facile ligand exchange with phosphines.

Phosphine groups, the most common ligand used to attach metal complexes to polymers, can be introduced into the polymeric structure through different courses (Figure 2). The first involves reaction of the halogenated polymer with $LiPPh_2$[92]. An alternate approach, leading to the same product, involves treatment of the halogenated polymer with butyllithium, followed by reaction with $ClPPh_2$[93]. A similar functionalized polymer can be formed by chloromethylating the polymer first with CH_3OCH_2Cl in the presence of $SnCl_4$ and then treating it with $LiPPh_2$[93].

Instead of functionalizing the polymer by first halogenating it and then transforming it to the phosphine analog, one can copolymerize styrene and divinylbenzene with the appropriate monomer to produce block copolymers. This product can be used for immobilization of highly substituted cluster compounds, while random copolymers lead to monosubstituted clusters[85].

An alternate route uses copolymerization of cluster bound monomer with another monomer. However, several technical problems, such as reaction of the cluster with the polymerization initiator or differences in reactivity between the different monomers, make this route less attractive.

In order to be useful as a support an organic polymer should possess properties such as good mechanical and thermal stability, limited solubility and inertness in the reaction medium, and readily accessible attachment sites. The intrinsic nature of the polymer, and to a lesser degree its structure and the extent of cross-linking, are the factors governing thermal and

Figure 2: Preparation methods for phosphine-functionalized poly(styrene-divinylbenzene).

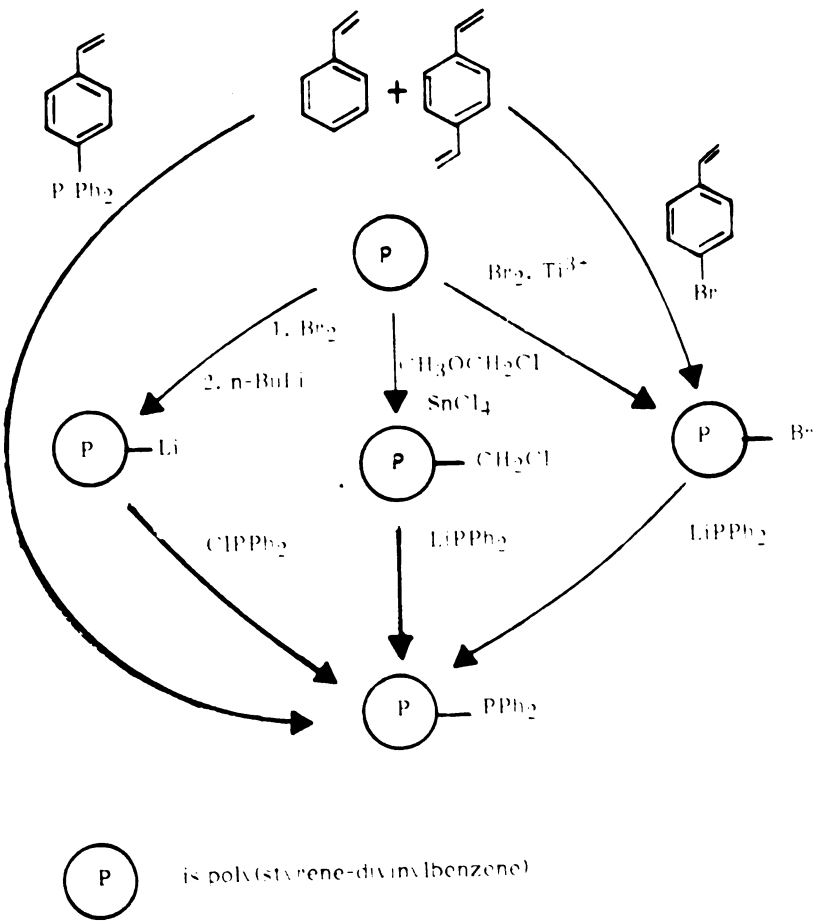

P is poly(styrene-divinylbenzene)

B.C. Gates and J. Lieto, Chemtech, 248 (1980).

mechanical stability.

Numerous literature reports describe synthetic methods that lead to polymer-supported metal cluster carbonyls. A summary of polymer-immobilized cluster carbonyl compounds of Ru, Os, and Ir pertinent to this work is given in Table 2.

3. Immobilized Metal Carbonyls on Inorganic Supports

Inorganic supports exhibit good thermal and mechanical stability because of their rigid structure and appear to be superior alternatives to organic polymers. The latter typically have an upper thermal stability limit around 150°C that overwhelms other advantages such as ease of functionalization and spectroscopic characterization. On the other hand, the limit of inorganic-supported cluster compounds greatly depends on the thermal stability of the complex itself. In fact, it has been reported that the thermal stability of a complex is enhanced as a result of the anchoring process[94].

The main route to functionalize an inorganic oxide involves reaction between surface hydroxyl groups and a readily hydrolyzable moiety[95-97].

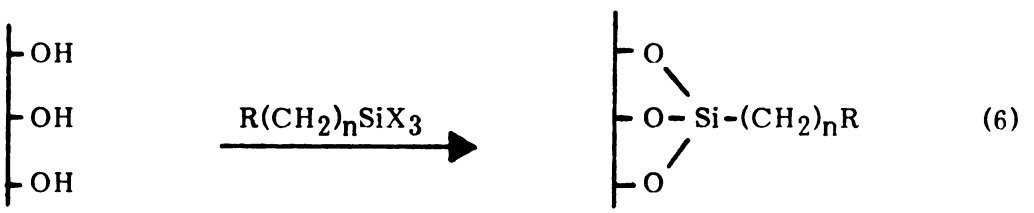

(6)

n = 0,1,2...

R: an organofunctional group, e.g.,

PPh_2, NH_2, C_5H_5

X: a hydrolyzable group, e.g.,

Cl, NH_2, OR, OCOR

Table 2

Polymer-Immobilized Cluster Carbonyls of Ru, Os, and Ir*

Initial Carbonyl	Support	Proposed Structure	Catalytic Reaction	Ref.
$H_4Ru_4(CO)_{12}$	phosphinated polystyrene	$H_4Ru_4(CO)_{11}(Ph_2P\text{-}Ⓟ)$ $H_4Ru_4(CO)_9(Ph_2P\text{-}Ⓟ)_3$ $H_4Ru_4(CO)_8(Ph_2P\text{-}Ⓟ)_4$	ethylene hydrogenation	104
$Ru_3(CO)_{12}$	poly(2-vinyl-pyridine)		hydroformylation	105
$Ru_3(CO)_{12}$	poly(acrylic acid)		1-pentene isomerization hydrogenation	106
$H_2Os_3(CO)_{10}$	phosphinated polystyrene	$H_2Os_3(CO)_{9,10}(Ph_2P\text{-}Ⓟ)$	olefin isomerization	107,108
$Ir(CO)_2$(P-toluidine)Cl	phosphinated polystyrene	$Ir_4(CO)_{11}(Ph_2P\text{-}Ⓟ)$ $Ir_4(CO)_{10}(Ph_2P\text{-}Ⓟ)_2$ $Ir_4(CO)_9(PPh_3)_{3-y}(Ph_2P\text{-}Ⓟ)_y$	ethylene cyclohexene hydrogenation	109

Ⓟ is polystyrene-divinylbenzene
* Partly taken from Ref. 54

This appears to be the most advantageous method because **1)** it involves a simple one-step reaction easy to perform under mild conditions; **2)** a number of $RSiX_3$ compounds can be used; and **3)** it affords a hydrolytically and thermally stable Si-C bond.

As with organic polymers, phosphine groups are the most common ligand used to attach metal cluster carbonyls to functionalized inorganic oxides. The process of immobilization involves again ligand exchange between the cluster and the support.

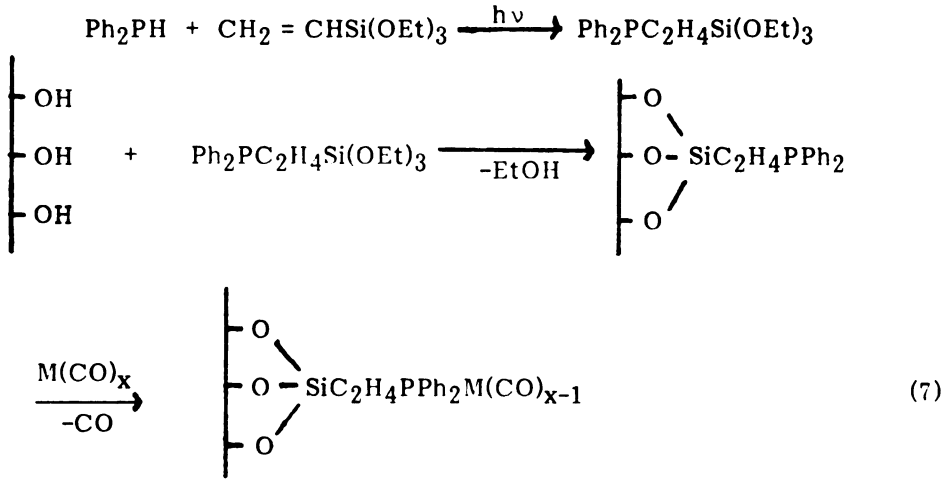

(7)

A slightly different method, leading to the same surface structure, involves first the reaction of the metal cluster with the phosphine-silane ligand, followed by reaction with surface hydroxyl groups.

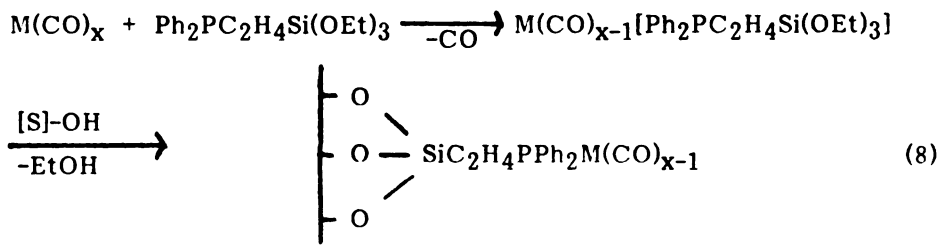

(8)

Anchoring a metal complex to an inorganic oxide through a pendant ligand normally leads to systems capable of catalyzing reactions under mild conditions. However, their use as catalysts under severe reaction conditions or catalyst precursors for the preparation of highly dispersed metal atoms is prohibited due to instability and decomposition of the organic ligand at elevated temperatures. Recent studies describe the preparation of supported metal clusters with well defined structures through direct interaction with surface -OH groups[54,75]. Several spectroscopic techniques have been used to characterize these supported clusters with unique structures and in a few cases they have been extracted from the surface by using ion-exchange methods[98,99]. It is believed that this development, besides being a route to the preparation of highly dispersed supported metals, will provide an insight into the relations between structure and catalytic activity.

A summary of supported cluster carbonyl compounds of Ru, Os, and Ir on inorganic oxides is given in Table 3.

E. Research Objectives

Smectite clays, having an ordered layer structure, provide certain advantages over amorphous metal oxides as complex supports[7]. The ability to control interlayer swelling by changing the polarity of the swelling solvent offers the possibility of inducing size or shape selectivity for catalytic reactions taking place in the interlayer region of the mineral[100]. Moreover, the capability of the interlamellar space to play an active and often constructive role in catalytic reactions[101] justifies the interest in investigating and using clay minerals as homogeneous catalyst supports.

Metal carbonyl cluster complexes represent a potentially important class of compounds for intercalation in layer silicates, because they may

Table 3

Selected Studies of Immobilized Cluster Carbonyls of Ru, Os and Ir on Inorganic Supports[a]

Initial Carbonyl	Support	Proposed Structure	Catalytic Reaction	Ref.
$Ru_3(CO)_{12}$	HY zeolite	$Ru_3(CO)_9$ ads		110
$Ru_3(CO)_{12}$	NaY zeolite SiO_2 Al_2O_3			111
$Ru_3(CO)_{12}$	γ-Al_2O_3		H_2 reduction of CO	112
$Ru_3(CO)_{12}$	SiO_2	$Ru_3(CO)_x$ ads	butene hydrogenation	113
$Ru_3(CO)_{12}$	n-Al_2O_3 SiO_2 MgO		hydrocarbon formation during decomposition	114
$Ru_3(CO)_{12}$ $H_4Ru_4(CO)_{12}$ $Ru_6C(CO)_{17}$	γ-Al_2O_3 SiO_2			115
$Ru_3(CO)_{12}$	SiO_2	$HRu_3(CO)_{10}$(O-Si≡)		116

Table 3 continued

$Ru_3(CO)_{12}$	SiO_2 TiO_2 Al_2O_3	$HRu_3(CO)_{10}$(O-Si)		117
$Ru_3(CO)_9L_3$[b]	SiO_2	$Ru_3(CO)_9(Ph_2P\text{-SIL})_3$[c]	olefin photoisomerization	118
$H_4Ru_4(CO)_8L_4$	SiO_2	$H_4Ru_4(CO)_8(Ph_2P\text{-SIL})_4$	ethylene hydrogenation	119
$H_2Os_3(CO)_{10}$	phosphinated SiO_2	$H_2Os_3(CO)_{9,10}(Ph_2P\text{-SIL})$	olefin isomerization ethylene hydrogenation	107,120
$Os_3(CO)_{11}L$	SiO_2	$Os_3(CO)_{11}(Ph_2P\text{-SIL})$	ethylene hydrogenation	120
$H_2Os_3(CO)_{10}L$	SiO_2	$H_2Os_3(CO)_{10}(Ph_2P\text{-SIL})$		121
$Os_3(CO)_{12}$	$\gamma\text{-}Al_2O_3$		hydrocarbon formation during decomposition	122
$Os_3(CO)_{12}$	SiO_2		H_2 reduction of CO	112
$Os_3(CO)_{12}$ $Os_6(CO)_{18}$	$n\text{-}Al_2O_3$		hydrocarbon formation during decomposition	114

Table 3 continued

$Os_3(CO)_{12}$	γ-Al_2O_3			123
$Os_3(CO)_{12}$	SiO_2 γ-Al_2O_3 TiO_2 ZnO	$HOs_3(CO)_{10}$(O-M)		124
$Os_3(CO)_{12}$	SiO_2	$HOs_3(CO)_{10}$(O-Si≡)	1-butene isomerization	125
$Os_3(CO)_{12}$	γ-Al_2O_3	$HOs_3(CO)_{10}$(O-Al≺)	1-hexene isomerization	126
$Os_3(CO)_{12}$ $H_2Os_3(CO)_{10}$ $Os_6(CO)_{18}$	SiO_2 n-Al_2O_3	$HOs_3(CO)_{10}$(O-M≺)	hydrocarbon formation during decomposition	127
$Os_3(CO)_{12}$	Al_2O_3	$HOs_3(CO)_{10}$(O-Al≺)		128
$Ir(CO)_2$(p-toluidine)Cl	phosphinated SiO_2	$Ir_4(CO)_{11}(Ph_2P\text{-SIL})$ $Ir_4(CO)_{10}(PPh_3)(Ph_2P\text{-SIL})$ $Ir_4(CO)_9(PPh_3)_2(Ph_2P\text{-SIL})$	ethylene hydrogenation	129
$Ir_4(CO)_{12}$	γ-Al_2O_3		hydrocarbon formation during decomposition	122

Table 3 continued

$Ir_4(CO)_{12}$	γ-Al_2O_3	>>	112
$Ir_4(CO)_{12}$	n-Al_2O_3	>>	114
$Ir_4(CO)_{12}$	γ-Al_2O_3 SiO_2	alkane hydrogenolysis	130
$Ir_4(CO)_{12}$	ZnO	H_2 reduction of CO	131
$Ir_4(CO)_{12}$	γ-Al_2O_3 SiO_2		132,133
$Ir_4(CO)_{12}$	SiO_2 γ-Al_2O_3		134
$Ir_4(CO)_{12}$	γ-Al_2O_3		123

a Abstracted in part from reference 54.

b L is $Ph_2PC_2H_4Si(OEt)_3$

c SIL is silica

exhibit interesting catalytic properties in their own right, or they may serve as precursors for the formation of atomically dispersed metal centers, as discussed earlier (vide supra). However, the known methods of immobilizing metal carbonyls on organic polymers or inorganic oxides are not suitable for intercalation of metal complexes in clays. Typically, the immobilization of metal complexes in smectites requires positively charged species capable of electrostatic binding to the negatively charged silicate layers.

The main objective of this study was to explore different approaches that would lead to intercalated metal cluster carbonyl complexes in clays. It appears that a net positive charge and solvolytic stability are the major requirements for a prospective candidate for intercalation in clay. On the other hand, size and/or shape of the intercalant play a relatively unimportant role, because even very large molecules such as enzymes can be accommodated in the silicate interlayer. This qualifies clays over zeolites, which are limited to intracrystalline immobilization of small molecules, because most of the pore openings are small (< 10 Å). However, the task of finding cationic cluster carbonyls capable of electrostatic binding is not so easy. Though there is an abundance of neutral or anionic cluster compounds, the number of positively charged species is small.

The first part of this work examines the reaction of the protonated metal carbonyl cluster $HOs_3(CO)_{12}^+$ with Na^+-hectorite. Remarkably, the binding of the cationic cluster leads to a preferential dispersal of $Os_3(CO)_{12}$ centers at the hydroxylated edge sites of the silicate layers rather than at the more abundant basal surfaces. This observation prompted further study of the interaction of neutral $Os_3(CO)_{12}$ cluster not only with natural Na^+-hectorite but also with fluorohectorite and laponite, synthetic hectorites with different layer-charge and morphology.

It became evident at this point that preparation of genuine intercalated metal carbonyl clusters in clays required an alternative approach. Pinnavaia and co-workers demonstrated that the phosphonium-phosphine ligand $Ph_2PCH_2CH_2\overset{+}{P}Ph_2CH_2Ph$ (abbreviated $P\text{-}P^+$) could be used for the transformation of well known, otherwise neutral, homogeneous rhodium catalysts to their cationic analogs, making them suitable for intercalation in clay minerals[102,103]. This earlier work, along with the known property of cluster carbonyl complexes to undergo substitution reactions with phosphine ligands, provided the rationale for the use of $P\text{-}P^+$ as a means of inducing positive charge on the cluster compounds. Thus, the second part of this dissertation describes the synthesis and intercalation of $Ru_3(CO)_9(P\text{-}P^+)_3$, $H_4Ru_4(CO)_8(P\text{-}P^+)_4$, $Ir_4(CO)_9(P\text{-}P^+)_3$, $Os_3(CO)_{11}(P\text{-}P^+)$, and $H_2Os_3(CO)_{9,10}(P\text{-}P^+)$ in hectorite.

Polyoxocation pillared clays constitute a new class of highly stable materials characterized by fixed porosity, high surface area, and intracrystal acidity. The pillaring reaction involves interaction of the negatively charged silicate layers with oligomeric cationic species and dehydroxylation at elevated temperatures to form small oxide aggregates which are stable in the interlamellar region. The recent advances in the area of direct immobilization of cluster carbonyls on inorganic oxides led us to investigate the interactions of carbonyl complexes with the aluminum oxide aggregates formed in the interlayer of smectites. Thus, the last part of this work examines the reaction of $Os_3(CO)_{12}$, $Ru_3(CO)_{12}$, $H_4Ru_4(CO)_{12}$, $H_2Os_3(CO)_{10}$, $Ir_4(CO)_{12}$, and $[CpFe(CO)_2]_2$ with alumina pillared clay.

CHAPTER II

EXPERIMENTAL

A. Materials

1. Natural Hectorite

Natural sodium hectorite with an idealized unit cell formula of $Na_{0.67}[Mg_{5.33}Li_{0.67}](Si_{8.00})O_{20}(OH,F)_4$ was obtained from the Baroid Division of National Lead Co. or the Source Clay Mineral Repository, University of Missouri, in the pre-centrifuged and spray dried form. The mineral was allowed to sediment 24 h as a 1 wt% aqueous slurry to remove dense impurities, saturated with Na^+ by reaction with excess aqueous NaCl, washed free of chloride by dialysis, and then freeze-dried.

2. Sodium Montmorillonite (Wyoming)

Na^+-montmorillonite with an idealized unit cell composition of $Na_{0.67}[Al_{3.33}Mg_{0.67}](Si_{8.00})O_{20}(OH)_4$ was obtained from the Source Clay Mineral Repository and was pretreated similarly to natural hectorite (vide supra).

The cation exchange capacity for hectorite and montmorillonite is 70 and 83 meq/100 g respectively.

3. Laponite®

This synthetic hectorite with a structural formula of

$Na_{0.22}Li_{0.14}[Mg_{5.64}Li_{0.36}](Si_{8.00})O_{20}(OH)_4$ was obtained in powder form from Laporte Company and used without further purification. The particle size of this mineral is approximately 10 Å thick with an average diameter of 200 Å and its cation exchange capacity is 55 meq/100 g.

4. Fluorohectorite

This clay is also a synthetic hectorite in which the octahedral lattice hydroxyl groups have been replaced with fluoride ions. It has a unit cell formula $Li_{1.6}[Mg_{4.4}Li_{1.6}](Si_{8.00})O_{20}(F)_4$. The mineral with particle size >> 2μ and cation exchange capacity of 190 meq/100 g was donated as an aqueous suspension by Corning Glass Works.

5. Solvents

All solvents used in syntheses and isomerization studies were reagent grade; spectrograde solvents were used for IR, UV-visible, and NMR spectroscopy. The solvents were deoxygenated by standard freeze-vacuum-thaw cycles.

6. Reagents

$Os_3(CO)_{12}$, $Ru_3(CO)_{12}$, $H_4Ru_4(CO)_{12}$, $Ir_4(CO)_{12}$ and $[CpFe(CO)_2]_2$ were purchased from Strem Chemicals Incorporated and used as received. Trimethylamine oxide dihydrate ($Me_3NO{\cdot}2H_2O$) and ammonium hexafluorophosphate were obtained from Aldrich Chemical Company and used without further purification. 1-hexene was purchased from Aldrich Chemical Company and was freshly distilled over activated alumina under an argon atmosphere prior to use as a substrate. Triphenylphosphine and benzylbromide were also obtained from Aldrich Chemical Company, while bis(1,2-diphenylphosphino)ethane was obtained from Pressure Chemical Company. Potassium hexafluorophosphate and sodium tetrafluoroborate were purchased from Alfa-Products-Ventron. Dowex (AG2-X8) anion exchange

resin, Cl-form, 50-100 mesh, was a gift from Dow Chemical Company.

B. Syntheses

All reactions were carried out under an inert atmosphere either in a nitrogen-filled glove box or on a vacuum line. Once the crystalline materials were synthesized, subsequent handling was conducted in the open atmosphere.

1. $H_2Os_3(CO)_{10}$

The hydrido-triosmium cluster was prepared by passing hydrogen gas through a solution of $Os_3(CO)_{12}$ (600 mg, 0.661 mmol) in refluxing octane (120 ml) for 2 h, according to the method of Kaesz et al.[66]. The solution was concentrated and chromatographed on silica gel with hexane as eluant. The deep purple band of $H_2Os_3(CO)_{10}$ was followed by a small band attributed to unreacted $Os_3(CO)_{12}$. IR ν(CO)(CH_2Cl_2) 2121 vw, 2076 s, 2063 s, 2025 vs, 2010 s, 1989 m cm^{-1}. ^1H NMR ($CDCl_3$) -11.49. λ_{max} 560, 339 nm.

2. $H_2Os_3(CO)_{10}(PPh_3)$

This compound was obtained by reaction of $H_2Os_3(CO)_{10}$ and triphenylphosphine by the procedure of Deeming and Hasso[67]. IR ν(CO)(CH_2Cl_2) 2100 m, 2060 s, 2042 s, 2018 vs, 1998 sh, 1976 m, 1962 m cm^{-1}.

3. $H_2Os_3(CO)_9(PPh_3)$

Pyrolysis of $H_2Os_3(CO)_{10}(PPh_3)$ in refluxing hexane for 1 h and layer chromatography afforded pure $H_2Os_3(CO)_9(PPh_3)$[67]. IR ν (CO)(CH_2Cl_2) 2090 m, 2052 s, 2005 vs, 1990 m, 1972 m, 1954 m cm^{-1}.

4. $[HOs_3(CO)_{12}](PF_6)$

This complex was prepared by adding concentrated (98%) sulfuric acid to osmium carbonyl, according to a method by Knight and Mays[65]. The solution was cooled to -30°C and added dropwise to a cold concentrated

aqueous solution of ammonium hexafluorophosphate. The precipitate was collected on a frit and washed quickly with the minimum amount of water. IR ν(CO)($MeNO_2$) 2134 s, 2102 s, 2077 vs, 2058 s, 2018 m cm^{-1}. λ_{max} (CH_3COCH_3) 366 nm.

5. $[HRu_3(CO)_{12}](PF_6)$

The preparatory procedure for this compound was similar to that of the osmium analog, described previously[65]. IR ν(CO)($MeNO_2$) 2128 s, 2100 s, 2077 vs, 2062 s, 2025 m cm^{-1}. λ_{max} (CH_3COCH_3) 403 nm.

6. $PH_2PCH_2CH_2PPh_2CH_2PhBr$

The bromide salt of the phosphonium-phosphine ligand was prepared by the reaction of bis(1,2-diphenylphosphino)ethane and benzyl bromide in toluene, according to known procedures[102,135]. The white crystals melt at 245-247°C.

7. BF_4^--Resin

The tetrafluoroborate form of (AG2-X8) Dowex anion exchange resin was prepared according to a method described by Quayle and Pinnavaia[102].

8. $(Ph_2PCH_2{}^1CH_2{}^2PPh_2CH_2{}^3Ph)(BF_4)$

The tetrafluoroborate form of $P\text{-}P^+$ was prepared by a method described previously[102]. In a nitrogen-filled glove box BF_4^--resin (31 g, 100 meq) was added to the methanol solution obtained from the preparation of $P\text{-}P^+Br$ (Section II.B.6). The slurry was stirred for 4 h and filtered. Fresh BF_4^--resin (31 g) was added to the filtrate and the procedure was repeated two more times. The solvent was removed under vacuum and the resulting white needle-like crystals were collected on a frit and washed with toluene. M.P. 188-189°C. ^1H NMR ($CDCl_3$) δH^1 2.55 m. δH^2 1.97 m, δH^3 4.26 d, J_{H3P^+} = 14.6 Hz.

9. $[Ru_3(CO)_9(P\text{-}P^+)_3](BF_4)_3$

$Ru_3(CO)_{12}$ (200 mg, 0.313 mmol) and $(P\text{-}P^+)BF_4$ (542 mg, 0.939 mmol) was refluxed in 100 ml MeOH for 6 h, in a manner analogous to a method by Piacenti et al.[136] for the preparation of $Ru_3(CO)_9(PPh_3)_3$. The solvent was evaporated under vacuum and the residue was washed with hexane to remove unreacted $Ru_3(CO)_{12}$. The residue was then treated with a minimum amount of acetone to dissolve the $[Ru_3(CO)_9(P\text{-}P^+)_3](BF_4)_3$ reaction product and the unreacted $P\text{-}P^+$ ligand was removed by filtration. Evaporation of the acetone solution afforded the pure compound. IR ν (CO)(CH_2Cl_2) 2048 m, 1980 s, 1962 s cm^{-1}. λ_{max} (CH_2Cl_2) 489, 362 sh nm.

10. $[Os_3(CO)_{11}(P\text{-}P^+)](BF_4)$

This compound was prepared by reaction of stoichiometric amounts of $Os_3(CO)_{11}(CH_3CN)$[137] (0.15 g, 0.163 mmol) and $(P\text{-}P^+)BF_4$ (94 mg, 0.163 mmol) in 30 ml $CHCl_3$ at 25°. The resulting precipitate was filtered, washed with a minimum amount of chloroform, and vacuum dried. IR ν (CO)(CH_2Cl_2) 2100 m, 2048 s, 2028 s, 2010 vs, 1998 sh, 1983 m, 1976 m cm^{-1}. λ_{max} (CH_2Cl_2) 407, 323 nm.

11. $[Ir_4(CO)_9(P\text{-}P^+)_3](BF_4)_3$

In a method analogous to that of Stuntz[71] for the preparation of $Ir_4(CO)_{12-x}L_x$ type complexes, solid $Ir_4(CO)_{12}$ (300 mg, 0.272 mmol) was added to refluxing THF (500 ml). To this solution $(P\text{-}P^+)BF_4$ (471 mg, 0.816 mmol) and solid $Me_3NO{\cdot}2H_2O$ (91 mg, 0.816 mmol) was added and heated at reflux for 10 min. After cooling the solvent was removed under vacuum and the product was taken up in a minimum amount of acetone. The unreacted $Ir_4(CO)_{12}$ and excess ligand remained undissolved and was removed by filtration. IR ν(CO)(CH_2Cl_2) 2039 m, 1995 sh, 1984 s, 1965 sh, 1832 vw, 1779 s cm^{-1}. λ_{max} (CH_2Cl_2) 383 sh, 301 nm.

12. $[H_4Ru_4(CO)_8(P\text{-}P^+)_4](BF_4)_4$

To a solution of $H_4Ru_4(CO)_{12}$ (200 mg, 0.269 mmol) in 100 ml $CHCl_3$ solid $Me_3NO{\cdot}2H_2O$ (119 mg, 0.108 mmol) and $(P\text{-}P^+)BF_4$ (620 mg, 0.108 mol) was added. After stirring overnight the solution became cloudy. Reducing the volume by half under vacuum and cooling gave $[H_4Ru_4(CO)_8(P\text{-}P^+)_4](BF_4)_4$ as a precipitate. Filtering the solution and washing the residue with $CHCl_3$ afforded a pure compound. IR $\nu(CO)(CH_2Cl_2)$ 2005 s, 1971 m, 1948 s cm^{-1}. λ_{max} (CH_2Cl_2) 404, 309 sh nm. ^1H NMR (d^6DMSO) $\delta(\mu\text{-}H)$ -16.50 quintet, $J_{P\text{-}H}$ = 7.0 Hz.

13. $[H_2Os_3(CO)_{10}(Ph_2PCH_2{}^1CH_2{}^2PPh_2CH_2{}^3Ph)](BF_4)$

To a solution of $H_2Os_3(CO)_{10}$ (100 mg, 0.117 mol) in $CHCl_3$ (25 ml) a stoichiometric amount of $(P\text{-}P^+)BF_4$ (68 mg, 0.117 mmol) was added according to a method reported by Deeming and Hasso[67] for the preparation of $H_2Os_3(CO)_{10}(PPh_3)$. The precipitate which formed after stirring for 1/2 h was collected on a frit, washed with $CHCl_3$, and vacuum dried. IR $\nu(CO)(CH_2Cl_2)$ 2100 m, 2060 s, 2042 s, 2018 vs, 1990 sh, 1976 m, 1960 m cm^{-1}. λ_{max} (CH_2Cl_2) 385, 331 nm. ^1H NMR ($CDCl_3$) (27°C) δH^1 2.94 m, δH^2 2.41 m, δH^3 4.42 d, J_{H3P^+} = 13.59 Hz; (-61°C) δ(H-Os) - 10.36 s, $\delta(\mu\text{-}H)$ -20.48 m. Anal. Calcd. for $C_{43}H_{33}BF_4P_2Os_3$: C, 36.06; H, 2.31; P, 4.32; Found: C, 35.69; H, 2.36; P, 3.29.

14. $[H_2Os_3(CO)_9(Ph_2PCH_2{}^1CH_2{}^2PPh_2CH_2{}^3Ph)](BF_4)$

A solution of $[H_2Os_3(CO)_{10}(P\text{-}P^+)](BF_4)$ (100 mg, 0.07 mmol) was refluxed in methanol (35 ml) under Ar for 2 h during which time the color changed from yellow to deep green. Removal of the solvent under vacuum and recrystallization from CH_2Cl_2-hexane afforded $[H_2Os_3(CO)_9(P\text{-}P^+)](BF_4)$ in the form of shiny flakes. IR $\nu(CO)(CH_2Cl_2)$ 2090 m, 2050 s, 2001 vs, 1989 s, 1948 m cm^{-1}. ^1H NMR ($CDCl_3$) δH^1 2.96 m, δH^2 2.43 m, δH^3

4.48 d, J_{H3P^+} = 14.26 Hz, δ(μ-H) -11.06 d, J_{HP} = 7.25 Hz. λ_{max} (CH_2Cl_2) 359, 304 nm.

C. Clay-Cluster Reactions

1. Reaction of Clay with $HM_3(CO)_{12}^+$ or $M_3(CO)_{12}$ (M=Os,Ru)

Na^+-hectorite (0.10 g, 0.070 meq) in 10 ml water was added with stirring to 0.007 mmol of $HM_3(CO)_{12}^+$ or $M_3(CO)_{12}$ dissolved in the minimum amount of acetone. After a reaction time of 10 min, the slurry was poured onto a polyethylene sheet and allowed to dry in air. The dried, self-supporting clay film was then removed from the polyethylene sheet and used for IR measurements. For some experiments the clay sample was freeze-dried instead of being dried in air.

2. Intercalation of Phosphine Substituted Cluster Carbonyls on Na^+-hectorite

In a typical experiment 0.1 g (0.070 meq) Na^+-hectorite in 10 ml water was added to a vigorously stirred acetone solution of the appropriate complex (0.070 meq). After a reaction time of 10 min, the mineral was collected by centrifugation, washed several times with acetone to remove physically adsorbed cluster molecules, and air-dried.

3. $H_2Os_3(CO)_9(P\text{-}P^+)$-hectorite

Decarbonylation of $H_2Os_3(CO)_{10}$-hectorite was achieved by heating the exchanged mineral at 80°C under vacuum for 2 h. IR ν(CO) (KBr) 2092 m, 2052 s, 2000 vs, 1978 s, 1950 sh cm^{-1}. λ_{max} (mull) 362, 315 nm.

4. $HOs_3(CO)_9(CH{=}CH_2)(P\text{-}P^+)$-hectorite

$H_2Os_3(CO)_9(P\text{-}P^+)$-hectorite (50 mg) was suspended in 50 ml acetone and acetylene gas, passed first through a trap at -78°C, was bubbled gently into the suspension at ambient temperature and pressure for 2 h. During

this time the color of the mineral changed from green to bright yellow. The solvent was drawn off and the clay was washed with acetone, dried, and characterized by infrared spectroscopy. IR ν(CO)(KBr) 2090 m, 2042 s, 1999 vs, 1962 sh cm^{-1}.

5. Alumina Pillared Clay (ALPILC)

The clay was prepared by reaction of natural Na^+-montmorillonite (Crook County, Wyoming) with an aluminum chlorohydrate solution, chlorohydrol® (Reheis Chemical Company), according to a previously described method[39]. The product was air-dried and then calcined at 350°C under Ar for 2 h. The unit cell composition, determined by plasma emission spectroscopy, is

$$[Al(OH)_{2.80}]_{2.87}[Al_{3.11}Fe_{0.42}Mg_{0.48}](Si_{7.92}Al_{0.08})O_{20}(OH)_4$$

and the N_2 BET surface area is approximately 300 m^2/g.

6. Reaction of ALPILC with $M_3(CO)_{12}$ (M=Os, Ru)

ALPILC (0.5 g) was degassed at 25°C under vacuum for 4 h and a solution of the metal cluster (0.020 mmol) dissolved in CH_2Cl_2 (35 ml) was added. The resulting slurry was stirred under Ar for 20 h at ambient temperature and pressure and then transferred to a nitrogen-filled glove box. The clay was collected on a frit, washed with CH_2Cl_2 to remove unreacted, weakly adsorbed cluster molecules and vacuum-dried.

7. Extraction of $HM_3(CO)_{12}^+$ Clusters From the Clay

The neutral cluster carbonyl was first reacted with the mineral and the portion which was not chemisorbed was removed by washing with CH_2Cl_2. The mineral was then treated with a solution of KPF_6 in acetone. After three successive washings the filtrates were combined and evaporated to dryness under vacuum.

8. Wet Impregnation of Clays with Neutral Clusters

A solution in CH_2Cl_2 containing an amount (0.007 mmol) of neutral cluster complex ($Os_3(CO)_{12}$, $Ru_3(CO)_{12}$, etc.) was added to the clay sample (0.1 g) and the mixture was stirred under Ar for a few hours. The solvent was then removed under vacuum and the mineral was stored under an inert atmosphere before further treatment.

9. Powder Pyrolysis Experiments

A powder clay sample or a self-supporting film was placed in a quartz tube fitted with two joints and stopcocks. The sample was pyrolyzed by using an external heating coil either while being pumped dynamically at approxiamtely 0.1 torr or while a stream of Ar gas was blowing over the sample.

10. Catalytic Reactions

$H_2Os_3(CO)_9(P\text{-}P^+)$-hectorite (30 mg, 0.010 mmol) was suspended in 5 ml of the appropriate solvent in a 15 x 150 mm pyrex culture tube fitted with a Teflon-linen screw cap and magnetic stir bar. To this suspension freshly distilled 1-hexene (1-3.5 ml, 0.008-0.028 mol) was added. The mixture was stirred either at ambient temperature and pressure or the tubes were immersed in an oil bath whose temperature was controlled (Parr Instrument Company, Model 4831 controller attached to an Iron-Constantan thermocouple). Catalytic activity was determined by withdrawing periodically a fraction of the reaction solution and analyzing the products by gas chromatography.

D. Physical Measurements

1. Infrared Spectroscopy

Infrared spectra were recorded on a Perkin-Elmer 283B or 475 model

grating spectrophotometer. Solution spectra were obtained by using 0.1 mm NaCl cells. Spectra of various clay intercalates were recorded by either mixing the samples with KBr and pressing them into a disk or using self-supporting films. These films were prepared by allowing an aqueous suspension of the mineral to evaporate on a polyethylene sheet. In some cases the spectrum was recorded by using mineral oil mulls placed between CsI disks. Samples of air or water sensitive intercalates were prepared in a nitrogen-filled glove box just prior to scanning to minimize decomposition.

2. X-ray Diffraction Studies

X-ray 00ℓ basal spacings were determined for oriented film samples either with a Siemens Crystalloflex-4 or a Philips X-ray diffractometer by using Ni-filtered Cu-K_α radiation (λ (K_α) = 1.5405 Å). The oriented film samples were prepared by evaporating an aqueous suspension of the mineral on a microscope slide. The diffraction was normally monitored over a range of $2° < 2\theta < 15°$. Peak positions, measured in degrees 2θ, were converted to interplanar d-spacings by using a standard chart.

3. UV-Visible Spectroscopy

Electronic spectra were obtained with a Varian Associates Cary 17 spectrophotometer. Solution spectra were recorded with matched 1 cm path-length quartz cells. Spectra of clay intercalates were acquired as mineral oil mulls placed between silica disks. To avoid scattering, a sample of the native mineral was put in the reference beam.

4. Proton NMR Spectroscopy

Proton nuclear magnetic resonance spectra were recorded on a Bruker WM-250 MHz spectrometer. Chemical shifts were measured either relative to tetramethylsilane as an internal standard or relative to the standard shift of the deuterated solvent and are reported in δ units.

5. Gas Chromatography

Gas phase chromatography of catalytic reaction products was performed either with a Varian Associates Model 920 GC equipped with a thermal conductivity detector or with a Hewlett-Packard model 5880 A GC supplied with a flame ionization detector. The columns were a 10 ft x 1/8 in. 10% UCW on 80-100 mesh chromosorb W and a capillary 12.5 m x 0.2 mm crosslinked dimethylsilicone. The reaction products were characterized by comparison of their retention times with chemically pure authentic samples.

6. Melting Points

Melting points were determined on a Thomas-Hocver Model 6406-H capillary melting point apparatus.

7. Elemental Analyses

Chemical analyses were performed by Schwarzkopf Microanalytical Laboratories, Wocdside, NY.

CHAPTER III

RESULTS AND DISCUSSION

A. Surface-Selective Dispersion of Cluster Carbonyls on Layered Silicates

1. Reaction of $HOs_3(CO)_{12}^+$ and $Os_3(CO)_{12}$ with Clays

The reaction of Na^+-hectorite (1.0 meq) in aqueous suspension with $HOs_3(CO)_{12}^+$ (0.10 mmol) in acetone results in a product (I) which contains a bound osmium carbonyl complex. The IR spectrum of I in the terminal CO stretching region is shown in Figure 3, along with the spectra of authentic samples of $[HOs_3(CO)_{12}][PF_6]$(II) and $Os_3(CO)_{12}$ (III). The CO stretching frequencies are provided in Table 4 for each compound; the band positions of electronic spectra are presented in Table 5.

It is apparent from the IR and electronic spectra that the osmium complex in I is immobilized on the clay surface as the neutral cluster $Os_3(CO)_{12}$ and not as the initial cation $HOs_3(CO)_{12}^+$. In addition, the x-ray diffraction pattern of I reveals an 001 spacing of 12.5 Å, a value which corresponds to an interlayer thickness of approximately 2.9 Å and the presence of a monolayer of water. Therefore, the bound $Os_3(CO)_{12}$ is not intercalated, but instead is bound to the external surfaces of the clay. These conclusions also are compatible with the observation that the neutral carbonyl complex is readily desorbed by washing with acetone.

Figure 3: Infrared spectra in the terminal CO stretching region: (I) $Os_3(CO)_{12}$-hectorite prepared from $HOs_3(CO)_{12}^+$ (film); (II) $[HOs_3(CO)_{12}]PF_6$ (KBr pellet); (III) $Os_3(CO)_{12}$ (KBr pellet); (IV) $Os_3(CO)_{12}$-hectorite prepared by impregnation with $Os_3(CO)_{12}$ (film); (V) sample I after heating in air at 150°C for 12 h.

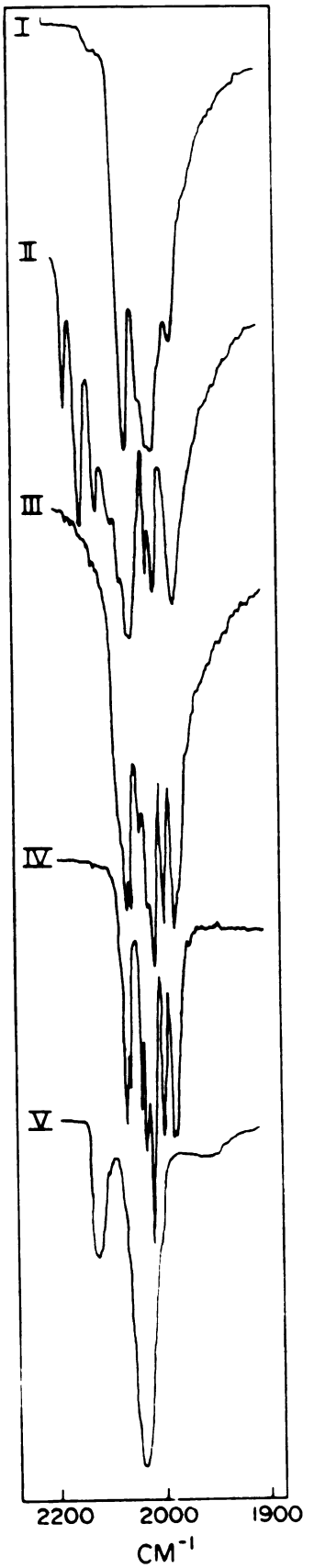
I
II
III
IV
V
2200
2000
1900
CM-1

Table 4

Infrared CO Stretching Frequencies for Reaction Products and Reference Compounds

Sample	Description	Medium	Frequencies, cm^{-1}
I	$[HOs_3(CO)_{12}]^+$ + hectorite reaction product	film	2066s,2060s, 2038m, 2025s,2017s,1997m, 1987m
II	$[HOs_3(CO)_{12}][PF_6]$	KBr	2177m,2148m,2119m, 2084m,2073s,2058vs, 2021s,2009s,1986s
III	$Os_3(CO)_{12}$	KBr	2068s,2060s,2040m, 2027s,2015vs,1998s, 1987s
IV	$Os_3(CO)_{12}$ + hectorite reaction product	film	2066s,2060m,2037m, 2027s,2014vs,1998s, 1986s
V	$[(\equiv SiO)_2Os(CO)_n]_x$-hectorite	film	2123m,2039s,1985m

Table 4 continued

VI	$[HOs_3(CO)_{12}]^+$ + fluorohectorite reaction product	film	2065s,2060s,2037m, 2026s,2014vs,1998m, 1988m
VII	$Os_3(CO)_{12}$ + Na^+-hectorite	mull	2115w,2071m,2055s, 2020vs,2001sh,1940m

Table 5

Electronic Spectroscopy Data for Reaction Products and Reference Compounds

System	Solvent	λ_{max} (nm)
$[HOs_3(CO)_{12}][PF_6]$	Acetone	366
$Os_3(CO)_{12}$	CH_2Cl_2	385,329
$[HOs_3(CO)_{12}]^+$ + hectorite reaction product	film	383,324
$Os_3(CO)_{12}$ + hectorite reaction product	film	387,329

To verify the presence of neutral metal carbonyl cluster in I, we investigated the binding of an authentic sample of $Os_3(CO)_{12}$ to Na^+-hectorite. The neutral carbonyl (0.10 mmol) in acetone solution was mixed at room temperature with a 1 wt% aqueous slurry of hectorite (1.0 meq), and the product was air-dried to form an oriented, self-supporting film. This method of sample preparation is analogous to the impregnation techniques typically used for supporting metal carbonyl clusters on silica and alumina. However, these latter supports, unlike clays, do not form highly oriented films when air dried.

The CO stretching frequencies for the clay-supported $Os_3(CO)_{12}$ prepared by impregnation of $Os_3(CO)_{12}$ (IV) are given in Table 4 and Figure 3. It is seen that the spectrum is similar to, but not identical with, the spectrum observed for the clay product prepared by reaction with $HOs_3(CO)_{12}^+$ (I). Significantly, the bands for I are broader and less resolved than those observed for IV. Also, the relative intensities of the bands differ for the two products. These spectral differences may be due in part to differences in cluster dispersion. For instance, IV exhibits sharp x-ray reflections characteristic of a segregated $Os_3(CO)_{12}$ phase. Phase segregation also is known to occur for metal carbonyls supported on silica and alumina by impregnation methods[123]. In marked contrast to the low degree of cluster dispersion in IV, product I shows no x-ray evidence for a segregated carbonyl phase. Thus we conclude that the supported carbonyl clusters derived from proton dissociation of $HOs_3(CO)_{12}^+$ are highly dispersed with an aggregate size less than 50 Å.

We next consider the type of surface occupied by the dispersed $Os_3(CO)_{12}$ clusters in I. There are two chemically distinct surfaces available for the binding of an adsorbate to a smectite clay particle: edge surfaces and basal

surfaces. As shown in Figure 4, the basal surfaces are composed of siloxane-type oxygen atoms, whereas the edge surfaces are hydroxylated. $Os_3(CO)_{12}$ is known to react with surface hydroxyls of silica and alumina[124,127,128] to give molecular species such as those represented in equation 9 for a silica surface.

$$2(\equiv SiOH) + Os_3(CO)_{12} \xrightarrow{\Delta} [(\equiv SiO)_2Os(CO)_n]_x \qquad (9)$$
$$n = 2,3$$

This reaction provides a chemical means of distinguishing between $Os_3(CO)_{12}$ at edge and basal plane sites. Under conditions where surface migration is slow, as is the case with our oriented film samples (see below), edge-bound clusters should react according to equation 9, whereas clusters adsorbed on basal planes should be stable.

In a typical smectite clay particle composed of a few tens of layers, each 9.6 Å thick and approximately 10^4 Å in diameter, the basal surface area is at least an order of magnitude greater than the edge surface area. In the case of IV, where much of the $Os_3(CO)_{12}$ is segregated as a separated phase, we might expect the cluster to migrate onto the basal surfaces and eventually to edge sites for reaction with hydroxyl groups. For instance, $Os_3(CO)_{12}$ supported on alumina by impregnation reacts according to eq. 9 at 150°C, even though the cluster initially is poorly dispersed at room temperature. However, the highly oriented nature of our clay film samples impedes migration of the metal clusters across the basal planes. Thus we observe no reaction of IV after 12 h at 150°C. The importance of sample orientation in impeding surface migration was demonstrated by impregnating a random, freeze-dried clay sample with $Os_3(CO)_{12}$ and observing reaction

Figure 4: Schematic illustration of the two types of external surfaces for a smectite clay. The edge surfaces are hydroxylated whereas the basal planes contain only siloxane oxygens. Sodium exhcange ions (not shown) occupy mainly the interlayer regions.

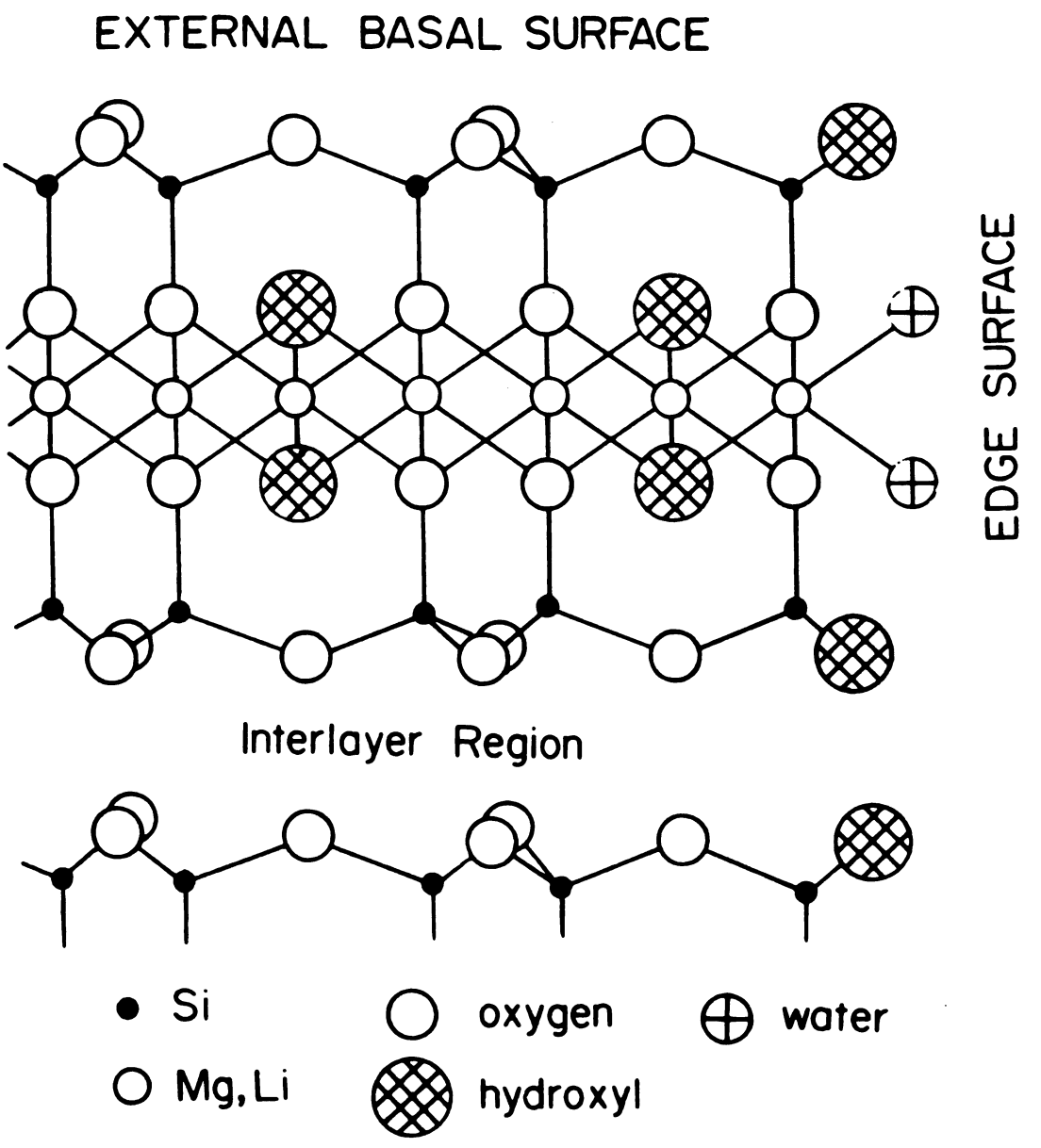
EXTERNAL BASAL SURFACE
EDGE SURFACE
Interlayer Region
Si
oxygen
water
Mg, Li
hydroxyl

according to eq. 9.

In contrast to the behavior of the neutral clusters in IV, the clusters in I do react in air at 150°C to form new surface species, despite the oriented condition of the sample. As shown in Figure 3 and Table 4 the new surface species exhibit three terminal CO stretching frequencies. These three bands are indicative[124,127,128] of both the molecular tricarbonyl (n=3) and the bicarbonyl (n=2) species depicted in eq. 9. On the basis of these observations, we may conclude that the initial binding of $HOs_3(CO)_{12}^+$ and the subsequent formation of $Os_3(CO)_{12}$ occurs at or near the edge surface sites.

The selective formation of $Os_3(CO)_{12}$ from $HOs_3(CO)_{12}^+$ at edge surfaces may be explained in terms of the following scheme wherein M = Os.

Scheme I

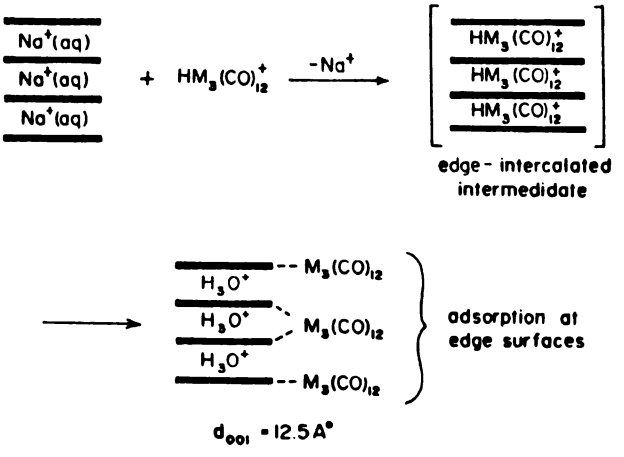

Unlike the neutral cluster the protonated cluster is capable of ion-exchange with intercalated Na^+. It is this exchange reaction which provides the driving force for the initial binding of the cluster cation near the edge of the clay platelet. However, the cluster cation is unstable because the aquated interlayer is more basic than the corresponding neutral cluster. Consequently, the proton is transferred to interlayer water and the neutral cluster is selectively formed in a dispersed state at edge sites where it has ready access to hydroxyl groups.

Although the initial intent of this work was to intercalate $HOs_3(CO)_{12}^+$ cluster cations in smectite clays, the cations proved to be unstable with regard to proton dissociation at exchange sites near the platelet edges. Nevertheless, the observed chemistry is unique in that the metal clusters are selectively dispersed at or near edge surface sites and the degree of cluster dispersion is much greater than can be achieved by impregnation of neutral clusters from solution.

These preliminary observations set up the basis for a more thorough investigation of the reaction of triosmium cluster carbonyl complexes with clays. It appeared to us we could control the dispersion of the metal cluster at different sites thus, allowing or preventing reaction with surface hydroxyl groups. We had studied briefly the influence of lamination or layer ordering on the reactivity of metal clusters towards OH groups. We next considered the role of size and morphology of the clay layers.

Reaction of fluorohectorite (100 mg) in aqueous suspension with $HOs_3(CO)_{12}^+$ (0.007 mmol) in acetone results in a product (VI) exhibiting an IR spectrum very similar to that of $Os_3(CO)_{12}$. In addition to the IR spectrum, which on the basis of band widths suggests the osmium clusters are bound to the external surfaces of the clay, the x-ray diffraction pattern

reveals a basal spacing of 12.1 Å, indicative of unexchanged clay with a monolayer of water. The difference between sample (I) and (VI) is apparent when the latter is heated at 150°C in air. Reaction under these conditions for 12 h causes only a fraction of the neutral clusters to react with surface hydroxyls, as evidenced by the appearance of CO absorptions at 2123 and 1958 cm^{-1}. The IR spectrum, apart from the weak absorptions characteristic of the mononuclear osmium complexes, remains basically unchanged even after extended reaction times.

The difference is reactivity between VI and I, the reaction product of $HOs_3(CO)_{12}^+$ with Na^+-hectorite, arises mainly from differences in morphology of the clay particles. Fluorohectorite with particle size >> 2μ, much larger than natural hectorite, is expected to possess significantly lower edge surface area. In addition, the number of OH groups in fluorohectorite is statistically lower because of the substitution at octahedral sites by fluoride ions. Thus, though the reaction is believed to proceed according to Scheme 1, the available surface is saturated quickly and the rest of the cluster molecules are forced to be deposited on the basal planes. Metal clusters deposited at or near the edges do react to form mononuclear osmium complexes. On the other hand, the highly oriented nature of the fluorohectorite film samples impedes migration of the metal clusters across the basal planes to reach and react with OH groups.

That the metal clusters do indeed selectively occupy first the edge surfaces before depositing on the basal planes is supported by comparison of the reaction of $HOs_3(CO)_{12}^+$ with Na^+-hectorite at two different molar ratios of metal complex to clay. An air-dried sample containing 0.035 mmol of complex per 100 mg of clay exhibits CO absorptions similar to those of unsupported $Os_3(CO)_{12}$. Heating at 150°C in air for 12 h results in partial

reaction of the osmium clusters with surface hydroxyl groups in contrast to a clay sample containing 0.007 mmol of $HOs_3(CO)_{12}^+$ (cf. I, Figure 3, Table 4).

As was noted earlier, the method of drying the mineral considerably influences the reactivity of metal clusters. Air drying leads to highly oriented samples that impede the migration of cluster molecules across the basal planes. If $Os_3(CO)_{12}$ is impregnated on Na^+-hectorite and the product freeze-dried as a powder rather than air-dried as a film, then heating in air leads to reaction with edge hydroxyl groups and to the formation of ensembles of atomically dispersed Os complexes evidenced, by the familiar three peak IR pattern (Figure 5). In contrast, heating the air-dried film sample (cf. IV, Figure 3, Table 4) does not lead to reaction with edge OH groups.

The observed dependence of the osmium cluster reactivity on drying most probably is related to the mechanism of layer aggregation in smectite clays. Furthermore, the degree of lamination or layer ordering in a flocculated clay system greatly depends on the size and morphology of the silicate platelets. Typical smectite clay particles, composed of a few tens of layers with a diameter in the range 10^2-10^4 Å, exhibit a pancake-like morphology. It is expected that layers with a large aspect ratio would favor face to face interactions of coagulated single-layer platelets. On the other hand, layers with a small aspect ratio would tend to aggregate through edge to edge and edge to face interactions resulting in a highly delaminated system.

A typical flocculated clay system should consist of laminated aggregates along with delaminated areas. The proposed model for a flocculated clay is illustrated in the central inset of Figure 6. Face to face aggregates are shown by a group of parallel layers, while single layers represent delaminated

Figure 5 Infrared spectra in the terminal CO stretching region: (a) Freeze-dried sample of $Os_3(CO)_{12}$ on Na^+-hectorite prepared by impregnation with $Os_3(CO)_{12}$ (mull); (b) after heating in air at 150°C for 12 h (mull).

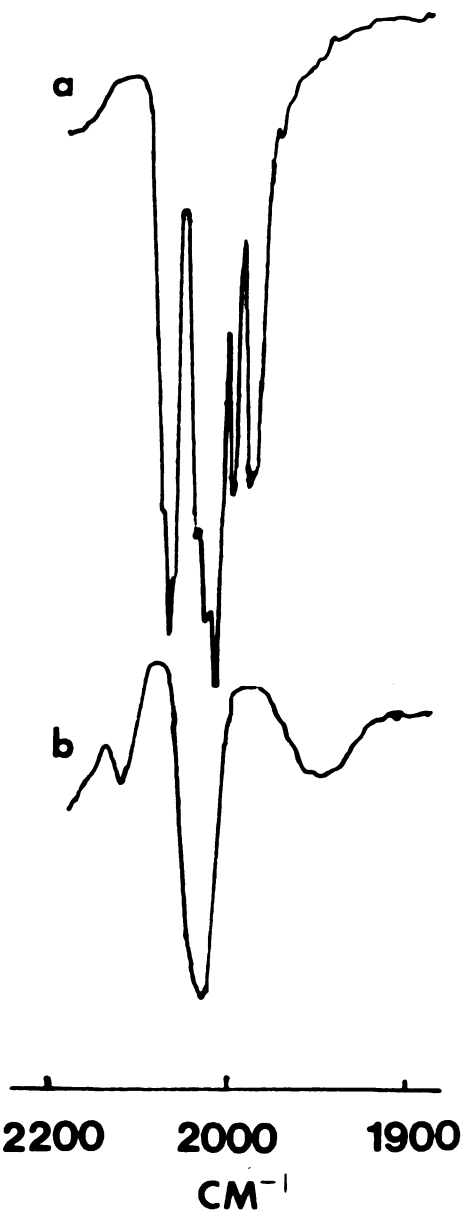
a
b
2200
2000
1900
CM⁻¹

Figure 6 (A) Model for a wet, flocculated clay system after impregnation with $Os_3(CO)_{12}$. Cycles represent aggregates of $Os_3(CO)_{12}$ cluster molecules of unspecified size; (B) Freeze-drying tends to preserve the flocculated structure. The sample contains both laminated and delaminated platelets; (C) Air-drying tends to promote face-to-face lamination of layers. Clusters are "trapped" and migration to edge sites is impeded.

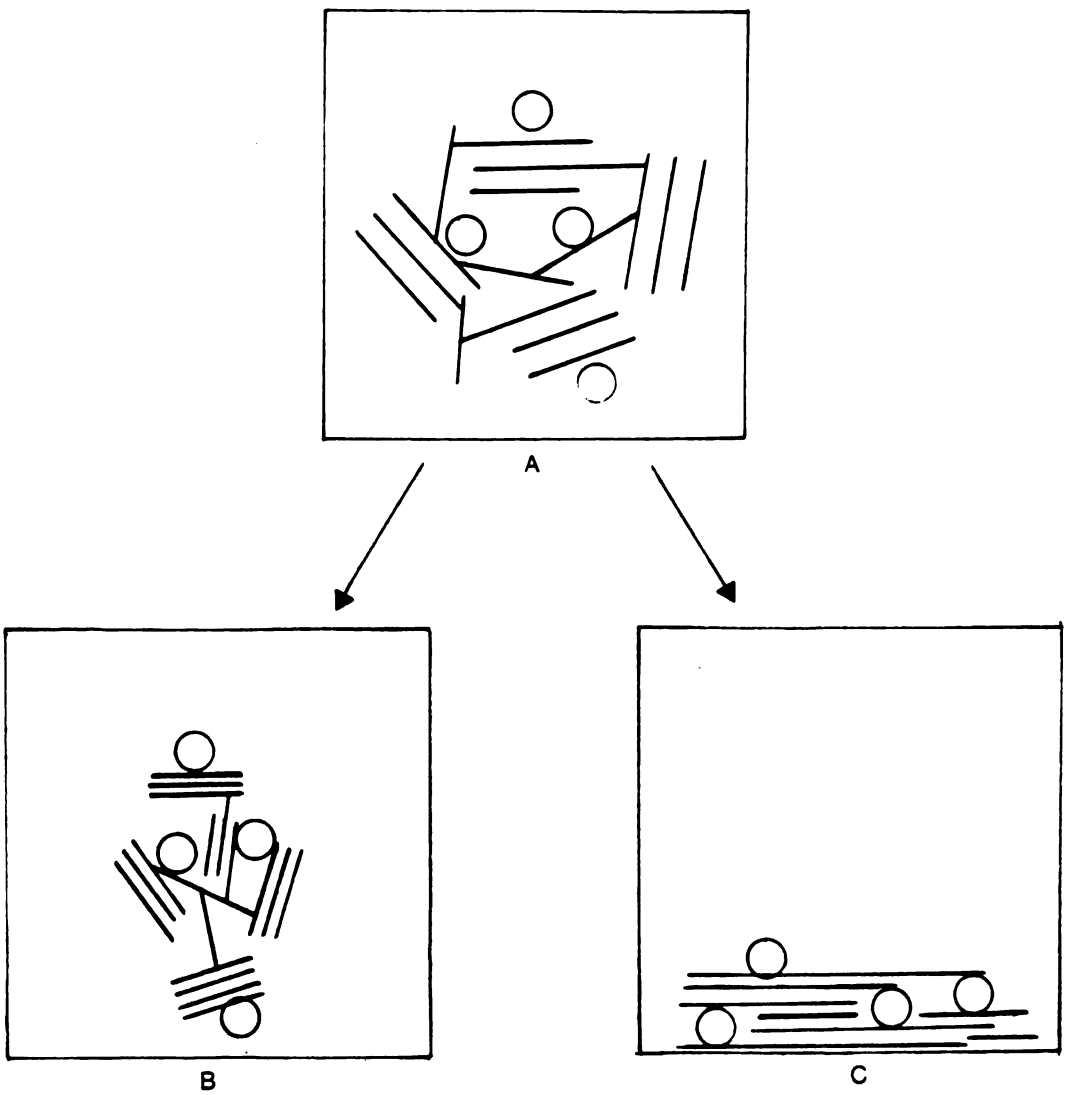
A
B
C

areas. Circles denote aggregates of $Os_3(CO)_{12}$ cluster of unspecified size. Freeze drying will generally preserve the structure of the flocculated clay, while the surface tension forces present under air-drying conditions will assist in a general reorganization. This rearrangement tends to optimize face to face interactions, ultimately leading to a highly oriented structure. Under these circumstances, migration of the segregated $Os_3(CO)_{12}$ onto the basal surfaces and eventually to edge sites for reaction with hydroxyl groups becomes highly probable for a random freeze-dried clay sample. Alternatively, the oriented nature of the air-dried samples hinders migration of the metal clusters across the basal planes.

It is important to recognize that this model of flocculation is valid only for aqueous clay suspensions. If, for example, an organic solvent is used for the impregnation of the metal cluster, then air-drying will not involve a reorganization mechanism that leads to highly laminated aggregates and the reaction of the metal cluster with surface hydroxyls is not impeded. Thus, when Na^+-hectorite (1.0 meq) is impregnated with a solution of $Os_3(CO)_{12}$ (0.1 mmol) in CH_2Cl_2 and then air-dried, the product exhibits a spectrum very similar to that of the unsupported cluster. Heating at 150°C in air for 12 h leads again to reaction with edge hydroxyls and the formation of mononuclear complexes, as evidenced by CO absorptions at 2019 m, 2032 s and 1950 m cm^{-1} (Figure 7).

To further verify the validity of our model for clay flocculation, we investigated the binding of authentic $Os_3(CO)_{12}$ to both laponite and fluorohectorite. Though both are synthetic hectorites, the former has a relatively small layer aspect ratio, while the latter is characterized by large particles. After impregnation with the osmium cluster molecules both clay samples were air-dried. However, the x-ray diffraction pattern of

Figure 7: Infrared spectra in the terminal CO stretching region: (a) $Os_3(CO)_{12}$-hectorite prepared by impregnation with $Os_3(CO)_{12}$ in CH_2Cl_2 (mull); (b) after heating in air at 150°C for 12 h (mull).

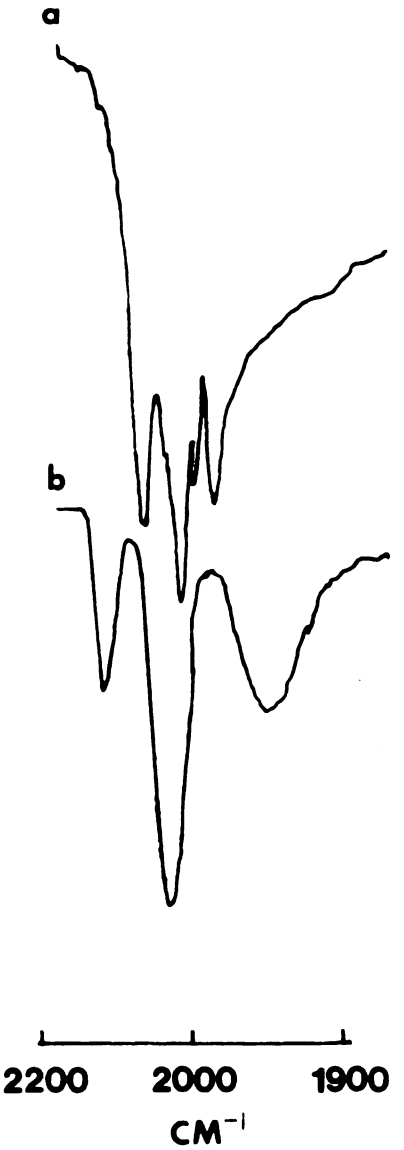
a
b
2200
2000
1900
CM⁻¹

fluorohectorite reveals a well ordered system, while laponite appears highly delaminated. As a result, the fluorohectorite clay sample remains unchanged on heating in air at 150°C (Figure 8). On the other hand, reaction of the metal clusters with OH groups in laponite under the same reaction conditions is highly favorable (Figure 9).

The wet impregnation technique that has been used for immobilization of metal carbonyls on refractory inorganic oxides usually requires a large amount of solvent due to the low solubility of the carbonyl complexes. After the reaction, evaporation of the solvent leads to segregation of the metal carbonyl, especially in systems with weak complex-support interactions. Howe et al.[138] found that materials prepared by impregnation are similar to those prepared by dry grinding techniques. Thus, impregnation methods generally lead to phase segregation of the carbonyl and such segregation can be observed by x-ray diffraction.

The x-ray diffraction data obtained utilizing $HOs_3(CO)_{12}^+$ and $Os_3(CO)_{12}$ with different particle size clays are summarized in Table 6. For samples prepared starting with the protonated $HOs_3(CO)_{12}^+$ cluster only the support was detected. The lack of an x-ray diffraction pattern due to supported carbonyl indicates these clusters are present in a highly dispersed state with an aggregate size less than 50 Å, the detection limit for the x-ray diffraction technique. On the other hand, products obtained by the impregnation technique starting with the neutral $Os_3(CO)_{12}$ cluster contain the metal species in the form of crystallites, regardless of the kind of clay or solvent used.

The different degrees of dispersion may be explained by the difference in the nature of the two metal clusters. The protonated cluster, because of its cationic character, is capable of ion-exchange with interlayer Na^+

Figure 8: Infrared spectra in the terminal CO stretching region: (a) $Os_3(CO)_{12}$-fluorohectorite prepared by impregnation with $Os_3(CO)_{12}$ and air-drying (film). The Os loading is 3.8 wt%; (b) after heating in air at 150°C for 12 h (film).

Figure 9: Infrared spectra in the CO stretching region: (a) $Os_3(CO)_{12}$--laponite prepared by impregnation with $Os_3(CO)_{12}$ and air-drying (mull). The Os loading is 3.8 wt%; (b) after heating in air at 150°C for 2 h (mull).

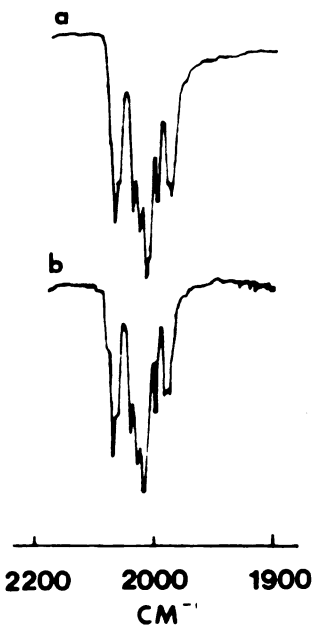

Figure 8

Figure 9

Table 6

X-Ray Diffraction Data for $Os_3(CO)_{12}$ and Clay-Supported Osmium Carbonyl Samples[a]

Sample	d Spacings (Å) for the Carbonyl Phase
$Os_3(CO)_{12}$	7.37,7.16,7.02, 6.75,6.60
$HOs_3(CO)_{12}^+$ + hectorite[b]	c
$HOs_3(CO)_{12}^+$ + fluorohectorite[b]	c
$Os_3(CO)_{12}$ + hectorite[b]	7.37,7.16,6.99, 6.75,6.60
$Os_3(CO)_{12}$ + fluorohectorite[b]	7.37,7.16,6.99, 6.60
$Os_3(CO)_{12}$ + laponite[b]	7.37,7.16,6.99, 6.75,6.60
$Os_3(CO)_{12}$ + hectorite[d]	7.40,7.19,7.13

a All clay samples are in the form of air-dried films.
b Clay in aqueous suspension, metal carbonyl in acetone
c No pattern due to supported carbonyl observed
d Clay in CH_2Cl_2, metal carbonyl in CH_2Cl_2

ions. The initially bound metal carbonyl transfers a proton to the interlayer water and the neutral cluster is selectively dispersed at or near the edges of the mineral. The electrical neutrality of the $Os_3(CO)_{12}$ cluster precludes any electrostatic interaction with the mineral and leads to a poorly dispersed metal carbonyl after evaporation of the solvent.

In an attempt to eliminate the formation of $Os_3(CO)_{12}$ crystallites on Na^+-hectorite, a clay sample (0.2 g) was first pretreated at 350°C under vacuum and then was refluxed with a solution of $Os_3(CO)_{12}$ (30 mg, 0.033 mmol) in octane (100 ml) for 24 h. After the reaction time the solution was filtered under nitrogen and the mineral was washed several times with CH_2Cl_2 to remove unreacted physically adsorbed osmium clusters. The random freeze-dried clay sample allows for reaction with the metal cluster through surface hydroxyls to form a new species (VII). The x-ray powder diffraction spectrum of VII shows no pattern due to supported carbonyl species, indicative of a high degree of dispersion of the metal species. However, the infrared spectrum is significantly different from those obtained by impregnation techniques (Figure 10, Table 4). The positions and intensities of the (CO) absorptions correspond well to those found by Crawford et al.[123] for $Os_3(CO)_{12}$ supported on alumina by an extraction technique. Although the structure of the osmium species cannot be unequivocally assigned, the IR data suggest that the framework of the cluster remains intact and interacts strongly with the support. It is possible that the spectrum of the clay sample is the superposition of those of the supported triosmium hydride cluster $HOs_3(CO)_{10}(O\text{-}Si\equiv)$ and ensembles a mononuclear osmium complexes of the type $[Os(CO)_n(O\text{-}Si\equiv)_2]_x$[124,127,128]. The osmium carbonyl species is stable in air, but heating at 150°C causes degradation and decarbonylation and produces the surface bound mononuclear complexes

Figure 10: Infrared spectra in the terminal CO stretching region: (a) clay sample prepared by refluxing $Os_3(CO)_{12}$ with freeze-dried Na^+-hectorite in octane (mull); (b) sample (a) after heating in air at 150°C for 2 h (mull).

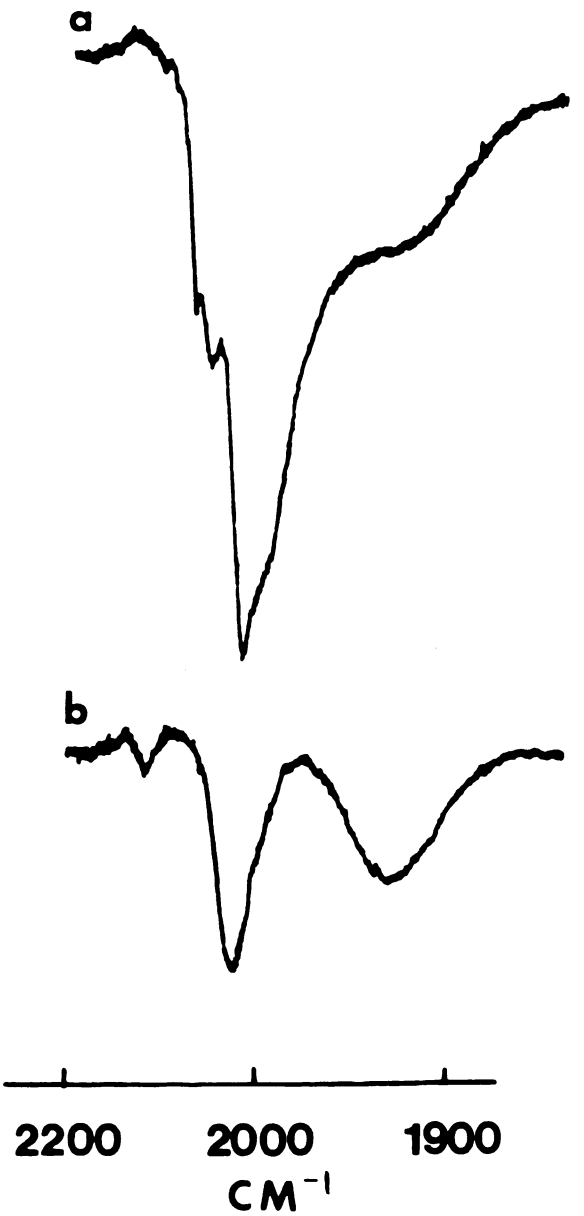
a
b
2200
2000
1900
CM⁻¹

(Figure 10).

The adsorption of metal cluster carbonyls on inorganic oxides has been extensively studied by several workers[54,75,78]. It is generally agreed that, unless the metal carbonyl is simply physisorbed on the surface of the support, interaction between surface hydroxyls and the cluster with concomitant metal oxidation accompanies adsorption from solution. Since $Os_3(CO)_{12}$ exhibits a high specificity towards the edge hydroxyl groups in clays, the reaction was used as a means of estimating the edge surface area of three different hectorites. Thus, the clays were refluxed with a solution of $Os_3(CO)_{12}$ in octane. Under the reaction conditions the edge surface is accessible to the metal clusters and the metal loading can provide an estimate of the available edge surface area. Elemental analysis data for fluorohectorite, natural hectorite, and laponite are provided in Table 7. Fluorohectorite, having the largest particle size, is expected to posses the lowest edge surface area and consequently binds the least amount of osmium. The metal loading in laponite is the highest, because of the abundance of edge surfaces due to the small size of the clay platelets. The osmium content in natural hectorite is within these two limits, as is its particle size.

Although the metal loadings for the three different clays are consistent with the trend in particle size, they only provide a relative estimate of the available edge surfaces. The ratio of edge sites for fluorohectorite, natural hectorite, and laponite from the metal loadings is calculated to be 1:3.3:4.4. In an independent experiment Kadkhodayan[139] measured the pseudo first-order rate constants for the reaction of alkyl bromides with NaCl using $Ni(Phen)_3^{2+}/SO_4^{2-}$ intersalated fluorohectorie, hectorite, and laponite as triphase catalysts. Since the substrate attack zone is limited to a very short distance at the edges of the clay, the rate constants would greatly depend

Table 7

Elemental Analysis of Os Complexes Supported on Hectorites

Clay	Particle Size (μ)	wt% Os	Normalized
Fluorohectorite	>> 2 μ	0.40	1.00
Hectorite, Baroid	< 2 μ	1.33	3.32
Laponite	0.02	1.76	4.40

on the particle size of the clay used. Interestingly, the normalized k_{obs} for fluorohectorite, hectorite, and laponite were 1:2.2:3.9, in qualitative agreement with the numbers obtained from metal loadings.

2. Reaction of $HRu_3(CO)_{12}^+$ and $Ru_3(CO)_{12}$ with Hectorite

$HRu_3(CO)_{12}^+$ was another candidate for site selective binding to a layered silicate surface. The reaction of Na^+-hectorite (1.0 meq) in aqeuous suspension with $HRu_3(CO)_{12}^+$ (0.1 mmol) in acetone results in a product (VIII) very similar to that obtained using authentic $Ru_3(CO)_{12}$ (XI). The IR spectra of VIII and XI in the terminal CO stretching region are shown in Figure 11 along with the spectra of molecular $[HRu_3(CO)_{12}][PF_6]$ (IX) and $Ru_3(CO)_{12}$ (X). The CO stretching frequencies for each compound are provided in Table 8. Electronic spectroscopy data are summarized in Table 9. In addition, the x-ray diffraction pattern of an oriented clay film of VIII indicates the presence of Na^+-hectorite with a monolayer of water. It is apparent from the experimental data that $HRu_3(CO)_{12}^+$ deprotonates to form neutral $Ru_3(CO)_{12}$ cluster molecules. The latter is not intercalated, but instead is bound to the external surfaces of the clay. The ruthenium complex appears to be well-dispersed, as judged from the absence of x-ray diffraction reflections for a segregated phase.

Although $HRu_3(CO)_{12}^+$ appears to parallel the behavior of $HOs_3(CO)_{12}^+$, further experimental evidence mitigates against this. Thus, heating samples (VIII) and (XI) at 110°C in air does not lead to any new surface species, in marked contrast to the behavior of sample (I) derived from $HOs_3(CO)_{12}^+$. $Ru_3(CO)_{12}$ is also known to react with surface hydroxyls of silica and alumina[115-117] to give molecular species such as those represented in equation 10 for a silica surface.

Figure 11: Infrared spectra in the terminal CO stretching region: (VIII) $Ru_3(CO)_{12}$-hectorite prepared from $HRu_3(CO)_{12}^+$(film); (IX) $[HRu_3(CO)_{12}]PF_6$(KBr pellet); (X) $Ru_3(CO)_{12}$ (KBr pellet); (XI) $Ru_3(CO)_{12}$-hectorite prepared by impregnation with $Ru_3(CO)_{12}$ (film).

Table 8

Infrared CO Stretching Frequencies for Reaction Products and Reference Compounds

Sample	Description	Medium	Frequencies, cm^{-1}
VIII	$[HRu_3(CO)_{12}]^+$ + hectorite reaction product	film	2064s, 2059 vs, 2044m 2032s, 2021s, 2001s, 1992m, 1987m, 1983m
IX	$[HRu_3(CO)_{12}][PF_6]$	KBr	2162w, 2133m, 2106m 2086s, 2069 vs,2048m, 2021m, 1989 w
X	$Ru_3(CO)_{12}$	KBr	2064s, 2058s, 2044m, 2031s, 2021 vs, 2002vs, 1993s, 1988m, 1984m
XI	$Ru_3(CO)_{12}$ + hectorite reaction product	film	2063s, 2058m,2041m 2032s, 2020vs, 2000vs, 1991m, 1985m, 1982m
XII	$[(\equiv SiO)_2Ru(CO)_2]_x$-hectorite	mull	2059s, 1988s

Table 9

Electronic Spectroscopy Data for Reactions Products and Reference Compounds

System	Solvent	λ_{max} (nm)
$[HRu_3(CO)_{12}][PF_6]$	Acetone	403
$Ru_3(CO)_{12}$	CH_2Cl_2	392
$[HRu_3(CO)_{12}]^+$ + hectorite reaction product	film	382
$Ru_3(CO)_{12}$ + hectorite reaction product	film	380

$$2(\equiv SiOH) + Ru_3(CO)_{12} \xrightarrow{\Delta} [(\equiv SiO)_2Ru(CO)_n]_x \qquad (10)$$

$$n = 2,3$$

Since the above reaction provides a chemical means of distinguishing between $Ru_3(CO)_{12}$ at edges and basal planes, it can be concluded that the clusters are more likely deposited at the more abundant basal surfaces.

The somewhat abnormal behavior of $HRu_3(CO)_{12}^+$ is consistent with its lower stability in solution when compared to its osmium analog. If deprotonation is faster than the rate of ion-exchange, the driving force that leads to initial binding of the cluster cation near the edges of the clay is absent. Consequently both $HRu_3(CO)_{12}^+$ and $Ru_3(CO)_{12}$ clusters result in the formation of similar products that contain the metal carbonyl on the basal surfaces. The highly oriented nature of the clay films impedes migration to the hydroxylated edge sites and precludes the formation of new surface species. The importance of sample orientation in hindering migration was demonstrated by freeze-drying sample (XI) and observing reaction according to equation 10 (Figure 12).

Heating the ruthenium-containing samples (VIII) and (XI) in air at 110°C results in a decrease in the intensities of the CO bands. The loss of intensity most likely results from the partial air-oxidation of $Ru_3(CO)_{12}$ to form RuO_2 and CO_2 by the reaction

$$Ru_3(CO)_{12} + 9O_2 \longrightarrow 3RuO_2 + 12CO_2 \qquad (11)$$

as observed previously for the supported ruthenium carbonyl complex[111].

Figure 12: Infrared spectra in the terminal CO stretching region: (a) Freeze-dried sample of $Ru_3(CO)_{12}$ on Na^+-hectorite (0.1 mmol/meq) prepared by impregnation with $Ru_3(CO)_{12}$ (mull); (b) sample (a) after heating in air at 100°C for 30 min (mull).

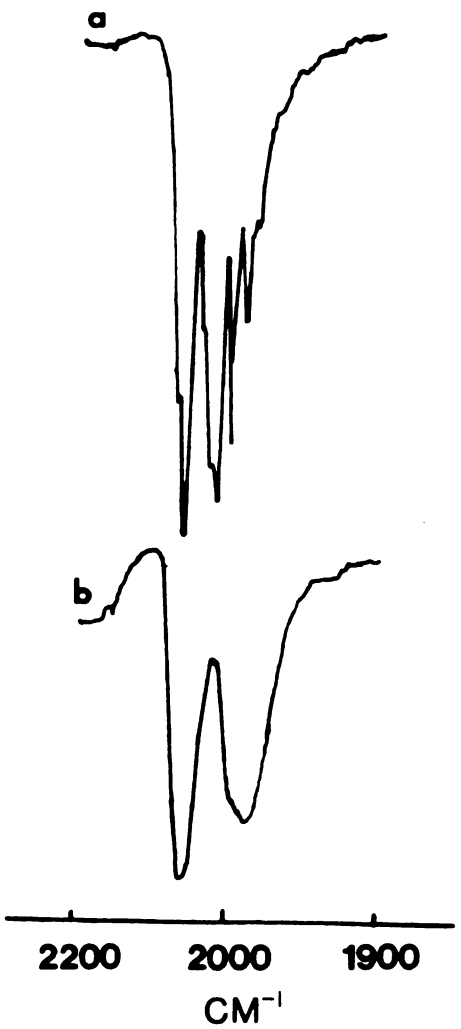
a
b
2200
2000
1900
CM⁻¹

B. Intercalation of Cationic Phosphine Substituted Carbonyl Clusters on Hectorite

Though the reactions of $HOs_3(CO)_{12}^+$ and $HRu_3(CO)_{12}^+$ with layered silicates provided an insight into clay-carbonyl systems, the initial intent of this work was to intercalate metal carbonyl clusters in clays. It was felt that a positive charge could be induced on the clusters by utilizing the phosphonium-phosphine ligand $Ph_2PCH_2CH_2\overset{+}{P}Ph_2CH_2Ph$, abbreviated $P\text{-}P^+$. Metal cluster carbonyls are capable of undergoing substitution reactions with neutral phosphine ligands. A similar approach has been used to prepare cationic analogs of well known, otherwise neutral, homogeneous rhodium catalysts[102,103].

1. Synthesis and Exchange Reactions

$Ru_3(CO)_9(P\text{-}P^+)_3$, $H_4Ru_4(CO)_8(P\text{-}P^+)_4$, $Ir_4(CO)_9(P\text{-}P^+)_3$, $H_2Os_3(CO)_{9,10}(P\text{-}P^+)$, and $Os_3(CO)_{11}(P\text{-}P^+)$ were prepared by the reaction of the parent neutral metal clusters with the positively charged phosphonium-phosphine ligand $P\text{-}P^+$ according to procedures, or slight modifications thereof, described earlier for the synthesis of $Ru_3(CO)_9L_3$[136], $Ir_4(CO)_9L_3$[71], $H_2Os_3(CO)_{9,10}L$[67], and $Os_3(CO)_{11}L$[137] in which L is a tertiary phosphine ligand:

$$Ru_3(CO)_{12} + 3P\text{-}P^+ \xrightarrow[MeOH]{\Delta} Ru_3(CO)_9(P\text{-}P^+)_3 + 3CO \qquad (12)$$

$$H_4Ru_4(CO)_{12} + 4P\text{-}P^+ + 4Me_3NO \xrightarrow{CHCl_3}$$

$$H_4Ru_4(CO)_8(P\text{-}P^+)_4 + 4CO_2 + 4Me_3N \qquad (13)$$

$$Ir_4(CO)_{12} + 3P\text{-}P^+ + 3Me_3NO \xrightarrow{THF}$$

$$Ir_4(CO)_9(P\text{-}P^+)_3^+ + 3CO_2 + 3Me_3N \tag{14}$$

$$H_2Os_3(CO)_{10} + P\text{-}P^+ \xrightarrow{CHCl_3} H_2Os_3(CO)_{10}(P\text{-}P^+) \tag{15}$$

$$H_2Os_3(CO)_{10}(P\text{-}P^+) \xrightarrow[MeOH]{\Delta} H_2Os_3(CO)_9(P\text{-}P^+) + CO \tag{16}$$

$$Os_3(CO)_{12} + Me_3NO \xrightarrow[CH_2Cl_2]{CH_3CN} Os_3(CO)_{11}(CH_3CN) + CO_2 + Me_3N \tag{17}$$

$$Os_3(CO)_{11}(CH_3CN) + P\text{-}P^+ \xrightarrow{CHCl_3} Os_3(CO)_{11}(P\text{-}P^+) + CH_3CN \tag{18}$$

Though complexes of the type $H_4Ru_4(CO)_8L_4$[140] have been obtained in the past by heating a solution of $H_4Ru_4(CO)_{12}$ in the presence of the appropriate phosphine ligand at approximately 100°C, the use of trimethylamine oxide in facilitating CO substitution in metal carbonyl complexes is well established. Thus, the reaction of one equivalent of $H_4Ru_4(CO)_{12}$ with four equivalents of $Me_3NO{\cdot}2H_2O$ in the presence of $(P\text{-}P^+)BF_4$ at room temprature results in the formation of only the tetrasubstituted phosphine product.

The infrared spectra of the cationic $P\text{-}P^+$ substituted complexes in the CO stretching region as well as their electronic spectra were in good agreement with those previously reported for their neutral analogues (Tables 10-12). Since the infrared spectrum of a metal carbonyl complex can serve as a fingerprint reflecting its structure and symmetry, IR spectroscopy can

Table 10

Infrared CO Stretching Frequencies for Molecular and Hectorite-Intercalated Metal Cluster Complexes[a]

Compound	ν (CO) cm^{-1}
$Ru_3(CO)_9(P\text{-}P^+)_3(BF_4)_3$	2048 m, 1980 s, 1962 s
$Ru_3(CO)_9(P\text{-}P^+)_3$-hectorite	2042 m, 1970 s, 1960 sh
$H_4Ru_4(CO)_8(P\text{-}P^+)_4(BF_4)_4$	2005 s, 1971 m, 1948 s
$H_4Ru_4(CO)_8(P\text{-}P^+)$4-hectorite	2002 s, 1965, sh, 1946 s
$Ir_4(CO)_9(P\text{-}P^+)_3(BF_4)_3$	2039 m, 1995 sh, 1984 s, 1965 sh, 1832 vw, 1779 s
$Ir_4(CO)_9(P\text{-}P^+)_3$-hectorite	2038 m, 1995 sh, 1980 vs, 1965 sh, 1835 vw, 1777 s
$Os_3(CO)_{11}(P\text{-}P^+)BF_4$	2100 m, 2048 s, 2028 s, 2010 vs, 1998 sh, 1983 m 1976 m,1940w
$Os_3(CO)_{11}(P\text{-}P^+)$-hectorite	2102 m, 2050 s, 2025 sh, 2001 vs, 1995 sh, 1975 s
$H_2Os_3(CO)_{10}(P\text{-}P^+)BF_4$	2100 m, 2060 s, 2042 s, 2018 vs, 1990 sh, 1976 m 1960 m
$H_2Os_3(CO)_{10}(P\text{-}P^+)$-hectorite	2100 m, 2062 s, 2042 s, 2010 vs, 1998 sh, 1980 m, 1970 m
$H_2Os_3(CO)_9(P\text{-}P^+)BF_4$	2090 m, 2050 s, 2001 vs, 1989 s, 1948 m
$H_2Os_3(CO)_9(P\text{-}P^+)$-hectorite	2092 m, 2052 s, 2000 vs 1978 s, 1950 sh
$HOs_3(CO)_9(CH{=}CH_2)(P\text{-}P^+)$-hectorite	2090 m, 2042 s, 1999 vs 1962 sh

Table 10 continued

$HOs_3(CO)_9$(vinyl)(P-P^+)-hectorie	2091 m, 2041 s, 2002 vs 1960 sh, 1940 sh
$HOs_3(CO)_9$(vinyl)(P-P^+)BF_4	2090 m, 2048 s, 2002 vs 1970 s, 1937 m

[a] All BF_4^- salts were run as CH_2Cl_2 solutions. All hectorite-intercalated products were run as KBr pellets.

Table 11

UV-Visible Spectroscopy Data for Hectorite-Exchanged Metal Clusters and Their Molecular Analogs

System	Solvent or Phase	Band Positions in nm
$Ru_3(CO)_9(P\text{-}P^+)_3(BF_4)_3$	CH_2Cl_2	489, 362 sh
$Ru_3(CO)_9(P\text{-}P^+)_3$-hectorite	mull	497, 360 sh
$H_4Ru_4(CO)_8(P\text{-}P^+)_4(BF_4)_4$	CH_2Cl_2	404, 309 sh
$H_4Ru_4(CO)_8(P\text{-}P^+)_4$-hectorite	mull	417, 310 sh
$Ir_4(CO)_9(P\text{-}P^+)_3(BF_4)_3$	CH_2Cl_2	383 sh, 301
$Ir_4(CO)_9(P\text{-}P^+)_3$-hectorite	mull	380 sh, 290
$Os_3(CO)_{11}(P\text{-}P^+)BF_4$	CH_2Cl_2	407, 323
$Os_3(CO)_{11}(P\text{-}P^+)$-hectorite	mull	415, 300
$H_2Os_3(CO)_{10}(P\text{-}P^+)BF_4$	CH_2Cl_2	385, 331
$H_2Os_3(CO)_{10}(P\text{-}P^+)$-hectorite	mull	380
$H_2Os_3(CO)_9(P\text{-}P^+)BF_4$	CH_2Cl_2	359, 304
$H_2Os_3(CO)_9(P\text{-}P^+)$-hectorite	mull	362, 315

Table 12

Infrared CO Stretching Frequencies and Electronic Absorptions of Cluster Carbonyl Compounds

Compound	ν(CO) cm^{-1}	λ_{max} nm	Ref.
$Ru_3(CO)_9[PPh_2C_2H_4Si(OEt)_3]_3$	2044 (240), 1970 (2790), 1940 (850)	488 (13200), 366 sh	118
$H_4Ru_4(CO)_8[PPh_2C_2H_4Si(OEt)_3]_4$	2008s, 1981m, 1948s, 1920w	407	119
$Ir_4(CO)_9(PPh_3)_3$	2047m, 2038sh, 1992s, 1973sh, 1799s, 1787sh		71
$Os_3(CO)_{11}(PPh_3)$	2108ms, 2055s, 2035s, 2019s, 2000ms, 1989ms, 1978m		137
$H_2Os_3(CO)_{10}[PPh_2C_2H_4Si(OEt)_3]$	2106 (1.00), 2066 (3.04), 2051 (3.55), 2025 (7.94), 2007sh, 1983 (1.41), 1972 (1.38)	385 (1.00), 332 (0.96)	121
$H_2Os_3(CO)_9[PPh_2C_2H_4Si(OEt)_3]$	2091 (1.00), 2052 (2.70), 2012 (4.75), 1988 (1.74), 1974 (0.82), 1954 (0.39)	560 (1.0), 354 (82), 300 (67)	121

be utilized as a sensitive technique in identifying products with various degrees of phosphine substitution.

Besides the CO absorptions, the IR spectra of the mixed phosphine metal clusters exhibit bands characteristic of the $P\text{-}P^+$ ligand as illustrated in Figure 13. The absroptions around 1600 cm^{-1} most likely are due to phenyl group skeletal vibrations. The strong band at 1440 cm^{-1} and the bands on either side of it could be assigned to the methyl group scissoring vibrations or they might be due to aryl skeletal vibrations. The bands in the region 1350-1150 cm^{-1} probably arise from phenyl group in-plane C-H bonding vibrations. The three relatively sharp absorptions at 850-600 cm^{-1} are assigned to phenyl group C-H out of plane bonding vibrations[141,159]. The broad strong band at 1060 cm^{-1} is characteristic of the tetrafluoroborate anion BF_4^-[160].

Metal cluster hydrides were further characterized by ^1H NMR spectroscopy. $H_2Os_3(CO)_{10}(P\text{-}P^+)$, having a terminal and a bridging hydride that exchange rapidly, shows no resonance in the hydridic region at room temperature (RT). Lowering the temperature to -61°C gives rise to a resonance at -10.36 ppm (terminal H), and another at -20.48 ppm (bridging H), similar to those observed for $H_2Os_3(CO)_{10}L$ complexes[67]. Refluxing a solution of $H_2Os_3(CO)_{10}(P\text{-}P^+)$ in methanol results in a slow loss of CO to give $H_2Os_3(CO)_9(P\text{-}P^+)$, which exhibits a proton doublet at -11.06 ppm (J_{HP} = 7.25 Hz), suggesting that both hydridic ligands bridge an Os-Os edge[67]. The ^1H NMR spectrum of $H_4Ru_4(CO)_8(P\text{-}P^+)_4$ shows, besides the $P\text{-}P^+$ ligand resonances, a quintet at -16.50 ppm (J_{HP} = 7.0 Hz) which agrees well with that observed for $H_4Ru_4(CO)_8L_4$ type complexes[140].

Preliminary attempts to exchange interlayer surface Na^+ ions with the cationic clusters from suspensions of the mineral in different polar organic

Figure 13: Infrared spectra of unsupported and hectorite-intercalated $Ir_4(CO)_9(P\text{-}P^+)_3$ in the region 2500-500 cm^{-1}: (a) $Ir_4(CO)_9(P\text{-}P^+)_3(BF_4)_3$ (KBr pellet); (b) $Ir_4(CO)_9(P\text{-}P^+)_3$-hectorite (film). Cross-hatched absorptions are also present in the native mineral.

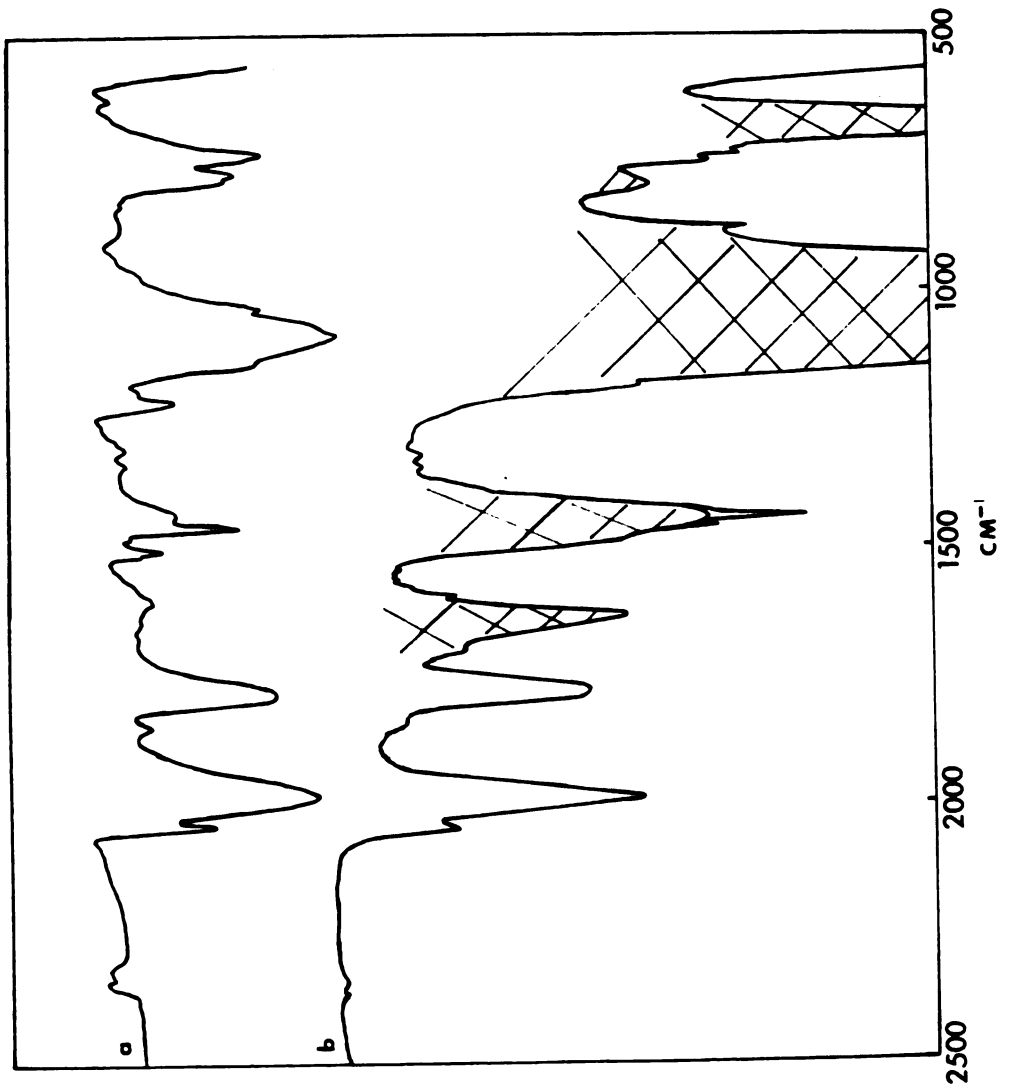
a
b
2500
2000
1500
1000
500
cm⁻¹

solvents were unsuccessful. An 001 spacing of about 12.6 Å, indicative of Na^+-hectorite with a water monolayer, was obtained even after continuous refluxing. Interestingly, successive washings of the clay with the organic solvent did not completely remove the metal complex from the external surface. The clay bound metal complex was shown by infrared spectroscopy to be unchanged.

The failure to exchange interlayer Na^+ ions by metal clusters containing $P\text{-}P^+$ can be explained in terms of the swelling properties of clays[10]. Polar organic solvents can cause a considerable swelling of silicate interlayers. Nevertheless, the interlayer expansion is generally limited to < 10 Å, making it difficult for the bulky complex to penetrate and displace Na^+ ions. In other words, the process expressed in equation 19, wherein the heavy lines represent the negatively charged silicate layers with a thickness of approximately 9.6 Å, and M_m^{n+} the cluster cations, is exceedingly slow.

$$\overline{\overline{nNa^+}} + M_m^{n+} \xrightarrow[\text{solvent}]{\text{organic}} \overline{\overline{M_m^{n+}}} + nNa^+ \qquad (19)$$

Since the edges of the smectite structure have broken bonds that contribute to the clay cation exchange capacity (CEC)[142], a small amount of the cluster satisfies the "edge charge" deficiency and remains on the surface even after repeated washings.

Despite the above limitations encountered in organic solvents, exchange of interlayer Na^+ by metal cluster complexes could be achieved by first suspending the clay in water and then adding this suspension to an acetone solution of metal cluster cation. Under these conditions the clay layers

are largely delaminated in aqueous suspension and the Na^+ ions on the basal surfaces are readily available for ion exchange. This is in contrast to the situation expressed in equation 19 where the clay layers are initially oriented face to face. Upon the addition of the clay suspension to the cluster cation solution, the Na^+ ions are replaced and the silicate layers reorient themselves in a face to face fashion. The overall process can be represented schematically as shown in equation 20.

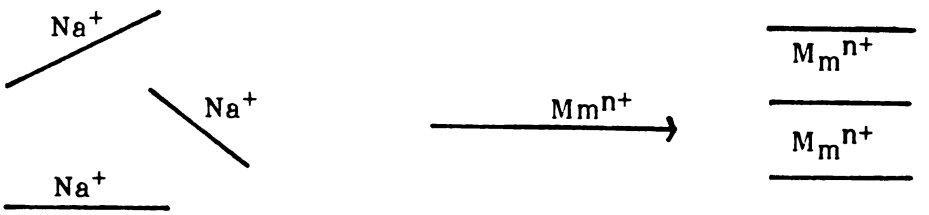

(20)

Intercalation of the different cluster cations in the interlamellar space of Na^+-hectorite results in a considerable increase in the 00ℓ spacing of the mineral (Table 13, Figure 14). The lack of more than two orders of reflection from the x-ray diffraction patterns indicates the presence of highly interstratified materials. The increase in spacing most probably is determined by the size of the phosphonium-phosphine ligand. The size and shape of the cluster framework might also play a minor role. Although one would expect intercalated cluster complexes of the same type but with higher degrees of $P\text{-}P^+$ substitution to yield materials with higher 00ℓ spacings, our results mitigate against this. Complexes with more than one $P\text{-}P^+$ ligand might adopt a more tightly-packed configuration in order to accommodate

Table 13

001 X-ray Basal Spacings of Hectorite-Intercalated Metal Cluster Carbonyl Complexes

Sample	d_{001} Å
$Ru_3(CO)_9(P\text{-}P^+)_3$-hectorite	22.1
$H_4Ru_4(CO)_8(P\text{-}P^+)_4$-hectorite	23.9
$Ir_4(CO)_9(P\text{-}P)_3$-hectorite	23.2
$Os_3(CO)_{11}(P\text{-}P^+)$-hectorite	27.6
$H_2Os_3(CO)_{10}(P\text{-}P^+)$-hectorite	26.8
$H_2Os_3(CO)_9(P\text{-}P^+)$-hectorite	26.0
$P\text{-}P^+$-hectorite	18.8

Figure 14: X-ray diffraction patterns of : (A) $Ru_3(CO)_9(P\text{-}P^+)_3$-hectorite; (B) $H_4Ru_4(CO)_8(P\text{-}P^+)_4$-hectorite; (C) $Ir_4(CO)_9(P\text{-}P^+)_3$-hectorite; (D) $Os_3(CO)_{11}(P\text{-}P^+)$-hectorite; (E) $H_2Os_3(CO)_{10}(P\text{-}P^+)$-hectorite; (F) $H_2Os_3(CO)_9(P\text{-}P^+)$-hectorite. Samples were prepared as oriented films on glass slides by first suspending the clay complex in water and allowing the suspension to evaporate on the slide at room temperature.

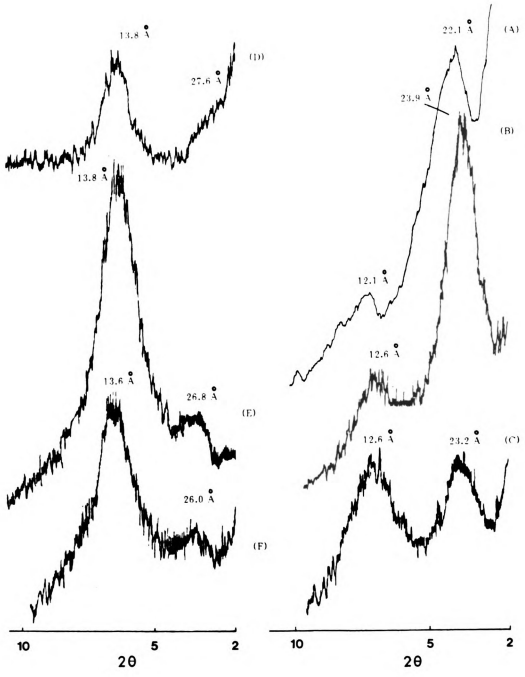
13.8 Å
27.6 Å
(D)
13.8 Å
13.6 Å
26.8 Å
(E)
26.0 Å
(F)
10
5
2
2θ
22.1 Å
(A)
23.9 Å
(B)
12.1 Å
12.6 Å
12.6 Å
24.2 Å
(C)
10
5
2
2θ

the bulky ligand molecules. On the other hand, substitution of $P\text{-}P^+$ for only one CO molecule leads to molecules with a less strained configuration and results in exchanged clays with higher spacings. The observed differences in interlayer expansion might also be due to the way the intercalated clusters are oriented toward the silicate sheets.

The intercalated metal carbonyl complexes were characterized by comparison of their carbonyl infrared spectra with those in solution (Table 10, Figures 15-19). The close similarity in band positions and relative intensities suggest that the cationic clusters remain unchanged upon intercalation, the interaction between host and intercalate being electrostatic. In addition to the CO absorptions and bands characteristic of the silicate framework, the infrared spectra of the clay-intercalates exhibit absorptions due to the $P\text{-}P^+$ ligand (Figure 13).

Another indication of the retention of chemical and structural constitution of the cluster complexes upon intercalation was provided by comparison of their electronic spectra with those obtained in solution. The transitions associated with M-M bonds in the cluster framework of the complexes are observed in the electronic spectra of the exchanged minerals and their molecular analogs (Table 11). The small deviation in λ_{max} between the intercalated clusters and those in solution can be attributed to the interaction of the former with the negatively charged silicate sheets, as well as to changes in the solvation environment.

The hectorite intercalated metal cluster complexes were further characterized by elemental analysis. The metal to phosphorus ratios, obtained by chemical analysis, were in good agreement with those predicted theoretically (Table 14). The loadings reported in the Table correspond to 26 to 82 meq/100 g of clay.

Figure 15: Infrared spectra in the CO stretching region of unsupported and hectorite-intercalated $Ru_3(CO)_9(P\text{-}P^+)_3$: (a) $Ru_3(CO)_9(P\text{-}P^+)_3(BF_4)_3$ in CH_2Cl_2 solution; (b) $Ru_3(CO)_9(P\text{-}P^+)_3$—hectorite (KBr pellet).

Figure 16: Infrared spectra in the CO stretching region of unsupported and hectorite-intercalated $H_4Ru_4(CO)_8(P\text{-}P^+)_4$: (a) $H_4Ru_4(CO)_8(P\text{-}P^+)_4(BF_4)_4$ in CH_2Cl_2 solution; (b) $H_4Ru_4(CO)_8(P\text{-}P^+)_4$-hectorite (KBr pellet).

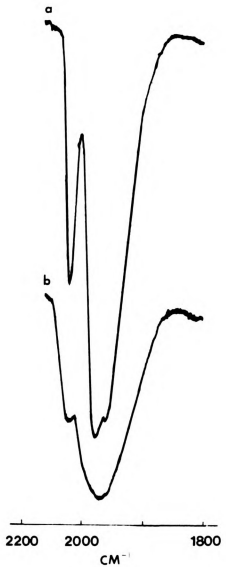

Figure 15

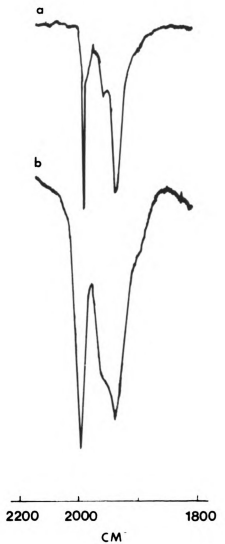

Figure 16

Figure 17: Infrared spectra in the terminal and bridging CO stretching region of unsupported and hectorite-intercalated $Ir_4(CO)_9(P\text{-}P^+)_3$: (a) $Ir_4(CO)_9(P\text{-}P^+)_3(BF_4)_3$ in CH_2Cl_2 solution; (b) $Ir_4(CO)_9(P\text{-}P^+)_3$-hectorite (KBr pellet).

Figure 18: Infrared spectra in the CO stretching region of unsupported and hectorite-intercalated $Os_3(CO)_{11}(P\text{-}P^+)$: (a) $Os_3(CO)_{11}(P\text{-}P^+)BF_4$ in CH_2Cl_2 solution; (b) $Os_3(CO)_{11}(P\text{-}P^+)$—hectorite (KBr pellet).

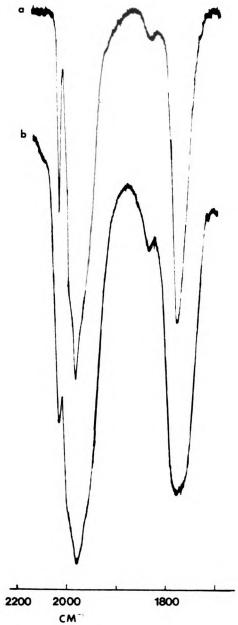

Figure 17

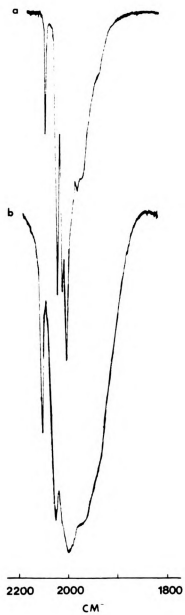

Figure 18

Figure 19: Infrared spectra in the CO stretching region:

(a) $H_2Os_3(CO)_{10}(P\text{-}P^+)(BF_4)$ in CH_2Cl_2 solution;

(b) $H_2Os_3(CO)_{10}(P\text{-}P^+)$-hectorite (KBr pellet);

(c) $H_2Os_3(CO)_9(P\text{-}P^+)(BF_4)$ in CH_2Cl_2 solution;

(d) $H_2Os_3(CO)_9(P\text{-}P^+)$-hectorite (KBr pellet).

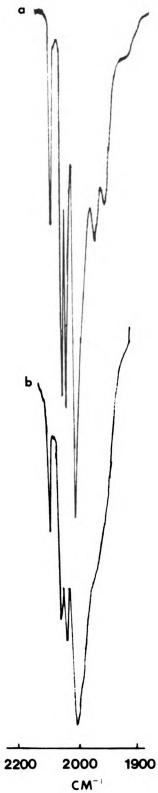
a
b
2200
2000
1900
CM⁻¹

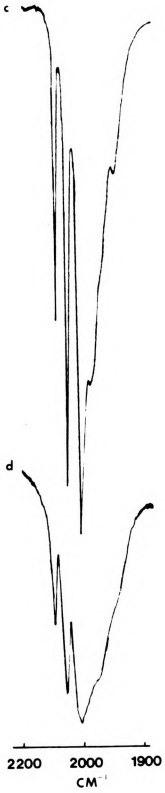
c
d
2200
2000
1900
CM⁻¹

Table 14

Elemental Analysis of Hectorite-Intercalated Cluster Carbonyls

System	wt%				M/P mole ratio	
	Ru	Ir	Os	P	Found	Calcd
$H_4Ru_4(CO)_8(P\text{-}P^+)_4$-hectorite	4.32			2.41	0.53	0.50
$Ru_3(CO)_9(P\text{-}P^+)_3$-hectorite	5.47			2.89	0.57	0.50
$Ir_4(CO)_9(P\text{-}P^+)_3$-hectorite		9.72		2.39	0.66	0.67
$H_2Os_3(CO)_9(P\text{-}P^+)$-hectorite			19.27	2.17	1.45	1.50
$Os_3(CO)_{11}(P\text{-}P^+)$-hectorite			10.92	1.31	1.37	1.50

2. Polarized Infrared Studies of $H_4Ru_4(CO)_8(P\text{-}P^+)_4$-Hectorite

Tetrasubstituted phosphine derivatives of the type $H_4Ru_4(CO)_8L_4$ with an even distribution of the phosphine ligands on the ruthenium atoms possess D_{2d} symmetry. Such a structure would exhibit three infrared-active CO stretching vibrations (B_2+2E) as shown in Figure 16 and Table 10. The weak band at about 1920 cm^{-1} is attributed to ^{13}C isotopic substitution[140]. The stretching frequency of B_2 symmetry is polarized in the z-direction while the doubly degenerate mode is x,y polarized.

The geometry of the molecule is preserved upon intercalation and the IR spectrum of $H_4Ru_4(CO)_8(P\text{-}P^+)_4$-hectorite, as an oriented film, exhibits CO absorptions at 2002 s, 1964 m, and 1942 s cm^{-1} (Figure 20). Because of the simplicity of the infrared pattern, we undertook a study to determine whether the intercalated molecules align themselves in a certain orientation towards the silicate sheets. Highly oriented films are built by stacking alternate arrays of silicate layers and interlayer cations in the crystallographic c-dimension. In a typical experiment the clay c-dimension is parallel to the IR beam ($\theta = 0°$). By rotating the clay film ($\theta \neq 0°$) the absorption that is polarized along an axis parallel to the c-dimension should increase in intensity while the bands polarized along the other two axes are expected to decrease.

The infrared spectra of $H_4Ru_4(CO)_8(P\text{-}P^+)_4$-hectorite for different angles towards the beam are shown in Figure 20. Since we observe no significant changes in the three CO absorptions we conclude that the clusters do not adopt any specific orientation but rather are intercalated in a random fashion.

Figure 20: Infrared absorbance spectra in the CO stretching region of $H_4Ru_4(CO)_8(P\text{-}P^+)_4$-hectorite at different angles of clay film relative to the direction of the IR beam: (a) $\theta = 90°$. The IR beam is perpendicular to the clay film; (b) $\theta = 110°$; (c) $\theta = 130°$.

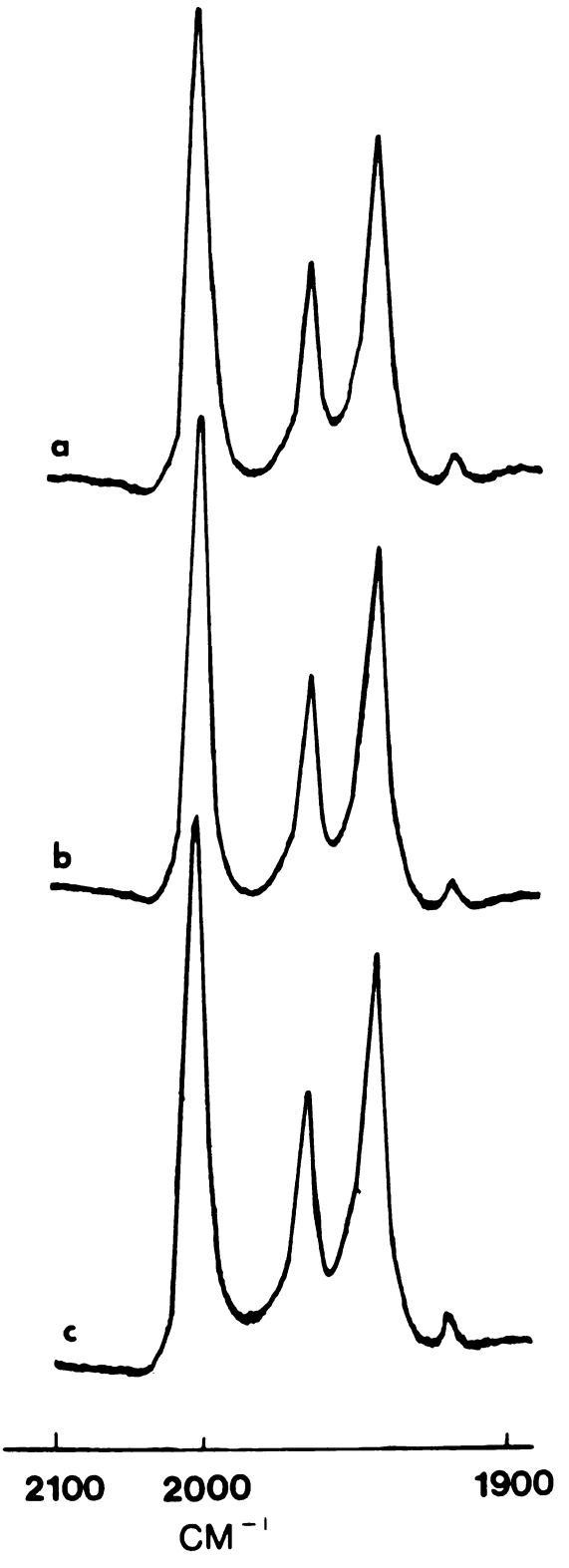
a
b
c
2100
2000
1900
CM⁻¹

3. Olefin Isomerization by Homogeneous and Hectorite-Intercalated $H_2Os_3(CO)_9(P\text{-}P^+)$ Catalysts.

The decarbonylation of $H_2Os_3(CO)_{10}(P\text{-}P^+)BF_4$ in refluxing methanol and $H_2Os_3(CO)_{10}(P\text{-}P^+)$-hectorite under vacuum at 80°C yields $H_2Os_3(CO)_9(P\text{-}P^+)BF_4$ and $H_2Os_3(CO)_9(P\text{-}P^+)$-hectorite, respectively, the resulting products having been identified by their infrared spectra (Figure 19, Table 10). Our results parallel those obtained for molecular and supported triosmium hydride carbonyl clusters, designated as $H_2Os_3(CO)_{10}PPh_3$ and $H_2Os_3(CO)_{10}PPh_2$-Support, which are known to lose CO on heating and become coordinatively unsaturated[67,107,108]. Because of their coordinative unsaturation they are able to react with electron pair donors such as acetylene and olefins.

We found both homogeneous and clay-intercalated triosmium clusters to be active olefin isomerization catalysts. Catalytic reactions of the soluble salt were carried out at ambient temperature and pressure in acetone without exclusion of air by using an initial substrate to cluster mole ratio of 800. 1-Hexene was isomerized to cis- and trans-2-hexene under homogeneous conditions producing 3300 moles of internal olefin per mole of triosmium cluster prior to catalyst cessation. After reaction the color of the solution had changed from deep green to yellow and the infrared spectrum indicated the presence of the saturated $HOs_3[CH_3(CH_2)_3CH{=}CH_2](CO)_9(P\text{-}P^+)BF_4$ with a bridging vinyl ligand[107] (Table 10).

Figure 21 illustrates the results for 1-hexene isomerization with $H_2Os_3(CO)_9(P\text{-}P^+)$-hectorite under the same reaction conditions used for the homogeneous catalyst. The dramatic difference in reaction rates for the three different solvents can be related to the extent of interlayer swelling. Among the three, toluene is the poorest swelling solvent and exhibits the

Figure 21: Isomerization of 1-hexene (1-3.3 M) to 2-hexene with $H_2Os_3(CO)_9(P\text{-}P^+)$-hectorite (0.01 mmol) in three different liquid media at ambient temperature and pressure. The clay catalyst contained 2.17 wt% P and 19.27 wt% Os.

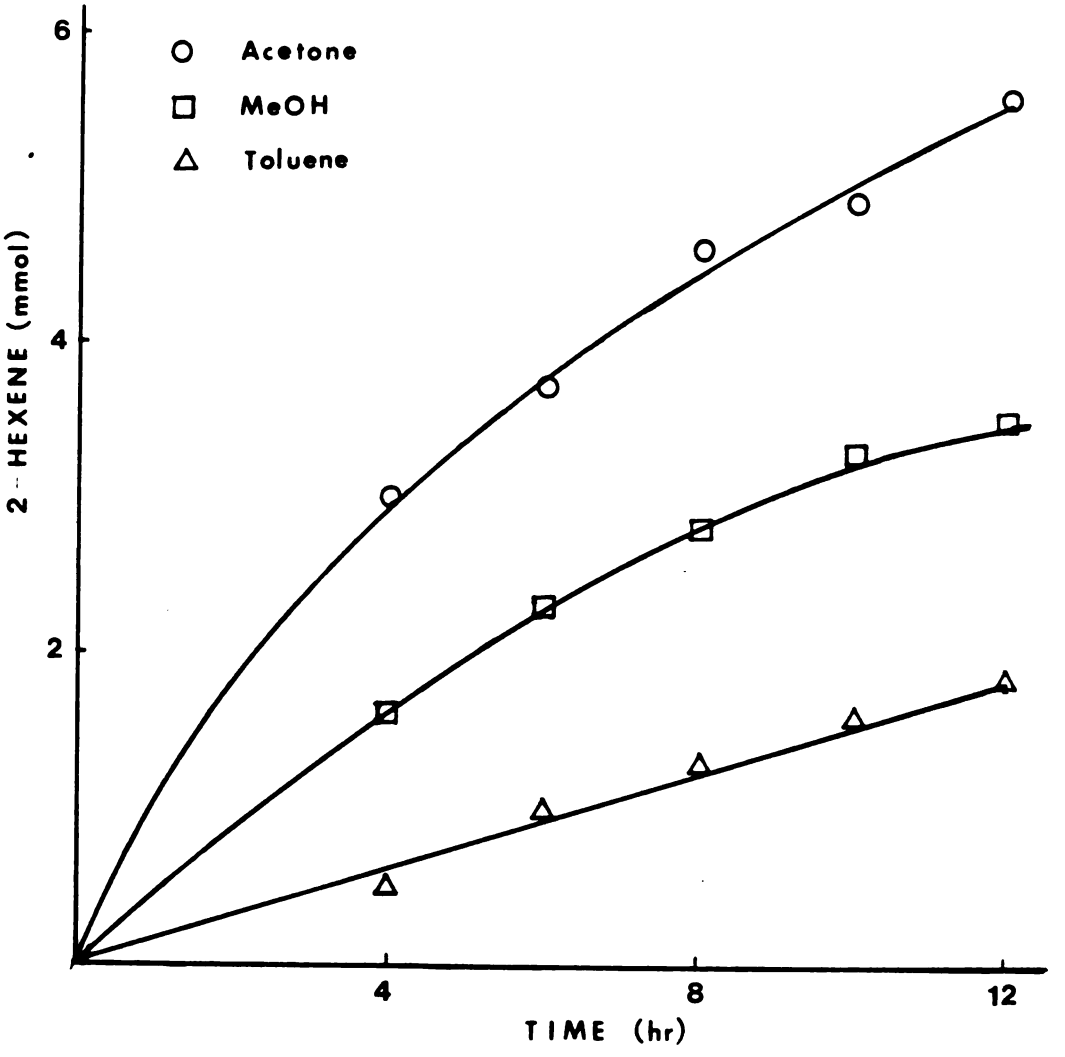
6
4
2
2-HEXENE (mmol)
Acetone
MeOH
Toluene
4
8
12
TIME (hr)

slowest rate. Contrary to previous results with clay-intercalated catalysts, we observe some catalytic activity that can be attributed to the large 00ℓ spacing observed for the mineral. In other words, the cationic complex acts as its own pillar making the interlayer accessible to substrate molecules even in the absence of a swelling solvent. The relative rate for the intercalated catalyst is higher in acetone than that observed in methanol, consistent with the differences in 00ℓ spacing obtained by solvating the mineral in these two solvents[141,161].

In all three reactions the color of the clay changed from deep green to shiny yellow, after which time the catalyst was no longer active. It can be inferred from the IR spectrum that catalytic cessation is due to the formation of a saturated complex. A similar complex with a bridging vinyl group is formed when acetylene is passed through a suspension of the intercalated catalyst in acetone (Table 10).

During the course of the reaction in methanol, but not acetone or toluene, a small amount of the metal complex is desorbed into the solution. Since electrical neutrality must be maintained within the clay, the desorbed complex most likely is not cationic. To investigate further the role of methanol we examined the desorption of clusters from hectorite in the absence of substrate. After stirring the clay suspension overnight in methanol, the color of the mineral changed from green to yellow, and a portion of the cluster was desorbed into the solution. No isomerization to internal olefin was observed when 1-hexene was added to this slurry. The infrared spectrum of the intercalated catalyst resembled that of the inactive catalyst obtained after reaction with the substrate. This observation suggests saturation of sites by methanol ligands in a manner analogous to that of the Os vinylidene complex. Furthermore, the spectrum of the filtrate exhibited terminal

CO bands at 2113 w, 2090 m, 2051 m, 2002 vs, 1940 m, br cm^{-1}, and no absorptions characteristic of the $P\text{-}P^+$ ligand. The complex pattern of the IR spectrum is an indication that the cluster remains intact.

Catalyst desorption may be atrributed to ligand dissociation and coordination of solvent molecules. Solvent coordination has been proposed to occur for some photoreactions of tungsten hexacarbonyl in methanol, though the product has not been isolated[143]. Dissociated $P\text{-}P^+$ molecules satisfy the negative charge of the silicate layers:

$$\underline{\overline{\text{H}_2\text{Os}_3(\text{CO})_9(\text{P-P}^+)}} \xrightarrow{\text{MeOH}} \underline{\overline{\text{P-P}^+}} + \text{metal cluster carbonyl (soln)} \quad (21)$$

The remaining intercalated clusters are incapable of isomerizing 1-hexene because they are coordinatively saturated with solvent molecules.

No desorption of catalyst was observed when either acetone or toluene was used as solvating agent. The filtrate after catalytic reaction exhibits neither catalytic activity nor IR absorptions in the CO stretching region. The reaction of the toluene-solvated intercalated catalyst at ambient temperature and pressure exhibits pseudo first-order behavior with K_{obs} = 0.022 h^{-1}. No homogeneous reaction was run in toluene because of the insolubility of the cluster in this solvent. For acetone and methanol a pseudo first-order behavior was not obtained, suggesting catalyst decomposition competes with the isomerization reaction.

In another series of experiments some data on the kinetics of 1-hexene isomerization, catalyzed by $H_2Os_3(CO)_9(P\text{-}P^+)$-hectorite in toluene at 75°C, were obtained. No catalyst decomposition was observed during the course of the reaction. We found the rate of the reaction to be proportional to the concentration of olefin as well as the concentration of the catalyst,

in agreement with results obtained by Gates and co-workers[107] for 1-pentene isomerization in the presence of $H_2Os_3(CO)_{10}$ in toluene at 75°C. In the same report these authors claimed that the silica supported catalyst was more stable than its soluble analog, yielding approximately 10^3 molecules of internal olefin per mole of cluster prior to catalytic cessation. In the present study, both the intercalated and soluble catalysts exhibited almost the same turnover number (3300 moles olefin/mole cluster), which is more than three times as large as the value obtained for the silica supported triosmium cluster. The similarity between soluble and intercalated catalysts is additional evidence that in sufficiently swollen smectites intercalated catalysts exhibit solution-like properties and do not lose appreciable activity compared to their homogeneous counterparts. The higher activity observed for the clay-intercalated triosmium cluster illustrates the advantage of using electrostatically supported catalysts. Immobilization of a metal complex through a covalent attachment will always reduce its mobility and consequently its catalytic activity.

The soluble and supported triosmium hydride clusters are the only examples for which well-established catalytic cycles involving a cluster complex have been proposed[67,107,108]. The overall catalytic cycle is illustrated in Figure 22. Our results are in agreement with previous observations[67,107] that during the reaction neither cluster fragmentation nor metal aggregation takes place, the catalyst being the intact cluster itself.

4. Thermal Stability of Hectorite-Intercalated Metal Cluster Carbonyls and Interaction with H_2 and O_2.

Decarbonylation of immobilized metal cluster carbonyl complexes leads to highly dispersed metallic particles on both organic and inorganic

Figure 22: Catalytic cycle for isomerization of α-olefins catalyzed by triosmium clusters[67,107]. The carbonyl ligands are omitted for simplicity. The $HOs_3(vinyl)(CO)_{10}$ is catalytically inactive.

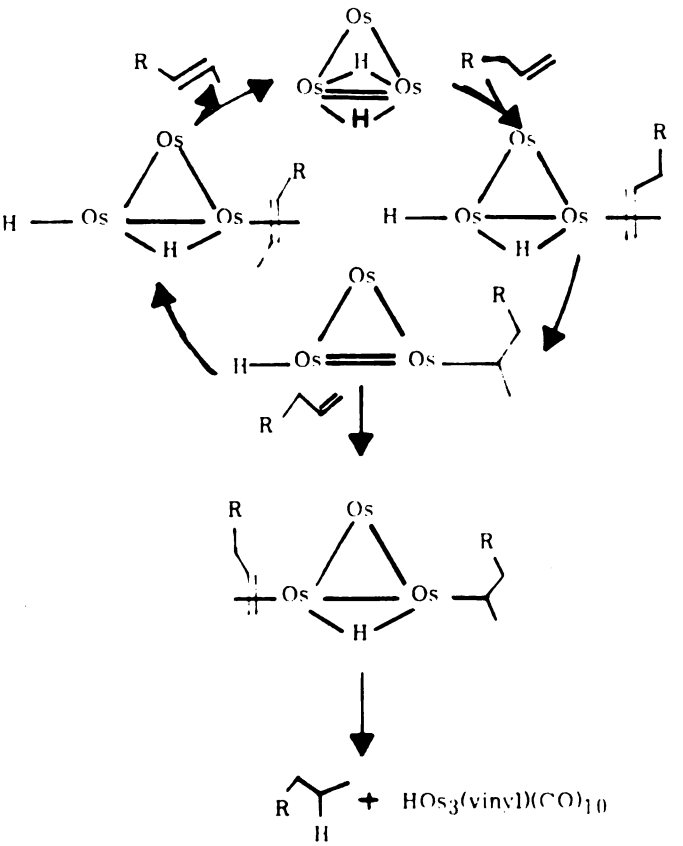

M.B. Freeman, M.A. Patrick and B.C. Gates, J. Catal., 73, 82 (1982).

supports[86,87]. Studies on the thermostability of the supported complexes usually yield valuable information in evaluating their catalytic properties. Characterization of the different subcarbonyl species can be accomplished by IR spectroscopy, the carbonyl absorptions serving as a fingerprint of the various metal species.

Figures 23 through 30 illustrate the effects of heating the clay-intercalated metal clusters under various conditions. Though unequivocal characterization of all metal subcarbonyl species is impossible at present due to the lack of soluble analogs exhibiting the same IR absorptions, an attempt will be made to rationalize the results obtained on thermolysis or oxidation. Simultaneous decomposition of the $P\text{-}P^+$ ligand adds an extra barrier in correlating surface species with authentic reference compounds.

The decomposition of immobilized clusters on typical metal oxides is likely to involve initially reaction of the metal atoms with surface hydroxyl groups[115,134]. Decarbonylation produces coordinatively unsaturated metal atoms, which in turn interact strongly with the support. In this case fragmentation and/or oxidation of the metal atoms can be anticipated. Complete decarbonylation would result in the formation of metal silicates or, when thermolysis is carried out in a H_2 environment, metal aggregates.

However, only the edge surfaces of clays are hydroxylated. This distinguishes edge sites from basal planes which are composed of siloxane-type oxygen atoms. Heating a clay film could cause migration of the metal clusters or their fragments from the interlayer region, where they are initially located, to the edges and reaction with surface hydroxyl groups. Such migration is in agreement with the observed reduction in 001 spacing to a value of approximately 16 Å after heating the clay sample above 200°C. The higher thermostability obtained for the intercalated carbonyl clusters compared

Figure 23: Infrared spectra in the CO stretching region of products formed by thermal decomposition of $Ru_3(CO)_9(P\text{-}P^+)_3$—hectorite: (a) $Ru_3(CO)_9(P\text{-}P^+)_3$-hectorite (film); (b) sample (a) after heating in vacuum at 110°C for 11 h; (c) followed by heating at 200°C for 9 h; (d) 300°C for 10 h; (e) sample (a) after heating in H_2 at 200°C for 10 h; (f) followed by heating at 300°C for 11 h.

Figure 24: Infrared spectra in the CO stretching region of products formed by oxidation of $Ru_3(CO)_9(P\text{-}P^+)_3$-hectorite in air: (a) $Ru_3(CO)_9(P\text{-}P^+)_3$-hectorite (film); (b) sample (a) exposed to air for 2 months; (c) sample (a) after heating in air at 110°C for 10 h; (d) followed by heating at 200°C for 45 min; (e) 200°C for 90 min; (f) 200°C for 3½ h; (g) 200°C for 10 h; (h) 300°C for 1 h.

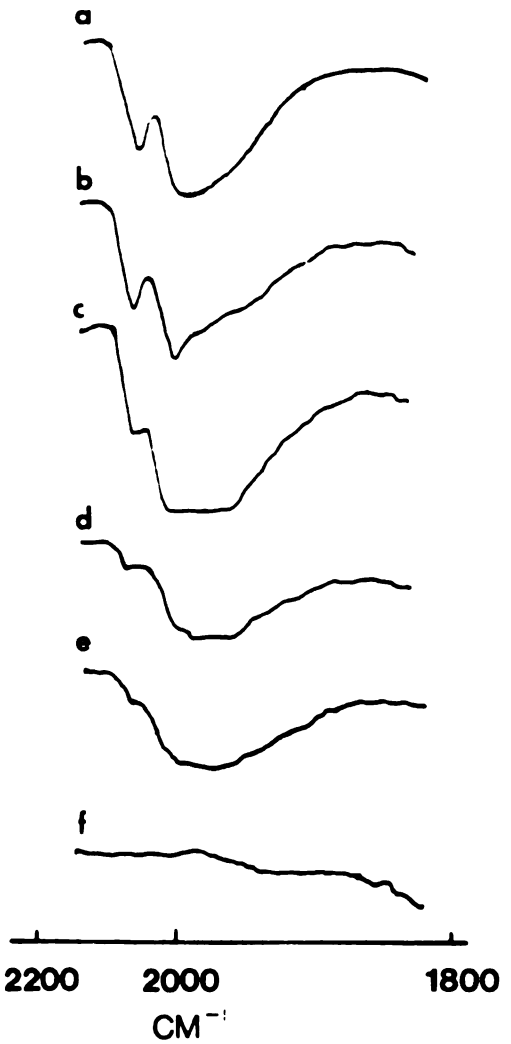

Figure 23

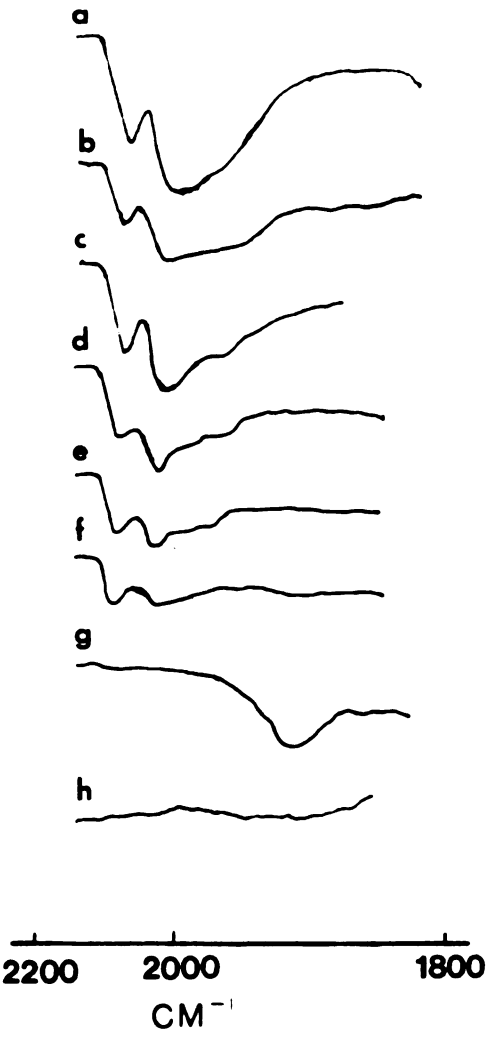

Figure 24

Figure 25: Infrared spectra in the CO stretching region of products formed by thermal decomposition of $H_4Ru_4(CO)_8(P\text{-}P^+)$—hectorite: (a) $H_4Ru_4(CO)_8(P\text{-}P^+)_4$-hectorite (film); (b) sample (a) after heating in vacuum at 110°C for 11 h; (c) followed by heating at 200°C for 9 h; (d) 300°C for 10 h; (e) sample (a) after heating in H_2 at 200°C for 10 h; (f) 300°C for 11h.

Figure 26: Infrared spectra in the CO stretching region of products formed by oxidation of $H_4Ru_4(CO)_8(P\text{-}P^+)_4$-hectorite in air: (a) $H_4Ru_4(CO)_8(P\text{-}P^+)_4$-hectorite (film); (b) sample (a) after heating in air at 110°C for 10 h; (c) followed by heating at 200°C for 45 min; (d) 200°C for 90 min; (e) 200°C for 3½ h; (f) 200°C for 10 h; (g) 300°C for 1 h.

Figure 27: Infrared spectra in the CO stretching region of products formed by thermal decomposition of $Ir_4(CO)_9(P\text{-}P^+)_3$—hectorite: (a) $Ir_4(CO)_9(P\text{-}P^+)_3$-hectorite (film); (b) sample (a) after heating in vacuum at 200°C for 9 h; (c) followed by heating at 300°C for 10 h; (d) sample (a) after heating in H_2 at 200°C for 10 h; (e) 300°C for 11 h.

Figure 28: Infrared spectra in the CO stretching region of products formed by oxidation of $Ir_4(CO)_9(P\text{-}P^+)_3$-hectorite in air: (a) $Ir_4(CO)_9(P\text{-}P^+)_3$-hectorite (film); (b) sample (a) after heating in air at 110°C for 10 h; (c) followed by heating at 200°C for 45 min; (d) 200°C for 10 h; (e) 300°C for 1 h.

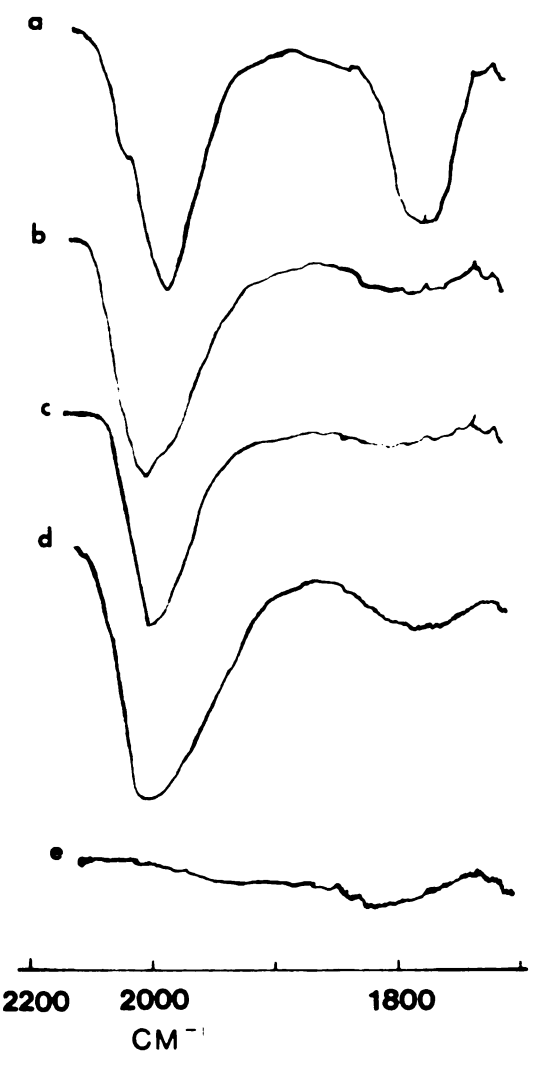

Figure 27

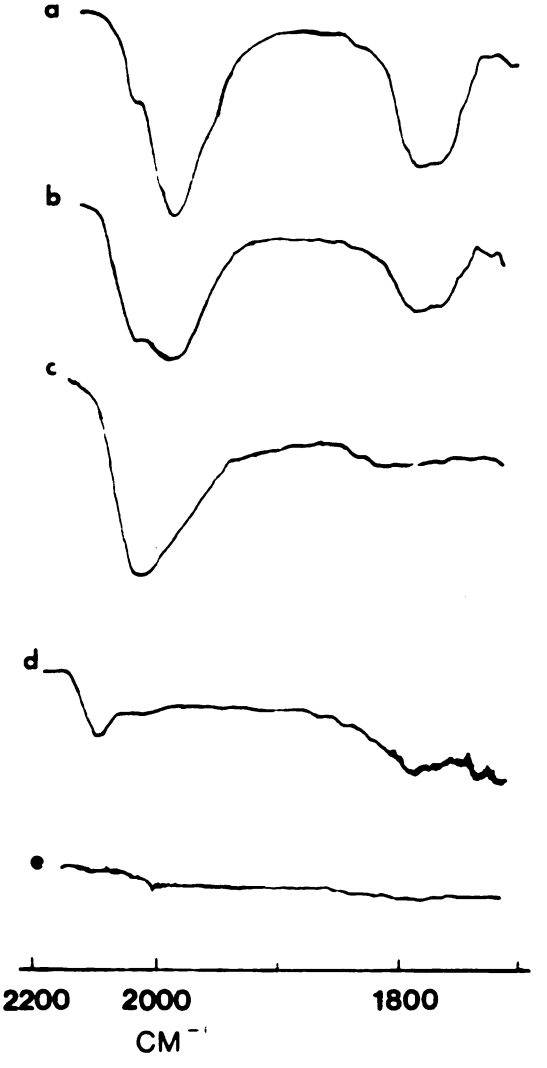

Figure 28

Figure 29: Infrared spectra in the CO stretching region of products formed by thermal decomposition of $Os_3(CO)_{11}(P\text{-}P^+)$—hectorite: (a) $Os_3(CO)_{11}(P\text{-}P^+)$-hectorite (film); (b) sample (a) after heating in vacuum at 200°C for 9 h; (c) followed by heating at 300°C for 10 h; (d) sample (a) after heating in H_2 at 200°C for 10 h; (e) 300°C for 11 h.

Figure 30: Infrared spectra in the CO stretching region of products formed by oxidation of $Os_3(CO)_{11}(P\text{-}P^+)$-hectorite in air: (a) $Os_3(CO)_{11}(P\text{-}P^+)$-hectorite (film); (b) sample (a) after heating in air at 110°C for 10 h; (c) followed by heating at 200°C for 45 min; (d) 200°C for 90 min; (e) 200°C for 10 h; (f) 300°C for 1 h.

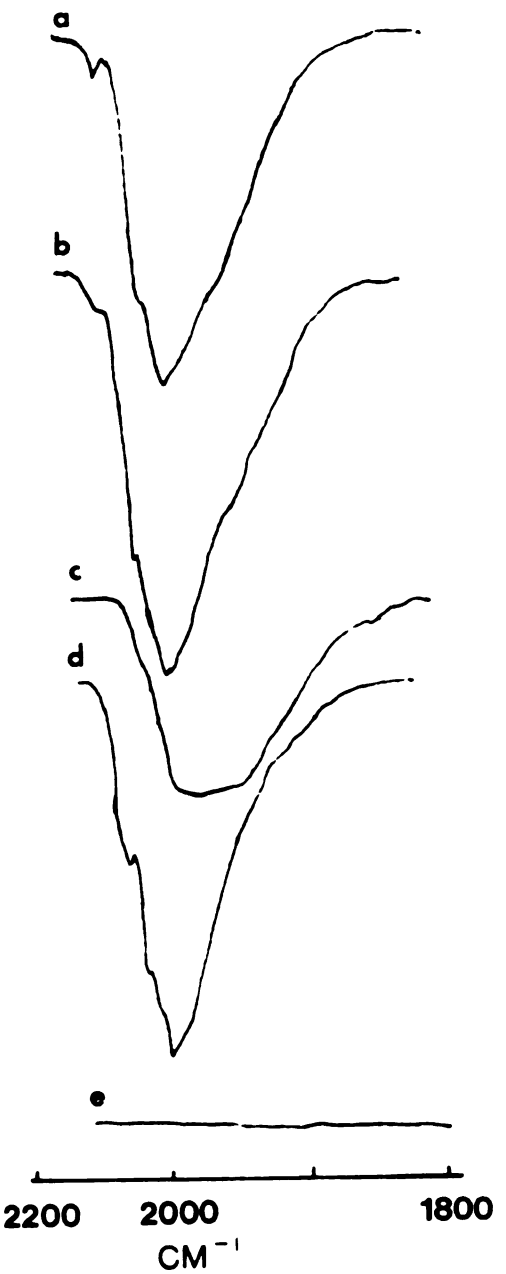

Figure 29

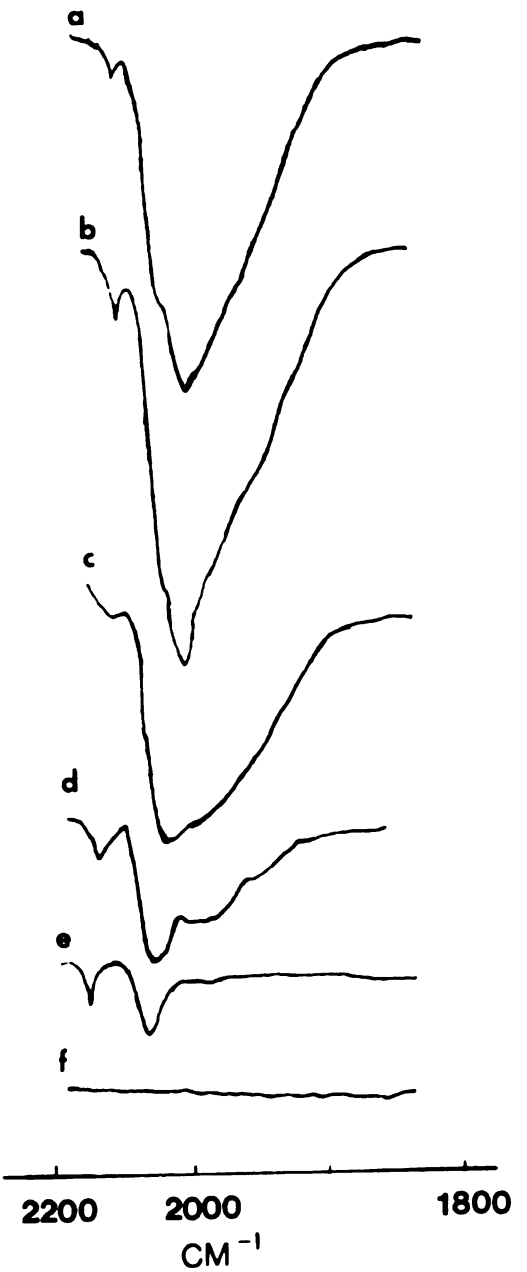

Figure 30

to their silica supported analogs is also in agreement with the proposed decomposition mechanism. Though oxidative degradation of the cluster by surface hydroxyl groups appears to be the principal decomposition process, adsorbed water or oxygen might be involved as well[128].

When $Ru_3(CO)_9(P\text{-}P^+)_3$-hectorite (designated hereafter Ru_3-HEC) is exposed to air at ambient temperature for a long time or heated in vacuum or in flowing O_2 (Figures 23 and 24) a similar spectral pattern is obtained. By analogy to the silica supported systems the bands located at 2060-2070 and 2000-2015 cm^{-1} can be assigned to two surface structures of the type $[Ru(CO)_2LX_2]_n$ or $[Ru(CO)_2X_2]_n$ in which L represents the phosphine ligand and X are likely to be oxygen atoms of the support. The band at 1950-1960 cm^{-1} is probably due to another surface species. The value of n, which depends on metal aggregation, cannot be specified on the basis of the present results. Persistent oxidation at 200°C leads to another species with a low frequency absorbance, most likely a species having one carbonyl per Ru atom. As the number of CO ligands decreases the availability of Ru d electrons for back bonding increases, shifting the CO absorbances to lower frequencies[144]. In the absence of O_2 the bands attributed to oxidized Ru species are less resolved and in the presence of H_2 the main surface structure is that exhibiting a broad band at 1960 cm^{-1}, further supporting our assignment. At 300°C decarbonylation is complete and Ru silicates or metal crystallites are likely to be formed. No attempt was made to identify metal aggregates by x-ray diffraction.

$H_4Ru_4(CO)_8(P\text{-}P^+)_4$-hectorite behaves similarly to Ru_3-HEC (Figures 25,26), though decomposition begins at much higher temperatures. The higher thermostability of the former has been attributed to its higher nuclearity[115].

Table 15

Vibrational Frequencies for Some Carbonyl Metal Complexes

Compound	ν(CO) cm^{-1}	Ref.
$RuI_2(CO)_2(PPh_3)$	2061 s, 2005 s	136
$[Ru(CO)_2I_2]_n$	2050 s, 1995 s, 1975 w(sh)	146
$[Ru(CO)_3I_2]_2$	2116 m, 2059 s, 2009 m	146
$Os(CO)_3(PEt_3)Cl_2$	2144 w, 2070 vs, 2023 s	147
$[Os(CO)_2(PPh_3)Cl_2]_2$	2051 s, 1981 s	147
$[Os(CO)_3I_2]_2$	2118 s, 2050 vs	127
$[Os(CO)_2I_2]_n$	2112 w, 2039 s(br), 1980 s(br)	127

At approximately 200°C $Ir_4(CO)_9(P\text{-}P^+)_3$-hectorite preferentially loses bridging carbonyls on heating in H_2 or under vacuum (Figure 27) as indicated by the loss of CO intensity in the region of approximately 1800 cm^{-1}, in agreement with results reported for $[Ir_4(CO)_9(PPh_3)_2PPh_2(CH_2)_3SIL]$, though decarbonylation of the latter starts at lower temperatures (approximately 100°C)[129]. Metal aggregation seems to be unlikely, but cannot be ruled out, because CO chemisorbed on Ir metal aggregates is expected to show broad bands in the 2050-2070 cm^{-1} region[145]. However, as the ligand coverage decreases, the absorbances shift to lower frequencies (1995-2030 cm^{-1})[134]. When the intercalated cluster is heated in O_2 the two-band pattern is believed to arise from a dicarbonyl iridium(I) species (Figure 28).

Evacuation of $Os_3(CO)_{11}(P\text{-}P^+)$-hectorite at 300°C leads to decomposition (Figure 29) and the spectrum resembles that reported for heated $[Os_3(CO)_{11}PPh_2(CH_2)_2SIL]$[120]. In the presence of H_2 a hydride is likely to be formed. Oxidation at 200°C leads to the appearance of new surface structures (Figure 30). At an early stage of decomposition there are probably two different species present. The bands at 2040 and 1990 cm^{-1} can be assigned to surface structure $[Os_3(CO)_2LX_2]_n$, while those at 2140 and 2060 cm^{-1} to $[Os(CO)_xX_2]_n$, (x = 2,3). Oxidation at 300°C leads to oxidized Os on the surface of the clay.

C. Cluster Carbonyl Interactions with Alumina Pillared Clay (ALPILC)

Polyoxocation pillared clays constitute a new class of highly stable materials characterized by fixed porosity, high surface area, and intracrystal acidity. In this portion of the dissertation discussion centers at infrared spectroscopy that was used to elucidate the interactions of $Os_3(CO)_{12}$, $Ru_3(CO)_{12}$, $H_2Os_3(CO)_{10}$, $H_4Ru_4(CO)_{12}$, $Ir_4(CO)_{12}$ and $[CpFe(CO)_2]_2$ with

alumina pillared clay. The same technique also allowed characterization of the metal surface species formed on thermal treatment under various conditions. An alumina pillared clay was prepared by reaction of Na^+-montmorillonite with aluminum chlorohydrate solution, as described previously (Section II.C.5), and allowed to equilibrate with air before use.

1. Adsorption of $Os_3(CO)_{12}$ on ALPILC

When $Os_3(CO)_{12}$ (0.02 mmol) in 40 ml CH_2Cl_2 is added under Argon to alumina pillared clay (0.5 g) which has been dried in vacuo at room temperature for 4 h, the mineral, after removal of the weakly adsorbed Os clusters by washing, exhibits IR carbonyl bands at 2134 s, 2100 s, 2074 vs, 2061 s, and 2023 m cm^{-1}. This set of bands, considered to belong to a single species, is nearly identical in frequency and intensity to that of $[HOs_3(CO)_{12}][PF_6]$ in $MeNO_2$ (Figure 31, Table 16). The Os loading of the dry mineral is 0.38 wt%.

The electronic spectrum of this material shows a maximum at 374 nm, whereas a value of 366 nm is observed for the molecular analogue $[HOs_3(CO)_{12}][PF_6]$ (Table 17). The small deviation in λ_{max} between intercalated and molecular cluster can be attributed to interactions with the negatively charged mineral and changes in its solvation environment.

It is noteworthy to point out that, if the impregnation of ALPILC is carried out in the presence of air, no significant carbonyl adsorption is observed after washing the support with CH_2Cl_2. The protonated osmium clusters are not stable in moist air and deprotonate, producing the neutral carbonyl[65].

The inability to extract $HOs_3(CO)_{12}^+$ from the surface of the pillared clay by a more polar solvent such as $CHCl_3$ or acetone is in agreement with its cationic character. However, it is possible to extract the protonated cluster by ion exchange with a solution of KPF_6 in acetone, presumably

Figure 31: Infrared spectra in the CO stretching region: (a) $HOs_3(CO)_{12}^+$/-ALPILC prepared by impregnation with $Os_3(CO)_{12}$ (mull); (b) $[HOs_3(CO)_{12}]PF_6$ in $MeNO_2$ solution; (c) sample (a) exposed to air at RT for 5 h (mull); (d) $Os_3(CO)_{12}$ in CH_2Cl_2 solution; (e) sample (c) after heating in vacuum at 100°C for 2 h (mull); (f) 250°C for 6 h; (g) sample (c) after heating in air at 110°C for 12 h.

Table 16

Infrared CO Bands of Molecular and ALPILC-Intercalated Metal Cluster Complexes

Compound	ν(CO) cm^{-1}	Reference
$[HOs_3(CO)_{12}]^+$/ALPILC[a]	2134 s, 2100 s, 2074 vs 2061 s, 2023 m	This work
$[HOs_3(CO)_{12}][PF_6]$[b*]	2134 s, 2101 s, 2077 vs 2058 s, 2018 m	This work
$[HOs_3(CO)_{12}][PF_6]$[b]	2135 s, 2102 s, 2080 s 2061 s, 2021 m	65
$[HOs_3(CO)_{12}][PF_6]$[b**]	2133 s, 2098 s, 2073 vs 2063 s, 2022 m	This work
$Os_3(CO)_{12}$/ALPILC[a#]	2068 s, 2034 s, 2014 m 2001 m	This work
$Os_3(CO)_{12}$[c]	2068 vs, 2034 s, 2013 m 2000 m	This work
$[HRu_3(CO)_{12}]^+$/ALPILC[a]	2128 s, 2099 s, 2077 vs 2060 s, 2030 s	This work
$[HRu_3(CO)_{12}][PF_6]$[b*]	2128 s, 2100 s, 2077 vs 2062 s, 2025 m	This work
$[HRu_3(CO)_{12}][PF_6]$[b]	2129 s, 2102 s, 2081 s 2068 sh, 2030 m	65
$[HRu_3(CO)_{12}][PF_6]$[b**]	2126 s, 2098 s, 2076 vs 2059 s, 2027 m	This work
$Ru_3(CO)_{12}$/ALPILC[a#]	2060 vs, 2029 s, 2010 m	This work
$Ru_3(CO)_{12}$[c]	2061 vs, 2029 s, 2011 m	This work
$HOs_3(CO)_{10}$(O-Al<)[a]	2101 m, 2068 vs, 2056 vs, 2019 s, 2005 m	This work
$HOs_3(CO)_{10}$(O-Al<)[d]	2107, 2068, 2055 2030	128
$HOs_3(CO)_{10}$(O-Al<)[d]	2107 w, 2068 s, 2056 s, 2023 vs, 2005 m	124

Table 16 continued

$HOs_3(CO)_{10}(O\text{-}Al<\ )$[d]	2107 w, 2067 s, 2055 s, 2027 vs, 2012 s (br)	127
$H_4Ru_4(CO)_{12}$/ALPILC[a]	2114 m, 2081 s, 2066 vs 2024 s	This work
$H_4Ru_4(CO)_{12}$[c]	2081 s, 2066 vs, 2024 s, 2009 m	This work
$Ir_4(CO)_{12}$/ALPILC[a]	2109 w, 2060 vs, 2026 s	This work
$Ir_4(CO)_{12}$[a]	2112 w, 2059 vs, 2020 s 2000 m	This work

a Nujol mull

b $MeNO_2$

c CH_2Cl_2

d Alumina disc

* Prepared in 98% H_2SO_4

** Isolated from the surface of ALPILC by exchange with KPF_6 in acetone

\# These samples were prepared from the corresponded protonated clusters by exposing the clay to moist air.

Table 17

Electronic Spectroscopy Data for Reaction Products and Reference Compounds

System	Solvent	λ_{max} (nm)
$[HOs_3(CO)_{12}]^+$/ALPILC[a]	mull	374
$[HOs_3(CO)_{12}][PF_6]$*	Acetone	366
$[HOs_3(CO)_{12}][PF_6]$**	Acetone	365
$Os_3(CO)_{12}$	CH_2Cl_2	385,329
$[HRu_3(CO)_{12}]^+$/ALPILC[b]	mull	410
$[HRu_3(CO)_{12}][PF_6]$*	Acetone	403
$[HRu_3(CO)_{12}][PF_6]$**	Acetone	401
$Ru_3(CO)_{12}$	CH_2Cl_2	392

* Prepared in 98% H_2SO_4

** Isolated from the surface of ALPILC by exchange with KPF_6 in acetone.

a Loading is 0.38 wt% Os

b Loading is 0.48 wt% Ru

according to the equation:

$$\underline{\underline{HOs_3(CO)_{12}^+}} \xrightarrow{KPF_6} \underline{\underline{K^+}} + HOs_3(CO)_{12}PF_6(soln) \qquad (22)$$

The yellow product was characterized by its infrared and electronic spectra as $[HOs_3(CO)_{12}][PF_6]$. Moreover, the presence of the proton was confirmed by the ^1H NMR resonance at -19.09 ppm.

When $HOs_3(CO)_{12}^+$ on ALPILC is exposed to air for a few hours, a new surface species is formed with terminal carbonyl absorptions at 2068 s, 2034 s, 2014 m, and 2001 m cm^{-1}, which are identical to those of $Os_3(CO)_{12}$ (Table 16, Figure 31). The similarity of the IR spectra along with the ability to extract the complex readily from the surface with CH_2Cl_2 suggests the new species to be $Os_3(CO)_{12}$ physisorbed on the support.

The presence of weakly adsorbed $Os_3(CO)_{12}$ on the surface of the mineral further supports our assignment of $HOs_3(CO)_{12}^+$ as the initial surface species. If there existed some other interaction involving loss of CO molecules and/or degradation of the cluster, the recovery of the neutral complex would have been impossible after exposure to air.

The protonated Os cluster can be reformed upon evacuation of the $Os_3(CO)_{12}$/ALPILC sample at 100°C for two hours. This reformation establishes the presence of an equilibrium between the two surface species which can be shifted in either direction by varying the water content of the mineral. A decrease in the amount of surface water increases the acidity of the support and favors the formation of the protonated cluster. On the other hand, increasing the amount of water on the surface by simple exposure to air diminishes the Bronsted acidity, which results in deprotonation to form neutral clusters.

When the $Os_3(CO)_{12}$/ALPILC sample is heated under vacuum at 150 to 300°C a new species is formed with IR carbonyl bands at 2032 s, 2045 vs and 1978 m cm^{-1} characteristic of ensembles of atomically dispersed $[Os(CO)_x(O\text{-}Al\lesssim)_2]_n$ (x = 2,3)[124,127,128]. This latter complex is believed to be formed after reaction of physisorbed $Os_3(CO)_{12}$ with surface hydroxyl groups with concomitant oxidation to divalent osmium. The same surface species is formed when the supported Os cluster is exposed to air for approximately two months, or when it is heated at 110°C for a few hours. IR spectra showed the dispersed mononuclear $[Os(CO)_x(O\text{-}Al\lesssim)_2]_n$ species to be stable under either vacuum or Ar at temperatures up to 300°C. At higher temperatures a progressive decarbonylation occurs with the formation of Os silicates.

2. Adsorption of $Ru_3(CO)_{12}$ on ALPILC

Adsorption of $Ru_3(CO)_{12}$ from a CH_2Cl_2 solution (5.1 x 10^{-3} M) onto ALPILC (0.5 g) leads again to a protonated surface species ($HRu_3(CO)_{12}^+$/ALPILC) with IR carbonyl bands at 2128 s, 2099 s, 2077 vs, 2060 s, and 2030s cm^{-1} (Figure 32, Table 16). The Ru loading of the dry mineral is 0.48 wt%. Both $Os_3(CO)_{12}$ and $Ru_3(CO)_{12}$ exhibit basic character and form fairly stable protonated clusters that can be isolated in the form of hexafluorophosphate salts. Since the intensity of the 2030 cm^{-1} band does not correlate well with that for the molecular analogue in $MeNO_2$, it is possible that some $Ru_3(CO)_{12}$, exhibiting an adsorption at 2029 cm^{-1}, is present along with the protonated surface cluster. This presence might be due to either fast deprotonation on the surface or very strong physisorption of Ru clusters, the latter factor inhibiting their extraction from the surface. The former seems the more realistic since $Ru_3(CO)_{12}$ is known to deprotonate faster in solution than its osmium cluster analogue. In addition, the electronic

Figure 32: Infrared spectra in the CO stretching region: (a) $HRu_3(CO)_{12}^+$/-ALPILC prepared by impregnation with $Ru_3(CO)_{12}$ (mull); (b) $[HRu_3(CO)_{12}]PF_6$ in $MeNO_2$ solution; (c) sample (a) exposed to air at RT for 5 h (mull); (d) $Ru_3(CO)_{12}$ in CH_2Cl_2 solution; (e) sample (a) exposed to air at RT for 24 h (mull); (f) sample (c) after heating in vacuum at RT for 24 h.

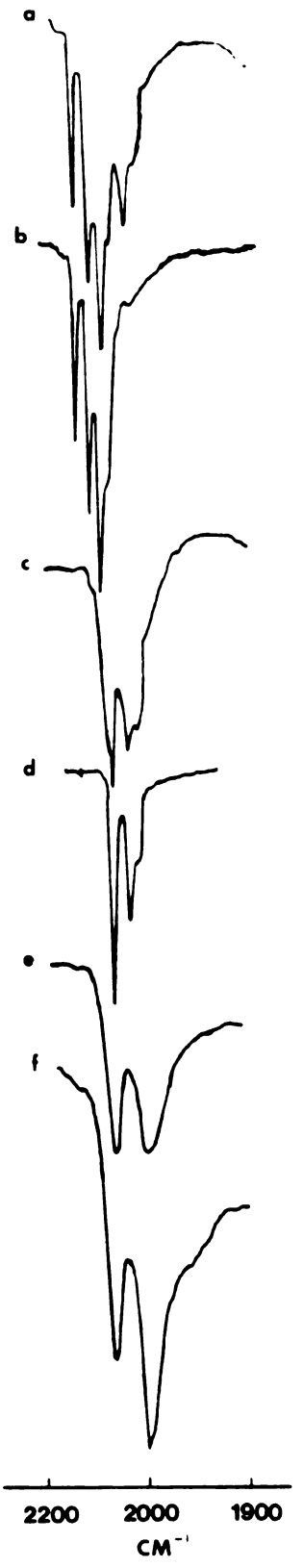
a
b
c
d
e
f
2200
2000
1900
CM⁻¹

spectrum of $HRu_3(CO)_{12}^+$/ALPILC exhibits a λ_{max} at 410 nm; the λ_{max} for $[HRu_3(CO)_{12}][PF_6]$ in acetone is 403 nm (Table 17).

In a parallel manner the protonated Ru surface species can be extracted from the support by using KPF_6 in acetone. The infrared and electronic spectra of the extracted ion agree well with those of $[HRu_3(CO)_{12}][PF_6]$. Moreover the NMR spectrum of the displaced ion exhibits a proton resonance at -18.67 ppm, in agreement with the -18.6 ppm reported for $[HRu_3(CO)_{12}][PF_6]$[65].

Though $Os_3(CO)_{12}$ refluxed in octane with alumina pillared montmorillonite for a few hours give rise only to the surface protonated cluster, $Ru_3(CO)_{12}$ under analogous conditions exhibits a more complex behavior. Thus, when $Ru_3(CO)_{12}$ is refluxed with the support in cyclohexane for about an hour, the infrared spectrum of this material exhibits the features of the protonated cluster superimposed on a broader spectrum. The latter might arise from some decomposition products.

When a $HRu_3(CO)_{12}^+$/ALPILC sample is exposed to air for a few hours the infrared spectrum exhibits at 2060 vs, 2029 s, and 2010 m cm^{-1} absorptions which are identical to those of $Ru_3(CO)_{12}$ (Table 16). Again, in the presence of moist air deprotonation with the formation of physisorbed Ru cluster molecules is observed. Prolonged exposure to air or treatment under vacuum at room temperature leads to anchored mononuclear ruthenium complexes[115-117] of the type $[Ru(CO)_2(O\text{-}Al\lessgtr)_2]_n$ with infrared absorptions at 2064 s and 1998 s cm^{-1}. The atomically dispersed ruthenium is formed by reaction of $Ru_3(CO)_{12}$ with surface hydroxyl groups. These species are not stable when heated in air and decarbonylation occurs to produce oxidized Ru atoms on the surface of the mineral.

3. Adsorption of $H_2Os_3(CO)_{10}$ on ALPILC

In the absence of air $H_2Os_3(CO)_{10}$ in CH_2Cl_2 (0.51×10^{-3} M) is adsorbed

on alumina pillared clay (0.5 g) to form two new surface species. The IR absorptions at 2101 m, 2068 vs, 2056 vs, 2019 s, and 2005 m cm^{-1} (Figure 33, Table 16) compare well with those reported for the surface bound hydridotriosmium cluster[124,127,128]. Additional bands at 2129 and 2032 cm^{-1} are assigned to a second species which is identified as a mononuclear osmium carbonyl complex $[Os(CO)_x(O\text{-}Al\leq)_2]_n$ (x = 2,3). The degradation of the cluster by surface-OH groups even at room temperature has been attributed to its reactivity[124]. That the species formed is indeed a surface bound hydridotriosmium cluster is further supported by the inability to extract it from the surface with any chlorinated solvent or with a solution of KPF_6 in acetone. This insolubility also rules out the possibility of cationic species being formed on the surface. The nature of $H_2Os_3(CO)_{10}$-surface complex will be discussed in a later section (see Section III.C.6).

Exposure to air or evacuation for a few hours leads to degradation of the bound triosmium cluster to form ensembles of atomically dispersed osmium (cf., Figure 33).

4. Adsorption of $H_4Ru_4(CO)_{12}$ on ALPILC

Stirring a solution of $H_4Ru_4(CO)_{12}$ (0.013 mmol) in CH_2Cl_2 (40 ml) with alumina pillared clay (0.5 g) and subsequent washing with CH_2Cl_2 results in no significant adsorption. Alternatively, if the solvent is evaporated under vacuum the resulting material exhibits IR absorptions at 2104 w, 2081 s, 2056 vs, and 2024 m cm^{-1}, which are identical in frequency and intensity to those of $H_4Ru_4(CO)_{12}$ (Figure 34, Table 16).

The physisorbed $H_4Ru_4(CO)_{12}$ cluster is stable and remains intact on exposure to air or evacuation at room temprature, in marked difference to the behavior of physisorbed $Ru_3(CO)_{12}$ molecules. However, heating at higher temperatures (100-200°C) in air or under vacuum leads to a material with

Figure 33: Infrared spectra in the CO stretching region of $H_2Os_3(CO)_{10}$ supported on alumina pillared clay: (a) $H_2Os_3(CO)_{10}$ supported by adsorption from CH_2Cl_2 solution (mull); (b) sample (a) exposed to air at RT for 24 h; (c) sample (a) after heating in air at 110°C for 2 h; (d) sample (a) after heating in vacuum at 150°C for 4 h.

Figure 34: Infrared spectra in the CO stretching region of unsupported $H_4Ru_4(CO)_{12}$ and $H_4Ru_4(CO)_{12}$ supported on alumina pillared clay: (a) $H_4Ru_4(CO)_{12}$ adsorbed on ALPILC from CH_2Cl_2 solution (mull); (b) $H_4Ru_4(CO)_{12}$ in CH_2Cl_2 solution; (c) sample (a) after heating in air at 100°C for 1 h (mull); (d) sample (a) after heating in vacuum at 150°C for 4 h.

two main IR absorptions at about 2070 and 2000 cm^{-1}, assigned to a surface structure of the type $[Ru(CO)_2(O\text{-}Al\lesssim)_2]_n$. The weak band which appears at about 2140 cm^{-1} is associated with surface structure $[Ru(CO)_3(O\text{-}Al\lesssim)_2]$ and disappears at longer periods of time or higher temperatures. At even higher temperatures (> 200°C) further decarbonylation occurs and leads to oxidized Ru atoms on the surface. The higher thermal stability of $H_4Ru(CO)_{12}$ compared with that of the trinuclear $Ru_3(CO)_{12}$ cluster has been attributed to its higher nuclearity[115].

5. Adsorption of $Ir_4(CO)_{12}$ on ALPILC

When $Ir_4(CO)_{12}$ is refluxed in cyclohexane (0.11×10^{-3} M) with alumina pillared montmorillonite (0.5 g) for two h, the IR spectrum of the resulting material exhibits bands at 2109 w, 2060 vs, and 2026 s cm^{-1} , in good agreement with those of $Ir_4(CO)_{12}$ (Figure 35, Table 16). Exposure to air does not result in any significant change in the IR spectrum. However, if the mineral is heated in air at 110°C a progressive diminishment of the 2026 cm^{-1} band and the appearance of a new band around 1990 cm^{-1} is observed. After two hours there appear only two bands at 2061 and 1988 cm^{-1}, assigned[123] to surface structure of the type $[Ir(CO)_2X]_n$, where X represents an oxygen atom of the support, which is then decarbonylated on further heating.

6. General Considerations on the Adsorption of Cluster Carbonyls on ALPILC

A schematic view of the reactions and the products of various metal cluster carbonyls and alumina pillared clay is represented in Figure 36 and 37. The initial product of the interaction of either $Os_3(CO)_{12}$ or $Ru_3(CO)_{12}$ with the support is the protonated trinuclear cluster. The H^+ ions of the support are produced by dehydration of the interlayering polymeric oxyaluminum cations during pretreatment at 350° under Ar[33]. The overall

Figure 35: Infrared spectra in the CO stretching region of unsupported $Ir_4(CO)_{12}$ and $Ir_4(CO)_{12}$ supported on alumina pillared clay: (a) $Ir_4(CO)_{12}$ adsorbed on ALPILC from cyclohexane solution (mull); (b) Nujol mull of $Ir_4(CO)_{12}$; (c) sample (a) after heating in air at 110°C for 2 h (mull).

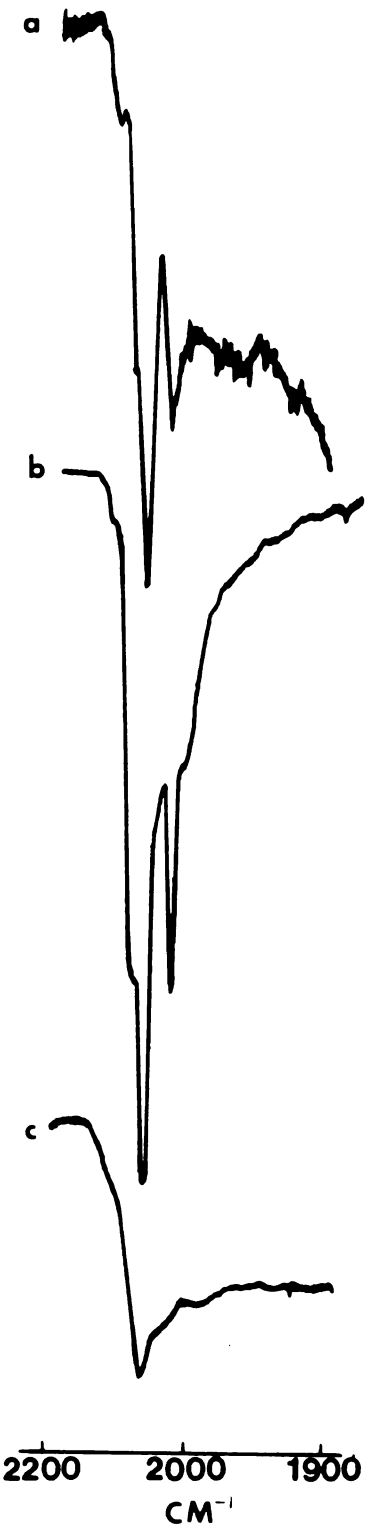
a
b
c
2200
2000
1900
CM⁻¹

Figure 36: Schematic representation of reactions and their products of $Os_3(CO)_{12}$ and alumina pillared clay (ALPILC).

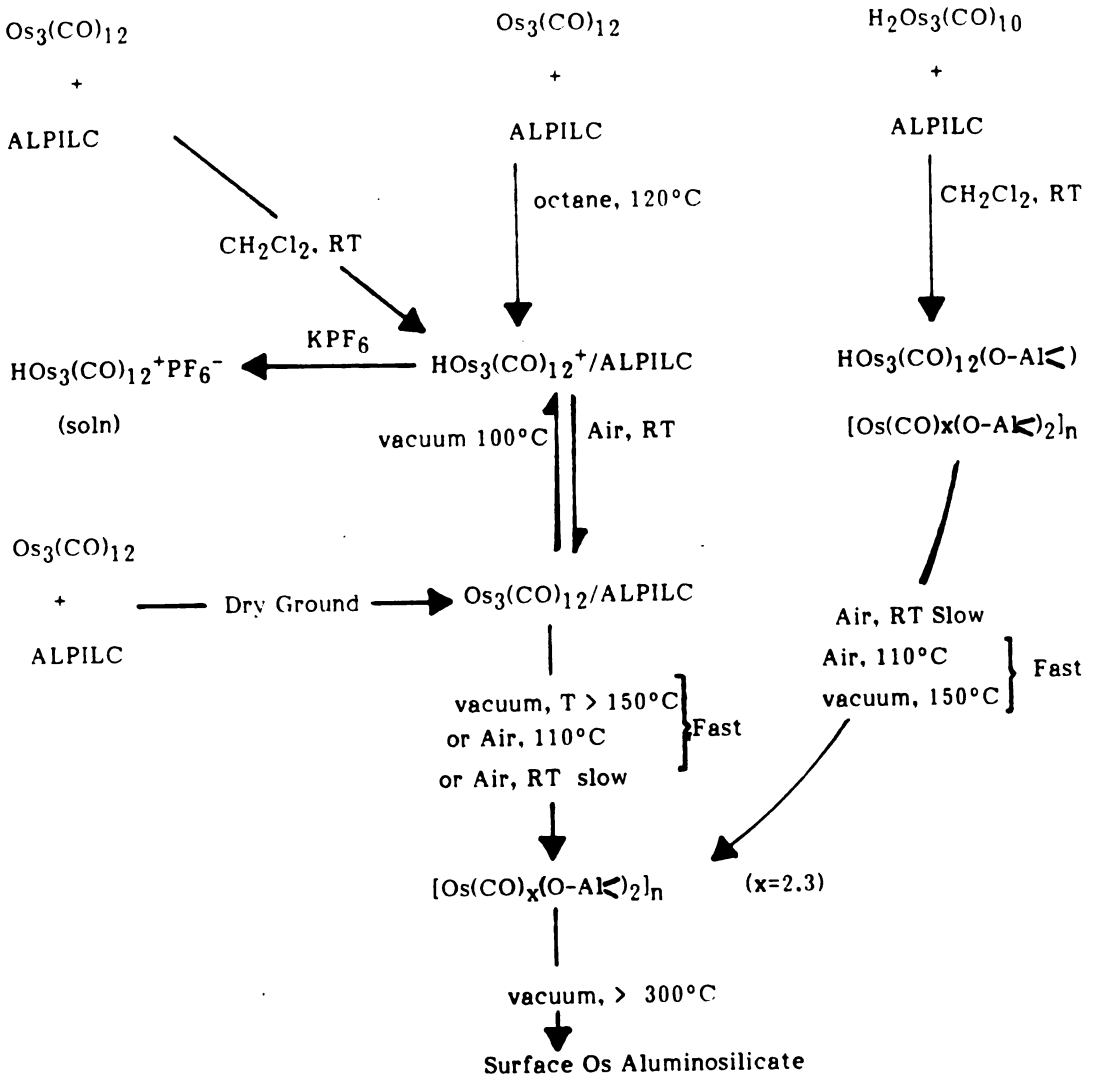
Os3(CO)12
+
ALPILC
CH2Cl2, RT
Os3(CO)12
+
ALPILC
octane, 120°C
H2Os3(CO)10
+
ALPILC
CH2Cl2, RT
KPF6
HOs3(CO)12+PF6-
(soln)
HOs3(CO)12+/ALPILC
HOs3(CO)12(O-Al≤)
[Os(CO)x(O-Al≤)2]n
vacuum 100°C
Air, RT
Os3(CO)12
+
ALPILC
Dry Ground
Os3(CO)12/ALPILC
Air, RT Slow
Air, 110°C
vacuum, 150°C
Fast
vacuum, T > 150°C
or Air, 110°C
or Air, RT slow
Fast
[Os(CO)x(O-Al≤)2]n
(x=2.3)
vacuum, > 300°C
Surface Os Aluminosilicate

Figure 37: Schematic representation of reactions and their products of supported $Ru_3(CO)_{12}$ on alumina pillared clay (ALPILC)

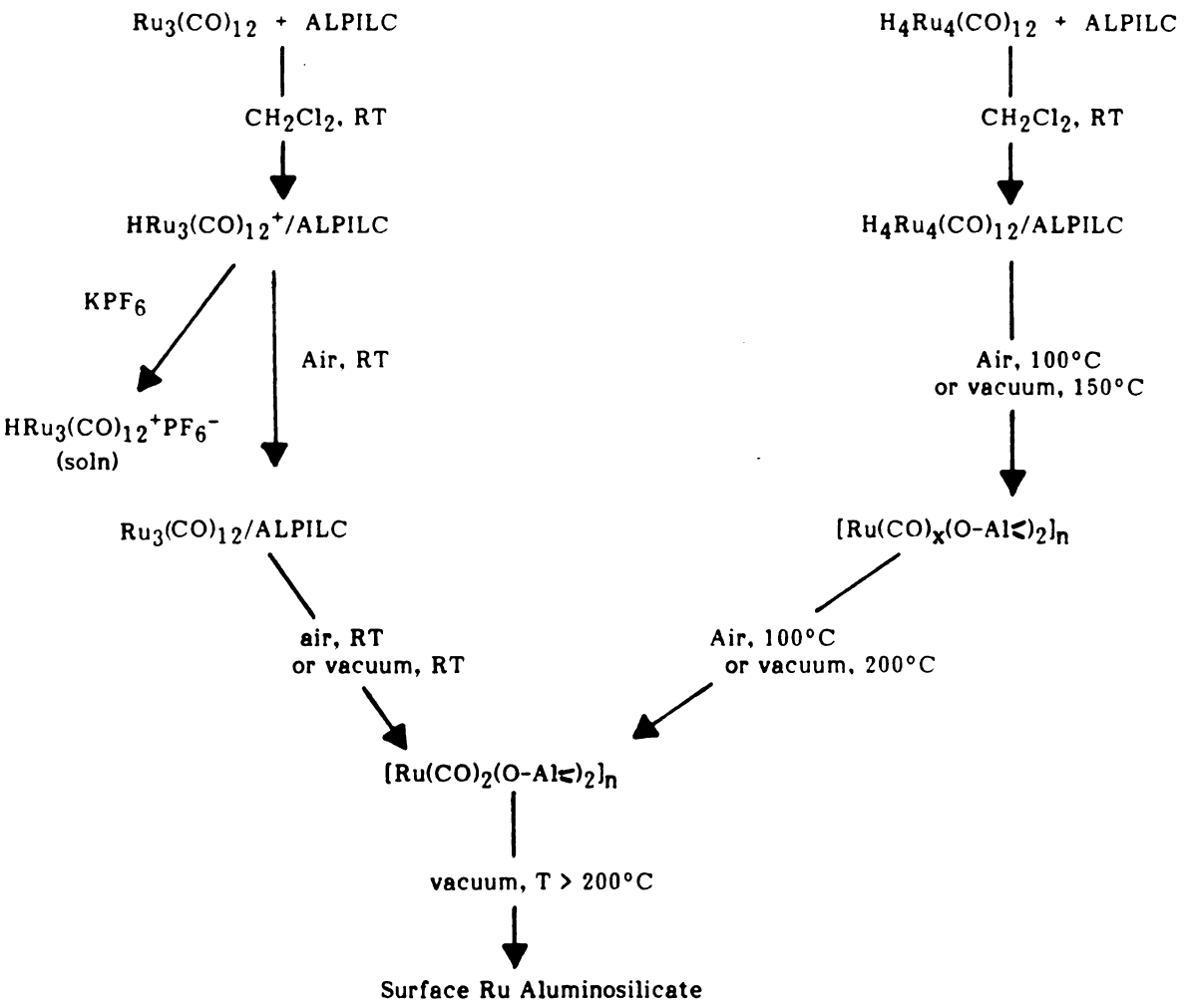
$Ru_3(CO)_{12}$ + ALPILC
CH_2Cl_2, RT
$HRu_3(CO)_{12}^+$/ALPILC
KPF_6
Air, RT
$HRu_3(CO)_{12}^+PF_6^-$
(soln)
$Ru_3(CO)_{12}$/ALPILC
air, RT
or vacuum, RT
$H_4Ru_4(CO)_{12}$ + ALPILC
CH_2Cl_2, RT
$H_4Ru_4(CO)_{12}$/ALPILC
Air, 100°C
or vacuum, 150°C
$[Ru(CO)_x(O\text{-}Al\leq)_2]_n$
Air, 100°C
or vacuum, 200°C
$[Ru(CO)_2(O\text{-}Al\leq)_2]_n$
vacuum, T > 200°C
Surface Ru Aluminosilicate

interlayer reaction may be represented by the following equation.

$$\underline{\overline{Al_{13}O_4(OH)_{28+n}^{(3-n)+}}} \xrightarrow{-H_2O} \underline{\overline{6.5\ Al_2O_3 + (3-n)\ H^+}} \qquad (23)$$

Bronsted acidity of alumina pillared clays was postulated to account for their catalytic activity as cracking catalysts[30,32]. Subsequent pyridine adsorption studies established the presence of both Bronsted and Lewis acid sites[38]. Though complexes of metal carbonyls are known to be formed with strong Lewis acids (i.e. $AlBr_3$)[148], we did not observe the formation of such an adduct. This might be due to the lower acidity of the support compared to that of $AlBr_3$.

It has been reported that by evacuating the pyridine-loaded alumina pillared clay at 150°C the number of Lewis-acid types is increased and that at 400°C the surface acidity is mostly of the Lewis type[38]. However, our evidence mitigates against this report. Increasing the activation temperature of the support from room temperature to 350°C under vacuum increases the amount of protonated cluster on the surface, as judged by IR, but presents no evidence for the formation of any other species. This implies that as the amount of surface water decreases, the protonic acidity increases.

The almost identical spectra of the supported protonated clusters and their molecular analogues as well as the ability to extract them from the surface by ion exhcange suggest the presence of only electrostatic interactions between host and intercalate. It is noteworthy that such a procedure leads to activation of surface protons for subsequent exchange with another cation. This possibility adds a new dimension to the surface chemistry of pillared clays since it has been claimed that they do not exhibit any cation exchange capacity.

Elemental analysis of the ruthenium and osmium bound clusters showed that the samples contained 0.48 wt% Ru and 0.38 wt% Os, respectively, when the clay was activated at 25°C. No attempt has been made to optimize the amount of surface bound metal carbonyls. These loadings correspond to a coverage of approximately 8 m^2 for the ruthenium and 3 m^2 for the osmium cluster per gram of clay, if the surface of the clusters is taken to be about 80 $\mathring{A}^2$. The low coverage of the surface most likely is due to the inaccessibility of the majority of the pores to the cluster molecules because of their comparable size[63,64]. That protonation takes place in the intracrystalline region of the support is further supported by the failure of alumina pillared fluorohectorite with a surface area of approximately 14 m^2/g and smaller pore opening to protonate metal cluster carbonyls. Significantly Al^{3+} -MONT (d_{001} = 11.6 $\mathring{A}$, at 350°C) only forms trace amounts of protonated cluster on external surfaces, as judged by IR.

In a similar experiment sodium-montmorillonite fails also to protonate either Os or Ru carbonyl clusters. The absence of acidic character from the naturally occuring mineral is attributed to the ability of Na^+ ions to enter the hexagonal recesses in the basal oxygen sheet during dehydration of the clay sample. These firmly fixed ions are stripped of their potentially acidic water molecules and are coordinated instead with oxygen atoms of the silicate framework[149].

Since protonation of metal cluster carbonyls can be only brought about by treatment with very powerful acidic media such as trifluoroacetic or 98% sulfuric acid[65,150], it is evident that the acidity of alumina pillared clays lies in the same range in terms of protonating capacity. This is not unusual for silicate minerals, which were shown to possess Bronsted acidity comparable in some cases to that of concentrated sulfuric acid. In these cases the most

important source of the acidity is polarized water molecules coordinated to polyvalent interlayer cations[15]. On the other hand, the acidity of pillared clays arises mainly from protons formed by dehydration of the interlayering polymeric oxyaluminum cations[33,38].

Of the five different carbonyl clusters examined in this work only $Ru_3(CO)_{12}$ and $Os_3(CO)_{12}$ form protonated surface species on contact with the support. This is not surprising since only the dodecacarbonyl triosmium and triruthenium clusters are known to form fairly stable protonated complexes that can be isolated in the form of hexafluorophosphate salts. The carbonyls $Ir_4(CO)_{12}$ and $H_2Os_3(CO)_{10}$ are also known to form solutions that exhibit high field ^1H NMR resonances upon treatment with strong acids, suggestive of the formation of protonated species even though solid salts have not been isolated[65,151].

Intracrystalline acidity distinguishes alumina pillared clays from other commonly used supports such as refractory metal oxides. Nevertheless, the small aluminum oxide aggregates sandwiched between the silicate layers exhibit reactivity which parallels that of bulk oxide. Thus, reaction of metal clusters with hydroxyl groups at elevated temperatures leads to degradation of the cluster with formation of subcarbonyl species bound to the support. That the hydroxyl groups of the small oxide clusters are involved rather than those present on the edges of the silicate framework is supported by the ability of the former to react with metal clusters at lower temperatures. The reactivity of the mineral silanol groups with neutral carbonyls is far less than that of the hydroxyl groups introduced by the molecular pillar (see Section III.A.1 and III.A.2).

Reaction of $H_2Os_3(CO)_{10}$ with ALPILC gives rise to a trinuclear supported osmium species which is probably formed by the following reaction:

$$H_2Os_3(CO)_{10} + \overline{H - O - Al\lessdot} \longrightarrow \overline{Os_3(H)(O\text{-}Al\lessdot)(CO)_{10}} + H_2 \quad (24)$$

A similar surface bound species is formed by interaction of OH groups of silica or alumina with either $Os_3(CO)_{12}$ or $H_2Os_3(CO)_{10}$. In addition to the similarity of its IR spectrum to that of a model compound prepared by the reaction of $Os_3(CO)_{12}$ with $HOSiPh_3$, EXAFS and Raman spectroscopy have shown the cluster framework to remain intact and suggest the following structure (I)[124,127,128].

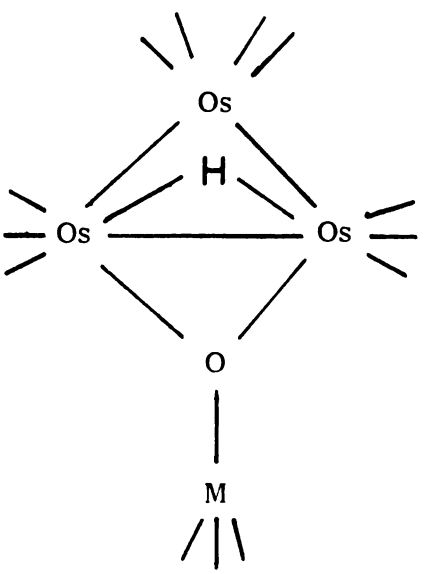

(I)

M = Si, Al, Ti or Zn

Treatment of this surface bound triosmium cluster at temperatures between 100° and 400°C under vacuum or an inert gas leads to a material with an IR spectrum similar to that observed for $[Os(CO)_2I_2]$[127], which has a polymeric structure with iodide atoms bridging the Os(II) ions. The transition from a surface bound trinuclear cluster to ensembles of atomically dispersed osmium, can be perceived as happening during formation of Os-O bonds with concurrent breaking of metal-metal bonds in the cluster framework[124,127]. Parallel behavior has been observed for $Ru_3(CO)_{12}$ supported on silica or alumina[116,117].

In the present work we do not observe formation of surface structure (I) with ALPILC-supported $Os_3(CO)_{12}$ or $Ru_3(CO)_{12}$. Instead, ensembles of atomically dispersed metal atoms of the type $[M(CO)_x(O\text{-}Al\lessgtr)_2]_n$ are formed by oxidation in air, evacuation, or thermal decomposition under Ar. Surface adsorbed water might be involved in the degradation of surface structure (I) upon thermal treatment of the mineral. The aforementioned mononuclear carbonyl complexes are also obtained with ALPILC-supported $Ir_4(CO)_{12}$, $H_2Os_3(CO)_{10}$ and $H_4Ru_4(CO)_{12}$. In the suggested structure the metal atoms are stabilized on the surface by firm interaction with oxygen atoms in the support lattice. In addition, every metal atom is coordinated to two or more CO molecules. However, the value of n cannot be designated at present and it depends on the particular cluster as well as the specific treatment conditions. If thermolysis does not induce aggregation of the metal centers, then the value of n is expected to lie between 1 and the number of metal atoms present in the original cluster. Alternatively, if metal conglomerates are formed, then n might be much higher.

The number and position of the IR bands in the CO region are dependent on the local symmetry, the oxidation state of the central atom and the extent

of metal aggregation. Complexes of the type $[M(CO)_3X_2]$, with pseudo C_{3v} symmetry, are expected to exhibit two IR carbonyl absorptions assigned to the A_1 and doubly degenerate E modes[152]. In addition structures containing two CO molecules per metal would also exhibit two major absorption bands associated with the symmetric and antisymmetric carbonyl stretching modes. Their position is determined by the number of CO molecules coordinated to the central atom. As the CO coverage on the surface decreases, the availability of metal d electrons for retroactive bonding increases. This leads to a strengthening of the M-C bond with concomitant weakening of the C-O bond, which in turn shifts the frequency to lower wavenumbers. In a similar manner as metal aggregation becomes more extensive the availability of d electrons decreases due to the formation of metal-metal bonds, which increases the vibrational frequency of the C-O bond.

As the mineral is treated at higher temperatures a progressive decarbonylation is observed. This leads to coordinatively unsaturated metal atoms that are likely to interact more strongly with the oxygen atoms of the support to form surface aluminosilicates. The strength of the metal-oxygen bonds determines the degree of metal-support interaction, which evidently plays a significant role in the formation of metal aggregates or atomically dispersed metal atoms.

7. Adsorption of $[CpFe(CO)_2]_2$ on ALPILC

Adsorption of $[CpFe(CO)_2)]_2$ from a CH_2Cl_2 solution (0.71×10^{-3} M) on alumina pillared montmorillonite (0.5 g) leads to a red-brown material which exhibits an IR spectrum significantly different from that of the unsupported cluster (Table 18). The new spectrum (Figure 38) shows CO bands at 2124 m, 2068 vs, and 2019 s cm^{-1}. The ability to extract the surface organometallic species into a solution of potassium hexafluorophosphate in

Table 18

Infrared CO Bands of Molecular and ALPILC Intercalated Metal Cluster Complexes

Compound	ν(CO) cm^{-1}	Reference
$[CpFe(CO)_{2,3}]^+$/ALPILC[a]	2124 m, 2068 vs, 2019 s	This Work
$[CpFe(CO)_3][PF_6]$[a] *	2124 m, 2067 s	This Work
$[CpFe(CO)_2(H_2O)][PF_6]$[b] *	2069 vs, 2023 vs	This work
$[CpFe(CO)_2]_2$[b]	1999 vs, 1958 s, 1777 vs 1772 vs	This Work
$CpFe(CO)_2I$[b]	2038 vs, 1999 vs	This Work
$[CpFe(CO)_3][PF_6]$[a]	2120, 2068	153
$[CpFe(CO)_2(H_2O)][BF_4]$[c]	2066 s, 2018 s	155
$CpFe(CO)_2I$[d]	2043 vs, 2005 vs	158

[a] Nujol mull; [b] CH_2Cl_2; [c] Acetone; [d] $CHCl_3$

* Isolated from the surface of ALPILC by exchange with KPF_6 in acetone.

Figure 38 Infrared spectra in the CO stretching region: (a) clay sample prepared by impregnation of alumina pillared clay with $[CpFe(CO)_2]_2$ in CH_2Cl_2 (mull); (b) $[CpFe(CO)_3]$-PF_6 extracted from the surface of ALPILC with a solution of KPF_6 in acetone (Nujol mull); (c) $[CpFe(CO)_2]$-PF_6 extracted from the surface with KPF_6 in acetone (CH_2Cl_2 solution).

acetone suggests their ionic character. When the mineral is washed with the aforementioned solution it becomes almost colorless. Removal of the acetone solvent under vacuum and replacement by CH_2Cl_2 produces a brown-red solution and an undissolved pale yellow material. The latter exhibits carbonyl absorptions at 2124 s and 2067 s cm^{-1} and a C_5H_5 resonance at 6.09 ppm, in good agreement with the spectra reported for $[CpFe(CO)_3][PF_6]$[153,154]. The CH_2Cl_2 soluble compound is also a metal carbonyl complex with ν(CO) at 2069 vs and 2023 vs cm^{-1}. Its ^1H NMR spectrum shows a C_5H_5 resonance at 5.60 ppm. Furthermore, it reacts quickly with KI to form a new complex with ν(CO) bands shifted to lower wavenumbers (2038 vs, 1999 vs cm^{-1}) and a single resonance in the NMR at 5.05 ppm. On the basis of the above results it is characterized as $[CpFe(CO)_2][PF_6]$[155]. The $CpFe(CO)_2^+$ cation is known to react with halides to form $CpFe(CO)_2X$ type complexes. The final IR spectrum of the clay sample is the superposition of those of the two surface species. The Fe loading of the dry mineral is 0.57 wt%.

The surface chemistry of $[CpFe(CO)_2]_2$ adsorbed on alumina pillared clay is far more complex than that observed for $Ru_3(CO)_{12}$ and $Os_3(CO)_{12}$. Adsorption of the dodecacarbonyl clusters on the support leads to the formation of the protonated $HM_3(CO)_{12}^+$ by intracrystal H^+ ions. In the case of iron, the lower stability of the metal-metal bonds leads to fragmentation of the dimer to form mononuclear complexes.

It has been known that cyclopentadienyl iron carbonyl compounds can abstract a proton from a strong acid to form a species containing metal-hydrogen bonds[156]. However, these salts are not very stable even in the presence of the acid. In addition to the carbonyl bands of the protonated dimer, CO absorptions from $CpFe(CO)_3^+$ appear and increase in intensity

Table 19

C_5H_5 Proton Chemical Shifts for Some Cyclopentadienyliron Carbonyl Compounds

Compound	δ ppm	Reference
$[CpFe(CO)_3][PF_6]$[a] *	6.09	This Work
$[CpFe(CO)_3][PF_6]$[a]	6.14	154
$[CpFe(CO)_2(H_2O)][PF_6]$[a]*	5.60	This Work
$[CpFe(CO)_2(H_2O)][BF_4]$	5.52	155
$CpFe(CO)_2I$[b]	5.05	This Work
$CpFe(CO)_2I$[b]	5.04	158

[a] CD_3COCD_3; [b] $CDCl_3$

* Isolated from the surface of ALPILC by exchange with KPF_6 in acetone.

with time[157]. In addition oxidation of the dimer in acetone and aqueous fluoroboric acid is known to form a reactive cationic intermediate identified as $CpFe(CO)_2^+$ (equation 25)[155]. This dicarbonyl complex undergoes substitution upon reaction with anionic (equation 26) or neutral ligands.

$$[CpFe(CO)_2]_2 + 2HBF_4 + H_2O + \tfrac{1}{2}O_2 \longrightarrow 2[CpFe(CO)_2(OH_2)]BF_4 \quad (25)$$

$$[CpFe(CO)_2(OH_2)]BF_4 + X^- \longrightarrow CpFe(CO)_2X + BF_4^- + H_2O \quad (26)$$

Adsorption of $[CpFe(CO)_2]_2$ on the support leads to the formation of both di and tricarbonyl clyclopentadienyl iron complexes. We believe these products are formed through different competing surface reactions. Reaction of the dimer with intracrystal protons results in the formation of the protonated complex which in turn decomposes to form the $CpFe(CO)_3^+$ ion according to equation 27.

$$[CpFe(CO)_2]_2 + ALPILC \rightleftharpoons [CpFe(CO)_2]_2H^+/ALPILC \longrightarrow$$

$$CpFe(CO)_3^+/ALPILC \quad (27)$$

On the other hand, the $CpFe(CO)_2^+$ complex might be produced through oxidation by molecular oxygen

$$[CpFe(CO)_2]_2 + ALPILC + O_2 \longrightarrow CpFe(CO)_2(H_2O)^+/ALPILC \quad (28)$$

or surface hydroxyl groups

$$\tfrac{1}{2}[CpFe(CO)_2]_2 + \underline{\overline{\quad}H\text{-}O\text{-}Al\langle\quad} \longrightarrow \underline{\overline{\quad}CpFe(CO)_2(O\text{-}Al\langle)\quad} + \tfrac{1}{2}H_2 \qquad (29)$$

The ability to extract the dicarbonyl complex from the surface by ion-exchange techniques suggests oxidation by O_2 in the presence of the acidic support according to equation 28 as the possible pathway. In addition, reaction of the dimer with a clay sample that has not been evacuated results in an almost exclusive production of the $CpFe(CO)_2^+$ ion on the surface. The formation of the protonated complex that in turn decomposes to the $CpFe(CO)_3^+$ ion can be only accomplished in the presence of strong acidic media. However, the Bronsted acidity of the support decreases as the amount of surface water increases. The molecular oxygen is probably strongly adsorbed on the support and cannot be removed upon evacuation. Surface water is also present even after treatment under vacuum at 300°C, as evidenced by the H_2O bending vibration frequency at about 1630 cm^{-1} in the IR spectrum of the mineral.

The ratio of the two surface products remains unchanged when shorter reaction times are employed. If the reaction is carried out in the presence of air a rusty material is obtained with no significant carbonyl absorption bands, likely iron oxide deposited on the exterior of the support.

Exposure to air of the $CpFe(CO)_x^+$, (x = 2,3), supported complexes results in a progressive decarbonylation. If the clay sample is heated at 100°C in air its IR spectrum exhibits mainly absorptions due to the $CpFe(CO)_3^+$ ion, however of diminished intensity. The same results are obtained when the mineral is heated at 100°C in flowing H_2. In this case decarbonylation is complete over a period of a few hours.

Removal of the CO ligands by either thermolysis or oxidation generates highly uncoordinated Fe atoms on the surface that interact strongly with

lattice oxygens of the clay framework. In this case Fe(II) and/or Fe(III) surface aluminates are likely to be formed.

D. Laponite-Supported Metal Cluster Carbonyls

The selective decoration of the edge surfaces of layered silicates with metal carbonyl complexes through reaction with surface hydroxyl groups was briefly studied in the last part of this work. Such decoration with heavy elements may be useful for studies of clay particle morphology by electron microscopy or it may have important implications for optimizing the turnover frequencies of clay supported metal catalysts. Laponite was used as a support because of the abundance of edge surfaces due to the small size of clay platelets. The impregnation was carried out in the absence of air and the solvent was removed under vacuum to eliminate decomposition of the cluster due to molecular O_2.

1. Adsorption of $H_2Os_3(CO)_{10}$ and $Os_3(CO)_{12}$ on Laponite

In the absence of air the hydrido cluster $H_2Os_3(CO)_{10}$ is easily physisorbed from CH_2Cl_2 solution on laponite. The IR spectrum of the reaction product is similar to that of the unsupported cluster (Figure 39, Table 20). Furthermore, the weakly adsorbed clusters can readily be extracted from the surface with CH_2Cl_2.

The effects of heating $H_2Os_3(CO)_{10}$ on laponite under vacuum and in Ar or air are illustrated in Figure 39. After heating in vacuum at 60°C, the spectrum of the crafted $Os_3(H)(O\text{-}Si\equiv)(CO)_{10}$ appeared accompanied by a drastic color change from red-violet to yellow. The surface species is most likely formed by the following reaction:

$$H_2Os_3(CO)_{10} + H\text{-}O\text{-}Si\equiv \longrightarrow Os_3(H)(O\text{-}Si\equiv)(CO)_{10} + H_2 \qquad (30)$$

Figure 39 Infrared spectra in the CO stretching region of $H_2Os_3(CO)_{10}$ supported on laponite (0.003 mmol/0.1 g): (a) $H_2Os_3(CO)_{10}$ physisorbed on laponite from CH_2Cl_2 solution (mull); (b) sample (a) after heating in vacuum at 60°C for 4 h; (c) followed by heating in vacuum at 150°C for 3 h; (d) sample (a) after heating under Ar at 150°C for 3 h; (e) sample (a) after heating in air at 100°C for 6 h.

Table 20

Infrared CO Bands of Molecular and Laponite-Supported Metal Cluster Complexes

Compound	ν(CO) cm^{-1}
$Os_3(CO)_{12}$/laponite[a]	2068vs, 2035s, 2016s, 1997m, 1983m
$Os_3(CO)_{12}$[b]	2068vs, 2034s, 2013m, 2000m
$[(\equiv Si\text{-}O)_2Os(CO)_x]_n$-laponite[a]	2118m, 2021vs, 1937s
$H_2Os_3(CO)_{10}$/laponite[a]	2114w, 2075s, 2064s, 2025vs, 2010s, 1992m
$H_2Os_3(CO)_{10}$[b]	2112vw, 2076s, 2063s, 2025vs, 2010s, 1989m
$HOs_3(CO)_{10}(O\text{-}Si\equiv)$-laponite[a]	2111w, 2074s, 2061s, 2023vs, 2009s, 1990m
$Ru_3(CO)_{12}$/laponite[a]	2059vs, 2030s, 2011m
$Ru_3(CO)_{12}$[b]	2061vs, 2029s, 2011m
$[(\equiv Si\text{-}O)_2Ru(CO)_2]_n$-laponite[a]	2051s, 1982s
$H_4Ru_4(CO)_{12}$/laponite[a]	2082s, 2065vs, 2024s
$H_4Ru_4(CO)_{12}$[b]	2081s, 2066vs, 2024s, 2009m

a Nujol mull

b CH_2Cl_2 solution

When the sample is heated at higher temperatures or at 100°C in air, surface species of the type $[(\equiv Si\text{-}O)_2Os(CO)_x]_n$ are formed, characterized by IR absorptions at around 2120 m, 2020 vs, and 1940 cm^{-1}.

Adsorption of $Os_3(CO)_{12}$ from a CH_2Cl_2 solution leads again to simple physisorption on the clay (Figure 40, Table 20). The clusters remain stable up to 100°C. When the clay sample was heated at higher temperatures we could not identify the formation of triangular clusters covalently attached to the support due to the complexity of the spectrum. At 150°C the spectrum of surface species $[(\equiv Si\text{-}O)_2Os(CO)_x]_n$, characterized by three IR absorptions, was observed.

The formation of the surface-supported hydride cluster $Os_3(H)(O\text{-}Si\equiv)(CO)_{10}$ requires an oxidative addition of a $\equiv Si\text{-}OH$ group to the Os-Os bond of the triosmium clusters. Such a transformation is easily achieved with $H_2Os_3(CO)_{10}$ which is a more suitable precursor than $Os_3(CO)_{12}$. In the latter case, loss of CO molecules is needed to form the trinuclear addition product. Heating at higher temperatures causes a breakdown of the cluster framework with simultaneous oxidation by surface-OH groups to two osmium(II) species of the type $[(\equiv Si\text{-}O)_2Os(CO)_x]_n$ according to equation 9 (see Section III.A.1). The stabilization of the mononuclear complexes on the surface of silica or alumina has been attributed to an extremely strong osmium-oxygen interaction and the steric repulsion between carbonyl ligands of neighboring surface complexes[128]. Hence the formation of metal aggregates is avoided on heating.

2. Adsorption of $Ru_3(CO)_{12}$ and $H_4Ru_4(CO)_{12}$ on Laponite

$Ru_3(CO)_{12}$ and $H_4Ru_4(CO)_{12}$ are readily physisorbed unaltered on laponite from a CH_2Cl_2 solution. The spectra of laponite-supported $Ru_3(CO)_{12}$ and $H_4Ru_4(CO)_{12}$ are presented in Figures 41 and 42, respectively. The CO

Figure 40: Infrared spectra in the CO stretching region of $Os_3(CO)_{12}$ supported on laponite (0.003 mmol/0.1 g): (a) $Os_3(CO)_{12}$ physisorbed on laponite from CH_2Cl_2 solution (mull); (b) sample (a) after heating in vacuum at 150°C for 3 h; (c) sample (a) after heating under Ar at 150°C for 3 h; (d) sample (a) after heating in air at 150°C for 6 h.

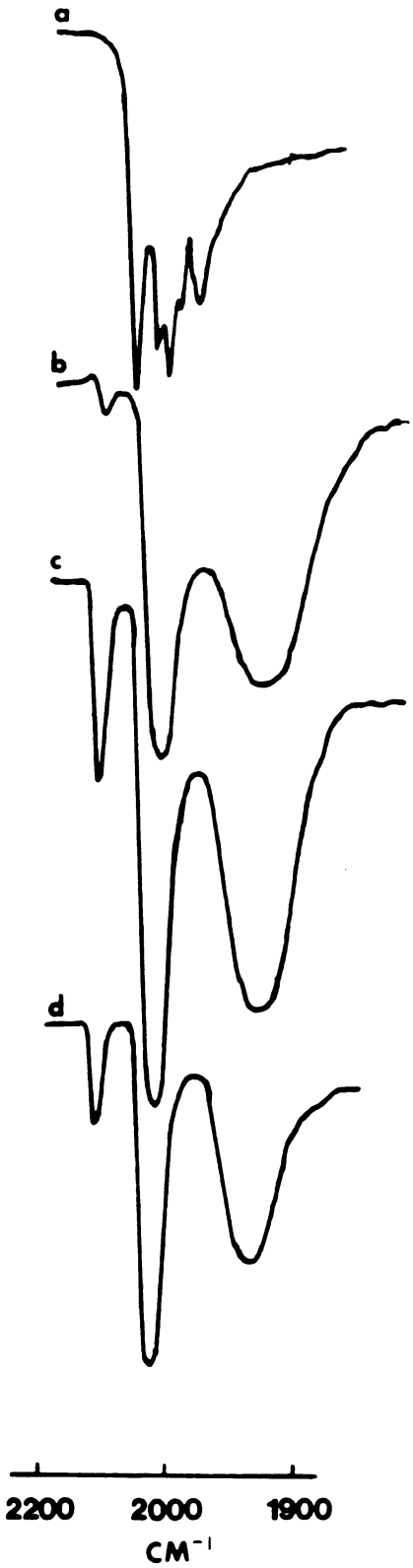
a
b
c
d
2200
2000
1900
CM⁻¹

Fig. 41 Infrared spectra in the CO stretching region of $Ru_3(CO)_{12}$ supported on laponite (0.003 mmol/0.1 g): (a) $Ru_3(CO)_{12}$ on laponite prepared by impregnation from CH_2Cl_2 solution (mull); (b) sample (a) after heating in vacuum at 60°C for 4 h; (c) sample (a) exposed to air for seven days; (d) sample (a) after heating in air at 90°C for 30 min.

Fig. 42 Infrared spectra in the CO stretching region: (a) $H_4Ru_4(CO)_{12}$ on laponite (0.003 mmol/0.1 g) prepared by impregnation from CH_2Cl_2 solution (mull); (b) sample (a) after heating in vacuum at 60°C for 6 h; (c) followed by heating at 120°C for 3 h; (d) sample (a) after heating in air at 90°C for 1 h.

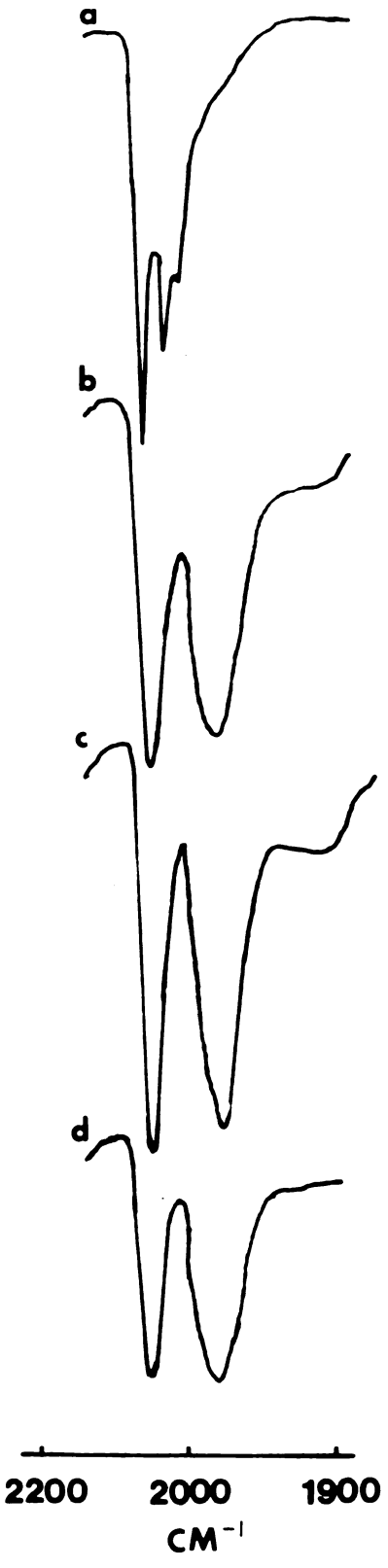

Figure 41

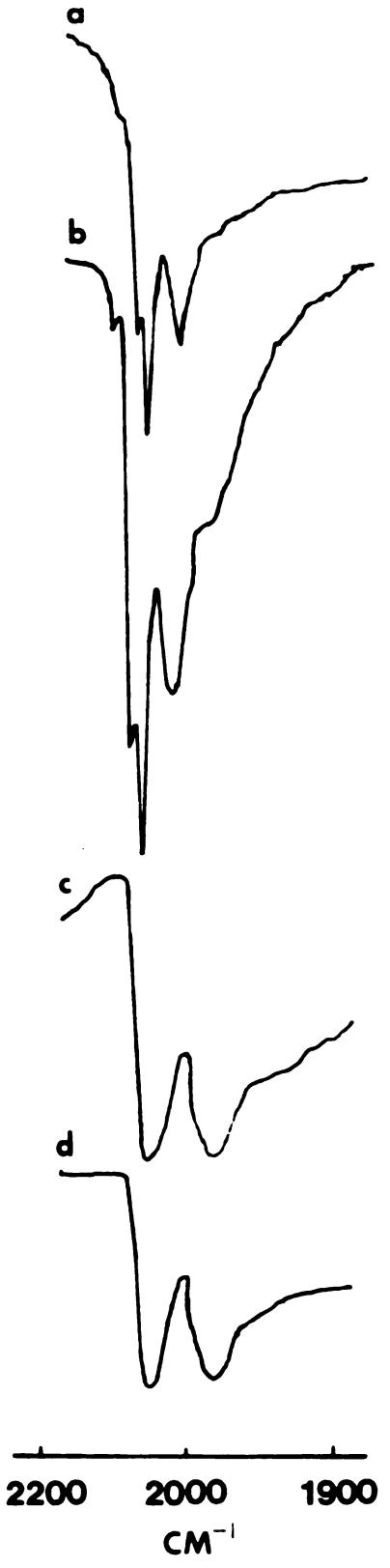

Figure 42

stretching frequencies along with those of molecular clusters are summarized in Table 20.

Heating the two clay samples in air or under vacuum leads to the formation of the surface structure $[(\equiv Si\text{-}O)_2Ru(CO)_2]_n$, characterized by IR absorptions at 2050 and 1980 cm^{-1} and independent of the original cluster composition. The observed higher stability of $H_4Ru_4(CO)_{12}$ is attributed to its higher nuclearity[115]. The formation of the mononuclear surface species most likely involves reaction with -OH groups according to equation 10 (see Section III.A.2).

REFERENCES

1. R.C. Mackenzie, Clays Clay Miner., 11, 11 (1963).
2. G. Brown, Ed., X-Ray Identification and Crystal Structure of Clay Minerals, Mineralogical Society, London, 1961.
3. G.W. Brindley and G. Brown, Eds. Crystal Structures of Clay Minerals and Their X-Ray Identification, Mineralogical Society, London, 1980.
4. U. Hoffman, Angew. Chem. Int. Ed., 7, 681 (1968).
5. J.B. Dixon, in "Minerals in Soil Environments", J.B. Dixon and S.B. Weed, Eds., Soil Science Society of America, Madison, WI, 1977, Chapter 11.
6. J.D. Russell and A.R. Frazer, Clays Clay Miner., 19, 55 (1971).
7. T.J. Pinnavaia, Science, 220, 365 (1983).
8. S.L. Swartzen-Allen and E. Matijec, Chem. Rev., 74, 385 (1974).
9. E.T. Uskova, N.G. Vasilev, and I.A. Uskov, Colloid J. (USSR), 30, 118 (1968).
10. H. Van Olphen, "An Introduction to Clay Colloid Chemistry", 2nd Ed. John Wiley, NY, 1977.
11. K. Norrish, Disc. Faraday Soc., 18, 120 (1954).
12. G.W. Brindley, K. Wiewiora and A. Wiewiora, Amer. Miner., 54, 1635 (1969).
13. K.V. Raman and M.M. Mortland, Proc. Soil Sci. Soc. Am., 33, 313 (1969).
14. V. Berkheiser and M.M. Mortland, Clays Clay Miner., 25, 105 (1977).
15. K.V. Raman and M.M. Mortland, ibid, 16, 393 (1968).
16. J.J. Fripiat, ACS Symp. Ser., 34, 261 (1976).

17. L.B. Ryland, M.W. Tamele and J.N. Wilson in "Catalysis", Vol. VII, P.H. Emmett, Ed., Reinhold, NY, 1960.

18. R.E. Grim, "Clay Mineralogy", 2nd Ed., McGraw-Hill, NY, 1968.

19. B.K.G. Theng, "The Chemistry of Clay-Organic Reactions", John Wiley, NY, 1974.

20. D.H. Solomon and D.G. Hawthorne, "Chemistry of Pigments and Fillers", John Wiley, NY, 1983.

21. T.J. Pinnavaia in "Advanced Techniques for Clay Mineral Analysis", J.J. Fripiat, Ed., Elsevier, NY, 1981, pp. 139-161.

22. W.E.E. Stone, ibid., pp. 71-112.

23. M.B. McBride in "Advanced Chemical Methods for Soil and Clay Mineral Research", J.W. Stucki and W.L. Banwart, Eds., Reidel, Holland, 1980, pp. 423-450.

24. R.M. Barrer and D.N. MacLeod, Trans. Faraday Soc., 51, 1290 (1955).

25. R.M. Barrer and D.L. Jones, J. Chem. Soc. (A), 2594 (1971).

26. M.M. Mortland and V.E. Berkheiser, Clays Clay Miner., 24, 60 (1976).

27. J. Shabtai, N. Frydman and R. Lazar, Proc. 6th Int. Congr. Catal., 2, 660 (1977).

28. V.E. Berkheiser and M.M. Mortland, Clays Clay Miner., 25, 105 (1977).

29. M.F. Traynor, M.M. Mortland and T.J. Pinnavaia, ibid., 26, 318 (1978).

30. G.W. Brindley and R.E. Sempels, Clay Miner., 12, 229 (1977).

31. S. Yamanaka and G.W. Brindley, Clays Clay Miner., 26, 21 (1978).

32. N. Lahav, U. Shani and J. Shabtai, ibid., 26, 107 (1978).

33. D.E.W. Vaughan and R.J. Lussier, Preprints, 5th Int. Conf. Zeolites, Naples, Italy, June 2-6, 1980.

34. J. Shabtai, Chim. L'Indust., 61, 734 (1979).

35. J. Shabtai and N. Lahav, U.S. Patent 4,216,188.

36. J. Shabtai, U.S. Patent 4,238,364.

37. D.E.W. Vaughan, R.J. Lussier and J.S. Magee, U.S. Patents, 4,176,090; 4,271,043; 4,248,739.

38. M.L. Occelli and R.M. Tindwa, Clays Clay Miner., 31, 22 (1983).

39. T.J. Pinnavaia, M.S. Tzou, S.D. Landau and R.H. Raythatha, J. Mol. Catal., 27, 195 (1984).

40. M.L. Occelli, S.D. Landau and T.J. Pinnavaia, J. Catal., 90, 256 (1984).

41. J.Y. Bottero, J.M. Cases, F. Flessinger and J.E. Poirier, J. Phys. Chem., 84, 2933 (1980).

42. J.C. Bailar, Catal. Rev.-Sci. Eng., 10, 17 (1974).

43. J.M. Basset and A.K. Smith in "Fundamental Research in Homogeneous Catalysis", M. Tsutsui and R. Ugo, Eds., Plenum Press, New York, 1977, Vol. 1.

44. S.L. Davydova and N.A. Plate, Coord. Chem. Rev., 16, 195 (1975).

45. R.H. Grubbs, Chemtech, 7, 512 (1977).

46. F.R. Hartley and P.N. Vezey, Adv. Organomet. Chem., 15, 189 (1977).

47. Z.M. Michalska and D.E. Webster, Plat. Met. Rev., 18, 65 (1974).

48. C.U. Pittman, Jr., and G.O. Evans, Chemtech, 3, 560 (1973).

49. A.L. Robinson, Science, 194, 1261 (1976).

50. Y.I. Yermakov, Catal. Rev.-Sci. Eng., 13, 77 (1976).

51. G.A. Somorjai, "Chemistry in Two Dimension:Surfaces", Cornell University Press, 1981.

52. W.A. Adamson, "Physical Chemistry of Surfaces", 3rd Ed., John Wiley, New York, 1976.

53. T.N. Rhodin and G. Ertl, Eds., "The Nature of the Surface Chemical Bond", North-Holland Publication Co., New York, 1979.

54. D.C. Bailey and S.H. Langer, Chem. Rev., 81, 109 (1981).

55. J. Manassen, Plat. Met. Rev., 15, 142 (1971).

56. J. Manassen and D.D. Whitehurst in "Progress in Catalysis", F. Basolo and R.L. Burwell, Jr., Eds., Plenum Press, New York, 1973.

57. Z.M. Michalska and D.E. Webster, Chemtech, 5, 117 (1975).

58. J.D. Corbett, Prog. Inorg. Chem., 21, 129 (1976).

59. R.L. Pruett, Adv. Organomet. Chem., 17, 1 (1979).

60. B.F.G. Johnson, Plat. Met. Rev., 22, 47 (1978).

61. A.P. Humphries and H.D. Kaesz, Prog. Inorg. Chem., 25, 146 (1978).

62. P. Chini, G. Longoni and V.G. Albano, Adv. Organomet. Chem., 14, 285 (1976).

63. R. Mason and A.I.B. Rae, J. Chem. Soc. (A), 778 (1968).

64. E.R. Corey and L.F. Dahl, Inorg. Chem., 1, 521 (1962).

65. J. Knight and M.J. Mays, J. Chem. Soc. (A), 711 (1970).

66. H.D. Kaesz, S.A.R. Knox, J. W. Koepke and R.B. Saillant, Chem. Commun., 477 (1971).

67. A.J. Deeming and S. Hasso, J. Organomet. Chem., 114, 313 (1976).

68. G.R. Wilkes, Ph.D. Thesis, The University of Wisconsin, Madison, WI, 1965.

69. R.D. Wilson, S.M. Wu, R.A. Love and R. Bau, Inorg. Chem., 17, 1271 (1978).

70. B.F.G. Johnson and J. Lewis in "Advances in Inorganic Chemistry and Radiochemistry", H.J. Emeleus and A.G. Sharpe, Eds., Academic Press, New York, 1981, Vol. 24.

71. G.F. Stuntz, Ph.D. Thesis, Univeristy of Illinois, Urbana-Champaign, IL, 1978.

72. W.R. Cullen and O.A. Harbourne, Inorg. Chem., 9, 1839 (1970).

73. E.L. Muetterties, T.N. Rhodin, E. Band, C.F. Brucker and W.R. Pretzer, Chem. Rev., 79, 91 (1979).

74. E.L. Muetterties, Science, 196, 839 (1977).

75. A.K. Smith and J.M. Basset, J. Mol. Catal., 2, 229 (1977).

76. M. Moskovits, Accts. Chem. Res., 12, 229 (1979).

77. R. Ugo, Catal. Rev.-Sci. Eng., 11, 225 (1975).

78. R. Whyman in "Transition Metal Clusters", B.F.G. Johnson, Ed., John Wiley, New York, 1980, Chapter 8.

79. R.M. Laine, J. Mol. Catal., 14, 137 (1982).

80. J.H. Sinfelt, Prog. Solid State Chem., 10, 55 (1975).

81. G.W. Parshall, J. Mol. Catal., 4, 243 (1978).

82. J. Falbe, J. Organometal. Chem., 94, 213 (1975).

83. J.F. Roth, J.H. Craddock, A. Hershman, and F.E. Paulik, Chem. Technol., 1, 600 (1971).

84. M.W. Farlow, U.S. Patent 2,518,608.

85. a) B.C. Gates and J. Lieto, Chemtech, 195 (1980);

b) B.C. Gates and J. Lieto, Chemtech, 248 (1980).

86. K. Iwatate, S.R. Dasgupta, R.L. Schneider, G.C. Smith and K.L. Watters, Inorg. Chim. Acta, 15, 191 (1975).

87. J.R. Anderson, "Structure of Metallic Catalysts", Academic Press, New York, 1975, p. 275.

88. A. Brenner and R.L. Burwell, Jr., J. Catal., 52, 353 (1978).

89. E. Mantovani, N. Palladino and A. Zanobi, J. Mol. Catal., 3, 285 (1978).

90. K.J. Klabunde, D. Ralston, R. Zoellner, H. Hattori and Y. Tanaka, J. Catal., 55, 213 (1978).

91. S.F.A. Kettle in "Topics in Current Chemistry", Springer Verlag, New York, 1977, Vol. 77, p. 111.

92. Y. Nonaka, S. Takahashi and N. Hagihara, Mem. Inst. Sci. Ind. Res. Osaka University, 31, 23 (1974).

93. G.O. Evans, C.U. Pittman, Jr., R. McMillan, R.T. Beach and R. Jones, J. Organomet. Chem., 67, 295 (1974).

94. L.L. Murrell in "Advanced Materials in Catalysis", J.L. Burton, R.L. Garten, Eds., Academic Press, New York, 1977, p. 235.

95. K.G. Allum, R.D. Hancock, I.V. Howell, S. McKenzie, R.C. Pitkethly and P.J. Robinson, J. Organomet. Chem., 87, 203 (1975).

96. I. Haller, J. Am. Chem. Soc., 100, 8050 (1978).

97. F.R. Wild, G. Gubitosa and H.H. Brintzinger, J. Organomet. Chem., 148, 73 (1978).

98. F. Hugues, J.M. Basset, Y.B. Taarit, A. Choplin, M. Primet, D. Rojas and A.K. Smith, J. Am. Chem. Soc., 104, 7020 (1982).

99. J.R. Budge, J.P. Scott and B.C. Gates, J. Chem. Soc. Chem. Commun., 342 (1983).

100 T.J. Pinnavaia, R. Raythatha, J.G.-S. Lee, L.J. Halloran and J.F. Hoffman, J. Am. Chem. Soc., 101, 6891 (1979).

101. R. Raythatha and T.J. Pinnavaia, J. Catal., 80, 47 (1983).

102. W.H. Quayle and T.J. Pinnavaia, Inorg. Chem., 18, 2840 (1979).

103. F. Farzaneh and T.J. Pinnavaia, Inorg. Chem., 22, 2216 (1983).

104. Z. Otero-Schipper, J. Lieto and B.C. Gates, J. Catal., 63, 175 (1980).

105. H.B. Gray, A. Rembaum and A. Gupta, U.S. Patent 4,127,506.

106. G. Braca, C. Carlini, F. Ciardelli and G. Sbrana, Preprints, 6th International Congress on Catalysis, London, 1976, paper A43.

107. M.B. Freeman, M.A. Patrick and B.C. Gates, J. Catal., 73, 82 (1982).

108. J.B.N. Effa, J. Lieto and J.P. Aune, J. Mol. Catal., 15, 367 (1982).

109. J. Lieto, J.J. Rafalko and B.C. Gates, J. Catal., 62, 149 (1980).

110. P. Gallezot, G. Coudurier, M. Primet and B. Imelic, Am. Chem. Soc., Symp. Ser., 144 (1977).

111. J.G. Goodwin, Jr., and C. Naccache, J. Mol. Catal., 14, 259 (1982).

112. D. Commereuc, Y. Chauvin, F. Hugues, J.M. Basset and D. Olivier, J. Chem. Soc., Chem. Commun., 154 (1980).

113. J. Robertson and G. Webb, Proc. R. Soc. London, Ser. A., 341, 383 (1974).

114. A.K. Smith, A. Theolier, J.M. Basset, R. Ugo, D. Commereuc and Y. Chauvin, J. Am. Chem. Soc., 100, 2590 (1978).

115. V.L. Kuznetsov, A.T. Bell and Y.I. Yermakov, J. Catal., 65, 374 (1980).

116. A. Theolier, A. Choplin, L. D'Ornelas, J.M. Basset, R. Ugo, R. Psaro, G. Zanderighi and C. Sourisseau, Polyhedron, 2, 119 (1983).

117. J. Evans and G.S. McNulty, J. Chem. Soc., Dalton Trans., 1123 (1984).

118. D.K. Liu and M.S. Wrighton, J. Am. Chem. Soc., 104, 898 (1982).

119. Y. Doi, K. Soga, K. Yano and Y. Ono, J. Mol. Catal., 19, 359 (1983).

120. S.C. Brown and J. Evans, J. Mol. Catal., 11, 143 (1981).

121. J.G. Bentsen and M.S. Wrighton, Inorg. Chem., 23, 515 (1984).

122. A. Brenner and D.A. Hucul, J. Am. Chem. Soc., 102, 2484 (1980).

123. J.E. Crawford, G.A. Melson, L.E. Makovsky and F.R. Brown, J. Catal., 83, 454 (1983).

124. M. Deeba and B.C. Gates, J. Catal., 67, 303 (1981).

125. R. Barth, B.C. Gates, Y. Zhao, H. Knozinger and J. Hulse, J. Catal., 82, 147 (1983).

126. X.-J. Li and B.C. Gates, J. Catal., 84, 55 (1983).

127. R. Psaro, R. Ugo, G.M. Zanderighi, B.Besson, A.K. Smith and J.M. Basset, J. Organomet. Chem., 213, 215 (1981).

128. H. Knozinger and Y. Zhao, J. Catal., 71, 337 (1981).

129. T. Castrillo, H. Knozinger and M. Wolf, J. Mol. Catal., 11, 151 (1981).

130. K. Foger and J.R. Anderson, J. Catal., 59, 325 (1979).

131. M. Ichikawa, Bull. Chem. Soc. Japan., 51, 2268 (1978).

132. R.F. Howe, J. Catal., 50, 196, (1977).

133. J.R. Anderson, P.S. Elmes, R.F. Howe, and D.E. Mainwaring, J. Catal., 50, 508 (1977).

134. K. Tanaka, K.L. Watters and R.F. Howe, J. Catal., 75, 23 (1982).

135. C. Ercolani, J.V. Quagliano and L.M. Vallarino, Inorg. Chim. Acta, 3, 421 (1969).

136. F. Piacenti, M. Bianchi, E. Benedetti and G. Braca, Inorg. Chem., 7, 1815 (1968).

137. B.F.G. Johnson, J. Lewis and D.A. Pippard, J. Chem. Soc., Dalton Trans., 407 (1981).

138. R.F. Howe, D.E. Davidson and D.A. Whan, J. Chem. Soc., Faraday Trans., 68, 2266 (1972).

139. A. Kadkhodayan, Ph.D. Thesis, Michigan State University, East Lansing, MI, 1984.

140. F. Piacenti, M. Bianchi, P. Frediani and E. Benedetti, Inorg. Chem., 10, 2759 (1971).

141. F. Farzaneh, Ph.D. Thesis, Michigan State University, East Lansing, MI 1981.

142. G.A. Borchardt in "Minerals in Soil Environments", J.B. Dixon and S.B. Weed, Eds., Soil Science Society of America, Madison, WI, 1977, Chapter 9.

143. A.J. Lees and A.W. Adamson, J. Am. Chem. Soc., 104, 3804 (1982).

144. A.A. Davydov ard A.T. Bell, J. Catal., 49, 332 (1977).

145. N. Sheppard and T.T. Nguyen, Adv. Infrared Raman Spectrosc., 5, 67 (1978).

146. M.J. Cleare and W.P. Griffith, J. Chem. Soc. (A), 372 (1969).

147. A.J. Deeming, B.F.G. Johnson and J. Lewis, J. Chem. Soc. (A), 898 (1970).

148. J.S. Kristoff and D.F. Shriver, Inorg. Chem., 13, 499 (1974).

149. J.A. Helsen, R. Drieskens and J. Chaussidon, Clays Clay Miner., 23, 334 (1975).

150. B. Delley, M.C. Manning, D.E. Ellis, J. Berkowitz and N.C. Trogler, Inorg. Chem., 21, 2247 (1982).

151. E.G. Bryan, G. Jackson, B.F.G. Johnson, J.W. Kelland, J. Lewis and K.J. Schorpp, J. Organomet. Chem., 108, 385 (1976).

152. P.S. Bratterman, "Metal Carbonyl Spectra", Academic Press, London, New York, San Francisco, 1975.

153. L. Busetto and R.J. Angelici, Inorg. Chim. Acta., 2, 391 (1968).

154. P.M. Treichel, R.L. Shubkin, K.W. Barnett and D. Reichard, Inorg. Chem., 5, 1177 (1966).

155. B.D. Dombek and R.J. Angelici, Inorg. Chim. Acta, 7, 345 (1972).

156. A. Davison, W. McFarlane, L. Pratt and G. Wilkinson, J. Chem. Soc. (A), 3653 (1962).

157. D.A. Symon and T.C. Waddington, ibid., 954 (1971).

158. T.E. Sloan and A. Wojcicki, Inorg. Chem., 7, 1268 (1968).

159. W.H. Quayle, Ph.D. Thesis, Michigan State University, East Lansing, MI, 1978.

160. M. Green, T.A. Kuc and S.H. Taylor, J. Chem. Soc. (A), 2334 (1971).

161. R.H. Raythatha, Ph.D. Thesis, Michigan State University, East Lansing, MI, 1981.